HOKKAIDO UNIVERSITY

Title	Key factors affecting the pozzolanic reaction of steel slag-dredged soil mixtures : From inorganic and organic perspectives
Author(s)	,
Citation	. ( ) 14452
Issue Date	2021-03-25
DOI	10.14943/doctoral.k14452
Doc URL	http://hdl.handle.net/2115/91539
Type	theses (doctoral)
File Information	Kanako_Toda.pdf

Instructions for use

Key factors affecting the pozzolanic reaction of steel slag-dredged soil mixtures

-From inorganic and organic perspectives-

Submitted by

Kanako Toda

For the degree of Doctor of Philosophy

Hokkaido University

Department of Sustainable Resources Engineering

February 2021

Acknowledgements

Abstract

Industrial byproducts and waste soils are environmentally low-impact resources for the construction industry. Construction materials made with such resources are particularly attractive for regional use close to the material sources, because of the feasibility in the transport and application associated with cost savings. Dredged soils, excavated sediments of water ways, and steel slags, byproducts of iron making processes, have potential to form civil engineering constructions close to seashores, as their mixtures develop strength. The utilization of such mixtures is still limited due to their unpredictable variation of strength development when different dredged soils or steel slags are applied. No previous studies have comprehensively investigated the key factors that affects the strength development of the mixtures. This study elucidates the key factors for the first time by identifying the contributions of both inorganic and organic components in steel slags and dredged soils to the strength development of the mixtures.

Chapter 1 reviews the literature on the general management of dredged soils and steel slags, current knowledge of technologies on their validation as construction materials, as well as the pozzolanic reaction, chemical reaction that develops strength of the mixtures, to identify the factors affecting the reaction.

Chapter 2 focuses on identifying the factors among inorganic components in dredged soils and steel slags affecting the strength development of the mixtures. Amorphous silica in dredged soils and portlandite in steel slags were identified as the key factors as major Si and Ca sources for the pozzolanic reaction, respectively.

Chapter 3 focuses on identifying the effect of organic components in dredged soils to the strength development of the mixtures. Characteristics of dredged soils such as high sulfur content in soil organic matters fraction exhibited the soft mixtures, which suggested the strength development inhibition by soil organic matters. Chapter 2 and 3 newly show that the quantification of particulars in inorganic and organic matters of steel slags and dredged soils

indicate the strength development of the mixtures. Discovery of the indicators would facilitate the evaluation processes of the applicability of the mixtures to constructions.

Chapter 4 experimentally verifies the inhibition of the pozzolanic reaction by soil organic matters, by designing an experiment of the pozzolanic reaction in coexistence of escalating amount of a model organic matter. The inhibition of the pozzolanic reaction with a threshold in the dosage of the organic matter indicated some soil organic components in soil organic matters to inhibit the strength development of soft mixtures, as speculated in chapter 3.

Chapter 5 experimentally compares the effectiveness of soil organic matter reagents to the inhibition of the pozzolanic reaction. Organic reagents caused the inhibition of the pozzolanic reaction at different dosages. Together with the characterization of the organic reagents, this study suggests that the dosage of reduced sulfur and/or phenolic groups may trigger the inhibition of the pozzolanic reaction. Chapter 4 and 5 newly show that the soil organic matters inhibit the pozzolanic reaction.

Chapter 6 characterizes the bulk soil organic matters extracted from dredged soils, to identify particulars that may affect the pozzolanic reaction in the mixtures. The sulfur indicator of soft mixtures, stated on chapter 3, was found to result from the difference in the content of reduced sulfur. Discoveries in chapter 5 and 6 suggest reduced sulfur as a key component that plays a role in the inhibition of the pozzolanic reaction.

Chapter 7 focuses on clarifying the interaction of soil organic matters with the pozzolanic reaction in microscopic scales. Additional to reduced sulfur and phenolic groups, the X-ray spectroscopic study on the distribution of carbon speciation in the mixtures and the synthesis products of the pozzolanic reaction suggested aromatic carbon to affect the pozzolanic reaction, as its content was commonly higher in the samples which the pozzolanic reaction was inhibited, in comparison to those which the reaction was not inhibited.

Chapter 8 concludes the key factors that affect the strength development of the mixtures in the context of waste validation and shows research impact. Outstanding insights are derived from half-splitting analysis of key components in raw materials that promote and

inhibit geochemical reactions in control of strength development of such construction materials. These findings in this study are unambiguously useful to enhance utilization of industrial byproducts and waste soils in the construction industry.

List of Contents

List of Figures

List of Tables

1. Introduction

1.1. Sustainable construction industry

The demand of construction material resources is projected to increase at least until 2060 [1]. Constructions that require primary resources such as cement, sands, and gravels have limitation in resources and their usages require material excavation from Earth's surfaces. The substitution of construction materials with industrial byproducts or waste soils have been actively studied and applied to validate wastes and to lower the utilization of primary construction resources. Waste validation in construction industry is a key to lower the environmental impact of the activity of the industry that would meet the current and future demand of construction materials with sustainability.

1.2. Steel slag-dredged soil mixtures, a case study

Feasible utilization of waste soils and industrial byproducts requires the materials to possess desired physical properties such as compressive strengths. One of the hurdles to utilize such materials is the unpredictable strength development, due to the variation in their components and compositions, caused by unknown components that contribute or inhibit the strength development. Different mixing conditions and combinations of the materials exhibit variation in their develop strength, with some that does not exhibit significant strength regardless to the length of the curing time, that distracts the application of such materials by increasing the demand of human resources to examine their physical properties prior to the application on engineering fields. However, once the components in starting materials that contribute to determine the strength development is clarified, the utilization wastes can be enhanced by facilitating the evaluation processes on their mixing design such as its mixing proportions with other additives, or by providing insights to suggest the modifications to improve the strength of the materials.

As an example of the construction materials that validates waste soils and industrial byproducts, this study focuses on elucidating the key factors that affect the strength development of construction materials made with dredged soils and steel slags, where significant amount of both materials is treated as wastes. The mixtures are hereafter called as steel slag-dredged soil mixtures.

The excavation of soil sediments in water ways for shipping safety produces significant volumes of dredged soils (e.g., [2–4]). In Japan, 16 million tons of marine soils were dredged in 2013 and used landfill (59%), made beach reclamation and sand covers (25%), or disposed in the ocean (5%) along with other minor options for use and disposal [5]. However, limitations on landfill sites and the environmental impact of its creation, which consumes land and other primary resources for site construction such as cement and aggregate, has highlighted the necessity of dredged soil utilization improvements.

The concretion of dredged soils by mixing alkaline activators [6–10] makes them useful as construction materials and offers the potential to promote their utilization. Furthermore, parts of the dredged soils have also been mixed with industrial waste such as fly ash, lime production waste, and steel slag. Steel slag is a by-product in the iron-making process, and it has the ability to develop the strength with dredged soils by mixing and curing at room temperature [11–13] (**Fig. 1-1**). It is a kind of alkaline activator of dredged soils. Steel slag-dredged soil mixtures are utilized in engineering works close to the seashore because of the ease of material transport and application (**Fig. 1-2**).
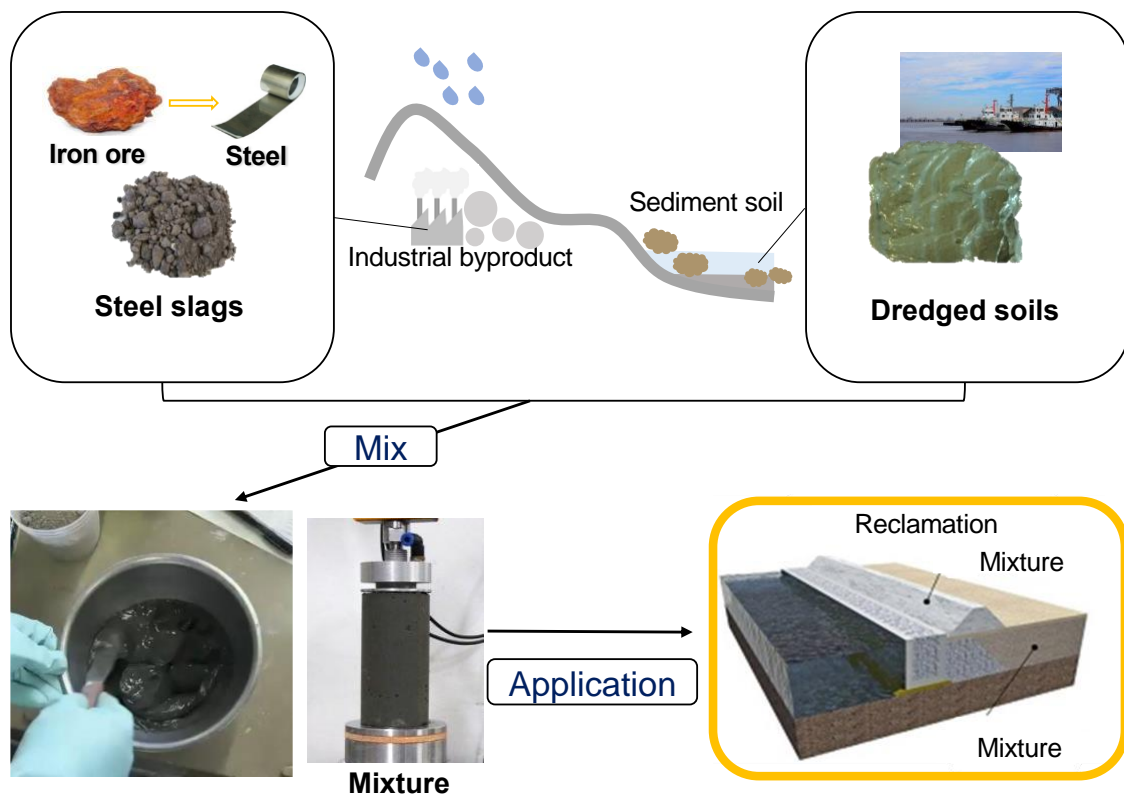
Fig. 1-1 Schematic diagram of steel slag and dredged soil utilization as construction materials close to seashore.
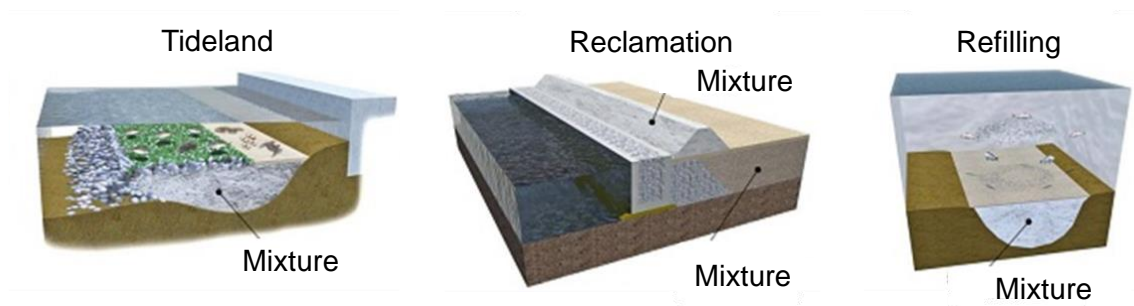
Fig. 1-2 Upper photo shows the onsite mixing of steel slag-dredged soil mixtures. Lower images show the examples of the mixture application.

However, as described in the general issue in the utilization of waste soils and industrial byproducts, some steel slag-dredged soil mixtures also exhibit weak strength in their construction. The mixtures made with dredged soils sampled from different ports cause variety in the strength development of their mixtures (**Fig. 1-3**). As shown on the **Fig. 1-3**, the final strength of the mixtures is unpredictable before mixing, which detracts from usefulness in the utilization of the mixtures.

(a)   (b)
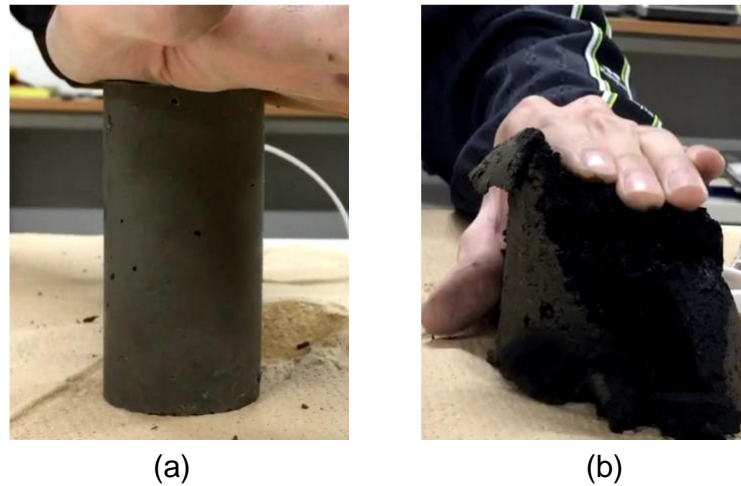
Fig. 1-3 Pictures of steel slag-dredged soil mixtures made with dredged soils from different ports, which (a) develops strength, that does not deform by pressing with hand, and (b) does not develop significant strength, that deforms by pressing with hand.

Fig. **1-4** shows the flowchart of the application of the mixtures. At the stage of environmental safety test and functionality test, the mixtures must pass the requirements to ensure the safety of the utilization. The application of the mixtures would not be straight forward when the properties of the mixtures do not match the requirements. Currently, the utilization of mixtures requires numerous strength tests with trial and error before the application, that corresponds to the trials on the mixing ratio determination and strengths tests on Fig. **1-4**.
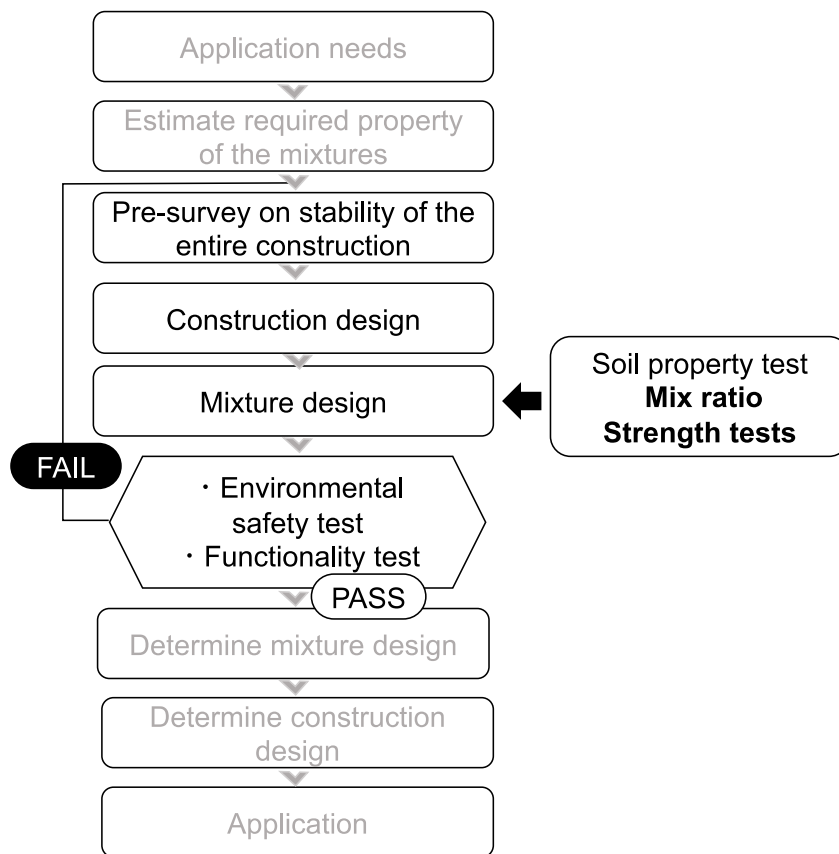
Fig. 1-4 Flowchart of the application of steel slag-dredged soil mixture (After [14][15]).

Unpredictable strength development especially results from the components of dredged soils where their effect on hardening is not fully elucidated. Such soils contain fine minerals, clay minerals, inorganic amorphous phases, and soil organic matters. Elucidation on the key components that affect the hardening reaction, would contribute to the enhancement of the utilization of the mixtures by facilitating the determination of the mixing ratio to achieve required strength development of the mixtures (**Fig. 1-4**).

1.2.1. Ca and Si sources are suggested as the key components that influence the strength development of the mixtures

The key factors affecting the strength development of the mixtures are suggested as the supply of calcium and silica [11,13]. The investigation on the factors originating in steel slags was studied extensively compared to that of the dredged soils, though the phases in steel slags that contribute to the strength development was not conclusive. Kiso et al., (2008) [11] suggested the content of free-CaO would be critical in promoting the strength development of the mixtures, though Hirai et al., (2011) [13] contradicted that the content of CaO was not influential to the strength development of the mixtures. Kiso et al., (2008) [11] discussed the importance of the quantity of soluble silica in dredged soils that influences the strength development of the mixtures, yet which silicate phases that contribute as the soluble silica supply remained unclarified.

The identification of the silicate phases and calcium bearing phases in dredged soils and steel slags, respectively, are necessary for the strength prediction of the mixtures.

1.2.2. Focus of the study: the pozzolanic reaction

The strength development of steel slag-dredged soil mixtures is presumably attributed to the extent of calcium silicate hydrate (C-S-H) phase formation [11,13]. C-S-H is known to act as a major binder in calcium-based cementitious materials (i.e., Lothenbach and Nonat, 2015). In this study, the formation reaction of C-S-H is hypothesized as the pozzolanic reaction, which refers to the formation of C-S-H from calcium supply such as portlandite $(Ca(OH)_2)$ and siliceous materials in moist conditions (formula 1-1). It is because, steel slags contain portlandite that can supply calcium other than free-CaO, which is rather soluble compared to other calcium bearing phases, such as calcium silicates. Chemical formula of the pozzolanic reaction can be simplified as formula 1-1 [11]:

$$Ca(OH)_2 + SiO_2 + nH_2O \rightarrow C-S-H \ (nCaO \cdot SiO_2 \cdot mH_2O). \quad (1-1)$$
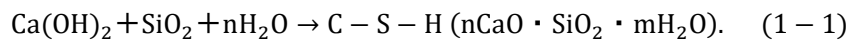
One of the stoichiometric reaction formula of C-S-H formation in thermodynamic database, Thermoddem of the French Geological Survey [17] is

$$Ca_{3.2}Si_2O_{8.2682}H_{2.1364}: 2.3446H_2O + 6.400H^+ = 3.200Ca^{2+} + 2.000H_4SiO_4 + 2.6128H_2O.$$
(1-2)
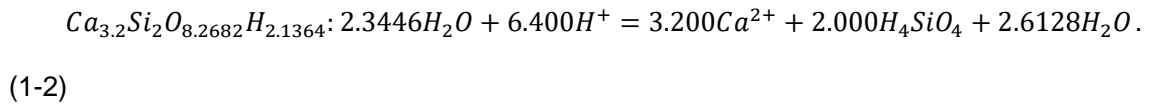
The pozzolanic reaction can be assumed as an iteration reaction as shown in **Fig. 1-5**. Portlandite, that possesses the equilibrium pH at 12.5 and calcium concentration at ca. 40 mmol/L makes the solution under alkaline conditions that allow the soluble silicate phases to dissolve, as silicates have high solubility under alkaline conditions, that let C-S-H to precipitate. Precipitation of C-S-H consumes dissolved silica and calcium, and decreases pH (formula 1-2), that undersaturates the solution composition against portlandite to allow the next iteration of the reaction to start. The factors which would affect the pozzolanic reaction would be the supply of calcium and silica as discussed in previous studies, also suggested from formula 1-1, or other factors that may interfere with the pozzolanic reaction.

However, no previous studies have comprehensively investigated the key factors which affects the strength development of the mixtures. Therefore, clarification of the key geochemical reactions for the strength development of the mixtures, presumably the pozzolanic reaction, and a total clarification of key components that affect the reaction, directly related to the strength development of the steel slag-dredged soil mixtures, will be carried out in this study. The clarification of the key factors that affect the strength development of the mixtures would make the evaluation processes faster with higher accuracy, which is expected to contribute to enhance the utilization of dredged soils and steel slags.
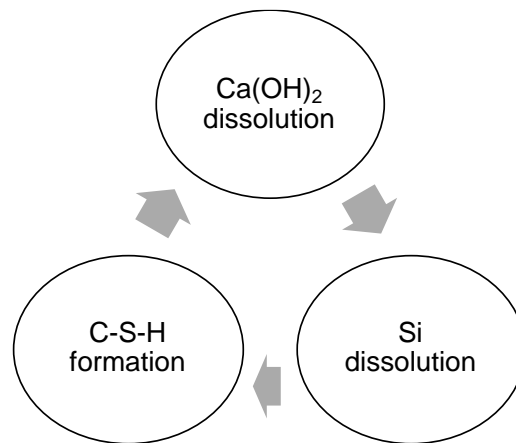
Fig. 1-5 Schematic diagram of the pozzolanic reaction.

1.2.2.1. Supply of Ca and Si sources

The calcium supply, attributed to steel slags, is hypothesized to be the dissolution of portlandite and it will be investigated in chapter 2 through characterization of steel slag samples and mineralogical and geochemical analysis of the steel slag-dredged soil mixtures, which will be compared between mixtures with and without significant strength development.

The silica supply, attributed to dredged soils, may originate in fine minerals, clay minerals and inorganic amorphous phases. Silicate phases which would supply silica for the C-S-H formation may exist in all classifications. The parameters that determine the feasibility of dissolution of the silicate phases, dissolution rate constants and specific surface area of some silicate phases that commonly compose soils are summarized in **Fig. 1-6**, **Fig. 1-7**, **Table 1-1**, and **Table 1-2**.

The parameters of silicate phases were compiled for: 1) minerals: quartz and albite; 2) clay minerals: kaolinite, chlorite, smectite, and illite; and 3) amorphous silica: volcanic glasses and diatomaceous materials, with synthetic amorphous silica. The phases that have higher dissolution rate constant and specific surface area would supply more silica to form C-S-H. Here, amorphous silica was shown to dissolve readily under alkaline conditions among other silicate phases, with highest dissolution rate constant two order higher than

other silicate phases, with specific surface area in the same range as clay minerals. Through characterization of dredged soils, the key silicate phases that supply silica to form C-S-H will be investigated in Chapter 2, by comparison of dredged soils that form mixtures with and without significant strength development.
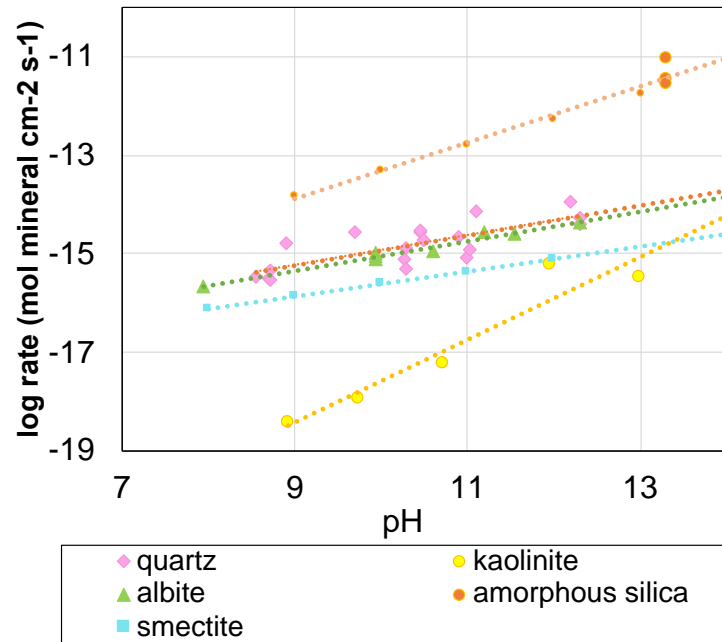
Fig. 1-6 Dissolution rate of silicates as a function of pH. Plots show the data compiled from previous studies and the fitted lines are shown on the diagram, that was used to calculate the dissolution rate constant of each phases. Data referred from [18–24].

Table 1-1 The dissolution rate constants of silicate phases as a function of pH.

Silicate phases	rate constant (mol cm^{-2} s^{-1})	References*
Quartz	$10^{(0.3041*pH-17.974)}$	Brady and Walther, 1990
		Wollast and Chou, 1988
		House and Orr, 1992
Albite	$10^{(0.3025*pH-18.068)}$	Chou and Wollast, 1985
Smectite	$10^{(0.25*pH-18.11)}$	Sato et al., 2004
Kaolinite	$10^{(0.8383*pH-25.967)}$	Huertas, 1999
Amorphous silica	$10^{(0.5739*pH-19.056)}$	Niibori et al., 2000
		Plettinck et al., 1994

*References from [18–25].
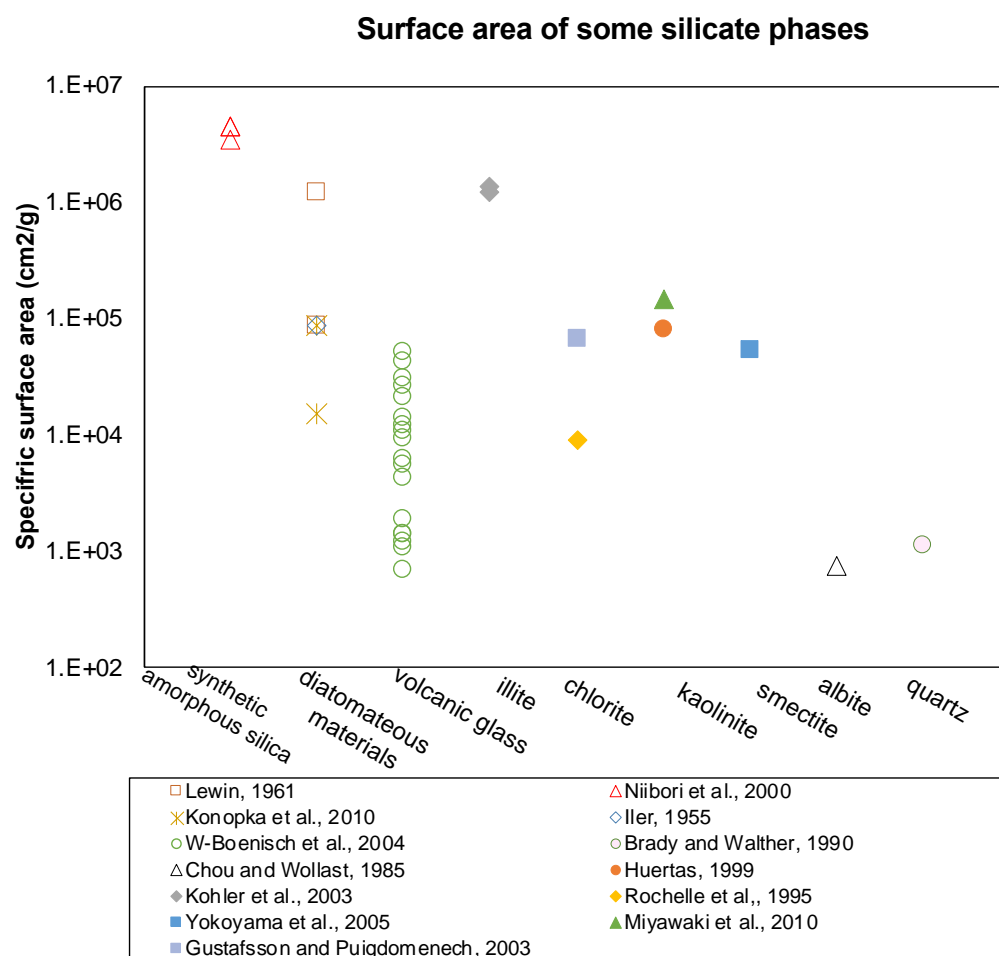
Fig. 1-7 Specific surface area of silicate phases.

Table 1-2 Values of specific surface area of silicate phases

Silicate phases	Surface area cm^2 g^{-1}	References*
quartz	1110	Brady and Walther, 1990
albite	750	Chou and Wollast, 1985
smectite	53000	Yokoyama et al., 2005
kaolinite	81600	Huertas, 1999
	148200	Miyawaki et al., 2010
illite	1240000	Kohler et al., 2003
	1370000	
chlorite	8900	Rochelle et al., 1995
	67000	Gustafsson and Puigdomenech, 2003
volcanic glasses	700~52200	W-Boenisch et al., 2004
diatomaceous materials	15200~1.23e+6	Iler, 1955, Lewin, 1961, Konopka et al., 2010
Synthetic amorphous silica	3.5e+6~4.5e+6	Niibori et al., 2000

References from [18,20,32–34,21,23,26–31].

1.2.2.2. Soil organic matters

Other than silicate phases in dredged soils, soil organic matters may also play a key role in the strength development of steel slag-dredged soil mixtures. Some organic matters including humic acids, an extractable fraction of soil organic matters, are known to inhibit the strength development of cementitious materials [35,36]. The removal of soil organic matter also improves strength development in cement treated soils [37]. Further, various organic reagents have been used to retard cement hydration rate in engineering fields [38–41]. Structural formula of major organic admixtures in cement industry are shown in **Fig. 1-8**, and an example of structural formula of soil humic acid is shown in **Fig. 1-9**. Organic admixtures compose of functional groups such as carboxylic group, that some of them also contain

sulfonates. The carbon species can be aliphatic or aromatic. On the other hand, soil organic matters compose of various organic constituents of carboxylic groups, esters, with aliphatic and aromatic carbon species. Sulfur bearing functional groups was also reported to exist in soil organic matters of sedimentary soils [42], such as thiols, polysulfides, and sulfonates. Soil organic matters are ubiquitous in environment, that has macromolecular structure with variety in their structural components. Comparison of the structures of the organic additives and soil organic matters spots out that soil organic matters would contain functional groups or structures as that or cement hydration retarders, or unique to soil organic matters that may interfere with the strength development of the steel slag-dredged soil mixtures.
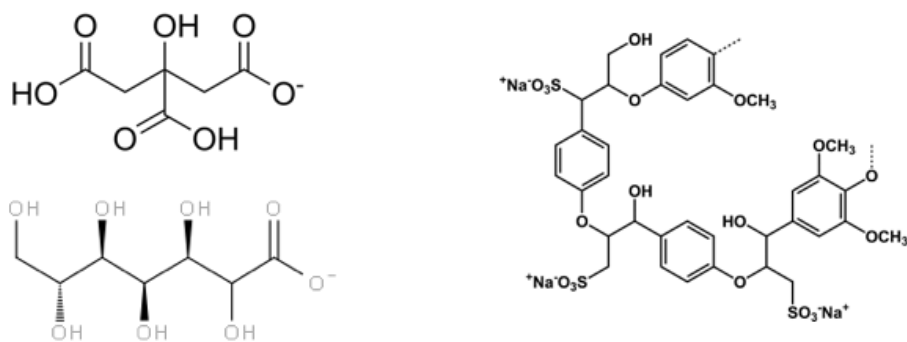
Fig. 1-8 Examples of organic admixtures in cement applications. Left structure formulas show carboxylic group bearing organic admixtures, and right structure formula show carboxylic and sulfonic group bearing organic admixtures [43]**.**
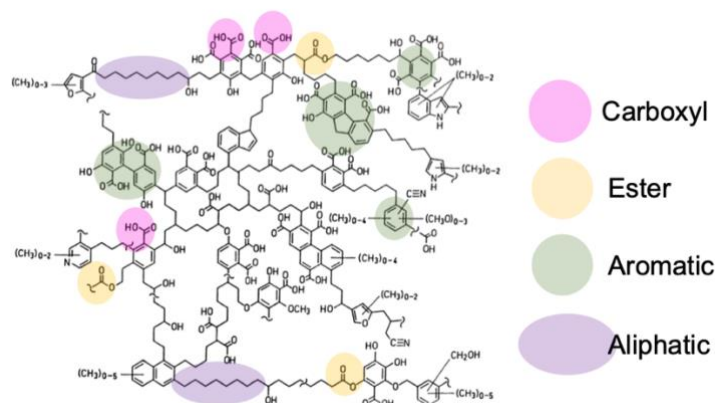
Fig. 1-9 Structural model of humic susbtances. (After Schulten and Schnizer, 1993 [44])

Organic matters could suppress pozzolanic reaction by: pH buffering capacity of soil organic matters, that is reported in the interaction of cement improved soils formed with additional humic acids[35]; calcium-organic matter complexation formation [45,46] that may decrease calcium supply to C-S-H formation; and, mineral surface poisoning, coverage of solid surfaces that occurs by the interaction of organic matters to inorganic phases surfaces, that may form impermeable layer to inhibit the hydration of starting minerals [40,47,48]. Hence, soil organic matters were hypothesized to retard, or inhibit the strength development of steel slag-dredged soil mixtures.

1.3. Aim of the study

This study aims to comprehensively elucidate the key factors that determine the strength development of the steel slag-dredged soil mixtures for the first time, by identifying the contributions of both inorganic and organic components in steel slags and dredged soils to the strength development of the mixtures.

The objective of each chapter are as follows. Chapter 2 aims to elucidate the inorganic components in steel slags and dredged soils that contribute to the supply of calcium and

silica in steel slag-dredged soil mixtures. Chapter 3 aims to clarify whether soil organic matters may indicate the weak strength development of the steel slag-dredged soil mixtures. Chapter 4 aims to elucidate whether soil organic matters inhibit the pozzolanic reaction. Chapter 5 aims to understand the effect of the compositional variety of soil organic matters to the pozzolanic reaction. Chapter 6 and 7 aims to elucidate the key components in soil organic matters that affect the pozzolanic reaction, which all results and discussions made from chapter 2 to chapter 7 will be summarized in chapter 8, to deliver the overview of the key factors which affect the strength development of the mixtures. Chapter 8 also suggests how facilitation of the application of the mixtures could be implemented, and how the research could apply to enhance the utilization of the mixtures.

References

[1]   Organization for Economic Co-operation and Development, Global Material Resources Outlook to 2060, 2019. https://doi.org/10.1787/9789264307452-en.

[2]   F. Onorati, C. Mugnai, M. Pulcini, M. Gabellini, A framework for the integrated assessment and management of dredged materials in Italy: A case study based on the application of Local Sediment Quality Guidelines, J. Soils Sediments. 13 (2013) 474–487. https://doi.org/10.1007/s11368-012-0636-4.

[3]   M.E. Bates, C. Fox-Lent, L. Seymour, B.A. Wender, I. Linkov, Life cycle assessment for dredged sediment placement strategies, Sci. Total Environ. 511 (2015) 309–318. https://doi.org/10.1016/j.scitotenv.2014.11.003.

[4]   J. Ministry of Land, Infrastructures, Transport and Tourism, On the Development of Technical Guideline on Ocean Disposal and Effective use of the Dredged Soils (In Japanese), Https://Www.Mlit.Go.Jp/Kisha/Kisha06/11/110619/01.Pdf. (2006).

[5]   P. and H.B. Ministry of land, Infratsurtucres, Transport and Tourism, Recycle guidelines for port / airport maintenance (Revised), (in Japanese), 2018.

[6]   V. Mymrin, J.C. Stella, C.B. Scremim, R.C.Y. Pan, F.G. Sanches, K. Alekseev, D.E. Pedroso, A. Molinetti, O.M. Fortini, Utilization of sediments dredged from marine ports as a principal component of composite material, J. Clean. Prod. 142 (2017) 4041–4049. https://doi.org/10.1016/j.jclepro.2016.10.035.

[7]   S. Lirer, B. Liguori, I. Capasso, A. Flora, D. Caputo, Mechanical and chemical properties of composite materials made of dredged sediments in a fly-ash based geopolymer, J. Environ. Manage. 191 (2017) 1–7. https://doi.org/10.1016/j.jenvman.2017.01.001.

[8]   V. Mymrin, R.C.Y. Pan, K. Alekseev, M.A. Avanci, J.C. Stella, C.B. Scremim, D.N. Schiavini, L.S. Pinto, R. Berton, S.L. Weber, Overburden soil and marine dredging sludge utilization for production of new composites as highly efficient environmental management, J. Environ. Manage. 236 (2019) 206–213. https://doi.org/10.1016/j.jenvman.2019.01.065.

[9]   Y.T. Kim, J. Ahn, W.J. Han, M.A. Gabr, Experimental evaluation of strength characteristics of stabilized dredged soil, J. Mater. Civ. Eng. 22 (2010) 539–544. https://doi.org/10.1061/(ASCE)MT.1943-5533.0000052.

[10]   T. Tsuchida, A. Porbaha, N. Yamane, Development of a geomaterial from dredged bay mud, J. Mater. Civ. Eng. 13 (2001) 152–160.

[11]   E. Kiso, M. Tsujii, K. Ito, M. Nakagawa, M. Gomyo, T. Nagatome, Method of dredged soil improvement by mixing with converter steel-making slag, Proc. Civ. Eng. Ocean. 24 (2008) 327–332.

[12]   M. Miraoui, R. Zentar, N.E. Abriak, Road material basis in dredged sediment and basic oxygen furnace steel slag, Constr. Build. Mater. 30 (2012) 309–319. https://doi.org/10.1016/j.conbuildmat.2011.11.032.

[13]   S. Hirai, M. Takaaki, K. Yoshiaki, K. Yuichiro, Study on Effect of Mixing Condition on Mechanical Properties of Mixture of Dredged Soil and Steel Slag (In Japanese), 2012.

[14]   Coastal development institute of technology, Technical manual for utilizing Calcia modified soil at ports, airports and coasts (in Japanese), 2017.

[15]   Constrution Design of Calcia-improved soils (in Japanese), Recearch Soc. Calcia-Improved Soil. (n.d.). http://calcia.jp/construction/index.html (accessed December 15, 2020).

[16]   B. Lothenbach, A. Nonat, Calcium silicate hydrates: Solid and liquid phase composition, Cem. Concr. Res. 78 (2015) 57–70. https://doi.org/10.1016/j.cemconres.2015.03.019.

[17]   P. Blanc, Thermoddem : Update for the 2017 version. Report BRGM/RP-66811-FR, 2017.

[18]   L. Chou, R. Wollast, Steady-state kinetics and dissolution mechanisms of albite., Am. J. Sci. 285 (1985) 963–993. https://doi.org/10.2475/ajs.285.10.963.

[19]   T. Sato, K. Masato, Y. Shingo, M. Tsutsui, K. Fukushi, T. Tanaka, S. Nakayama, Dissolution mechanism and kinetics of smectite under alkaline condition, in: Proc. Int. Work. Bentonite-Cement Interact. Repos. Environ., 2004: pp. A3-38 to A3-41.

[20]   F.J. Huertas, L. Chou, R. Wollast, Mechanism of kaolinite dissolution at room temperature and pressure Part II: Kinetic study, Geochim. Cosmochim. Acta. 63 (1999) 3261–3275. https://doi.org/10.1016/S0016-7037(99)00249-5.

[21]   Y. Niibori, M. Kunita, O. Tochiyama, T. Chida, Dissolution rates of amorphous silica in highly alkaline solution, J. Nucl. Sci. Technol. 37 (2000) 349–357. https://doi.org/10.1080/18811248.2000.9714905.

[22]   S. Plettinck, Kinetics and Mechanisms of Dissolution of Silica at Room Temperature and Pressure, Mineral. Mag. 58A (1994) 728–729. https://doi.org/10.1180/minmag.1994.58a.2.116.

[23]   P.V. Brady, J.. V. Walther, Kinetics of quartz dissolution at low temperatures, Chem. Geol. 82 (1990) 253–264.

[24]   W.A. House, D.R. Orr, Investigation of the pH dependence of the kinetics of quartz dissolution at 25°C, J. Chem. Soc. Faraday Trans. 88 (1992) 233–241. https://doi.org/10.1039/FT9928800233.

[25]   R. Wollast, L. Chou, Rate Control of Weathering of Silicate Minerals at Room Temperature and Pressure, Published by Kluwer Academic Publishers, 1988.

[26] S. Yokoyama, M. Kuroda, T. Sato, Kinetics and Mechanism of Smectite Dissolution, Clays Clay Miner. 53 (2005).

[27] S.J. Köhler, F. Dufaud, E.H. Oelkers, An experimental study of illite dissolution kinetics as a function of ph from 1.4 to 12.4 and temperature from 5 to 50°C, Geochim. Cosmochim. Acta. 67 (2003) 3583–3594. https://doi.org/10.1016/S0016-7037(03)00163-7.

[28] C.A. Rochelle, K. Bateman, R. MacGregor, J.M. Pearce, D. Savage, P.D. Wetton, Experimental Determination of Chlorite Dissolution Rates, MRS Proc. 353 (1994) 149. https://doi.org/10.1557/PROC-353-149.

[29] D. Wolff-Boenisch, S.R. Gislason, E.H. Oelkers, C. V. Putnis, The dissolution rates of natural glasses as a function of their composition at pH 4 and 10.6, and temperatures from 25 to 74℃, Geochim. Cosmochim. Acta. 68 (2004) 4843–4858. https://doi.org/10.1016/j.gca.2004.05.027.

[30] J.C. Lewin, The dissolution of silica from diatom walls, Geochim. Cosmochim. Acta. 21 (1961) 182–198. https://doi.org/10.1016/S0016-7037(61)80054-9.

[31] K. Konopka, A. Danelska, M. Szafran, Diatoms as a Source of New Materials, Ceram. Mater. 62 (2010) 521–524.

[32] R. Miyawaki, T. Sano, F. Oohashi, M. Suzuki, T. Kogure, T. Okumura, J. Kameda, T. Umezome, T. Sato, D. Chino, I. Hiroyama, Y. Yamada, K. Tamura, K. Morimoto, S. Uehara, T. Hatta, 日本粘土学会参考試料の分析・評価, Nendo Kagaku. 48 (2010) 158–198.

[33] B.Å. Gustafsson, I. Puigdomenech, The effect of pH on chlorite dissolution rates at 25°C, in: Symp. II – Sci. Basis Nucl. Waste Manag. XXVI, 2002.

[34] R.K. Iler, The collid chemistry of silica and silicates, 1955.

[35] H. Tremblay, J. Duchesne, J. Locat, S. Leroueil, Influence of the nature of organic compounds on fine soil stabilization with cement, Can. Geotech. J. 39 (2002) 535–546. https://doi.org/10.1139/t02-002.

[36] G.-O. Kang, T. Tsuchida, Y.-S. Kim, W.-J. Baek, Influence of humic acid on the strength behavior of cement-treated clay during various curing stages, J. Mater. Civ. Eng. 29 (2017) 1–18. https://doi.org/10.1061/(ASCE)MT.1943-5533.0001919.

[37] M. Kamon, S. Tomohisa, K. Sawa, On stabilization of hedoro by using cement group hardening materials, Zairyo. 432 (1989) 1092–1097.

[38] M. Bishop, A.R. Barron, Cement hydration inhibition with sucrose, tartaric acid, and lignosulfonate: Analytical and spectroscopic study, Ind. Eng. Chem. Res. 45 (2006) 7042–7049. https://doi.org/10.1021/ie060806t.

[39] G. Möschner, B. Lothenbach, R. Figi, R. Kretzschmar, Influence of citric acid on the hydration of Portland cement, Cem. Concr. Res. 39 (2009) 275–282. https://doi.org/10.1016/j.cemconres.2009.01.005.

[40] N.L. Thomas, J.D. Birchall, The retarding action of sugars on cement hydration, Cem. Concr. Res. 13 (1983) 830–842.

[41] V.S. Ramachandran, M.S. Lowery, Conduction calorimetric investigation of the effect of retarders on the hydration of Portland cement, Thermochim. Acta. 195 (1992) 373–387. https://doi.org/10.1016/0040-6031(92)80081-7.

[42] M.A. Vairavamurthy, D. Maletic, S. Wang, B. Manowitz, T. Eglinton, T. Lyons, Characterization of sulfur-containing functional groups in sedimentary humic substances by X-ray absorption near-edge structure spectroscopy, Energy and Fuels. 11 (1997) 546–553. https://doi.org/10.1021/ef960212a.

[43] H.F.W. Taylor, Cement chemistry, Cem. Chem. (1997). https://doi.org/10.1680/cc.25929.

[44] H.R. Schulten, M. Schnitzer, A state of the art structural concept for humic substances, Naturwissenschaften. 80 (1993) 29–30. https://doi.org/10.1007/BF01139754.

[45] C. J. Milne, D. Kinningburgh, J. C.M. De Wit, W. H. Van Riemsduk, L. K. Koopal, Analysis of metal-ion binding by a peat humic acid using a simple electrostatic model, J. Colloid Interface Sci. 175 (1995) 448–460. https://doi.org/10.1016/j.jcis.2008.12.029.

[46] J.G. Hering, F.M.M. Morel, Humic Acid Complexation of Calcium and Copper, Environ. Sci. Technol. 22 (1988) 1234–1237. https://doi.org/10.1021/es00175a018.

[47]   J. Plank, M. Gretz, Study on the interaction between anionic and cationic latex particles and Portland cement, Colloids Surfaces A Physicochem. Eng. Asp. 330 (2008) 227–233. https://doi.org/10.1016/j.colsurfa.2008.08.005.

[48]   J. Plank, C. Hirsch, Impact of zeta potential of early cement hydration phases on superplasticizer adsorption, Cem. Concr. Res. 37 (2007) 537–542. https://doi.org/10.1016/j.cemconres.2007.01.007.

2. Effect of amorphous silica to strength development in steel slag-dredged soil mixtures

Abstract

Some of the steel slag from ironworks and dredged soils from marine and waterfront engineering work are partially treated as waste. However, a mixture of these two kinds of waste has the potential to be used as construction materials when mixed, due to chemical reactions forming secondary phases. Utilizing waste of such kind as a resource, will help to improve sustainability in society by reducing waste and replacing virgin resources such as cement. Recently, it was reported that mixtures of steel slag and dredged soil hardens under specific conditions. The phase compositions of dredged soils and steel slags vary depending on the quantity of each component, which results in unpredictable strength development of mixtures. The effect of the variations in the phases of the starting materials on strength development of the mixtures is not yet clarified, limiting the utilization of the mixtures. Understanding the hardening mechanisms of the mixtures will enable the prediction of strength development. Focusing on the variations in the components in steel slags and, especially of dredged soils, this study aims to identify the components in both materials that affect the secondary phases formation that are responsible for strength development. We found support for suggestions that calcium silicate hydrate, C-S-H is one of the secondary phases responsible for the strength development of the mixtures. From a comparison of two kinds of steel slags and various dredged soils, the amount of portlandite in the steel slags and the amount of amorphous silica in the dredged soils are suggested as one of the key components of starting materials involved in the C-S-H formation.

2.1. Introduction

The effect of a partial substitution of starting materials to form cement and concrete has been widely studied as it would make it possible to decrease the environmental impact of cement production and/or improve the properties of cement and concrete. The ASTM C618 [1] defines mineral admixtures that can be used for mixing concrete, such as diatomaceous earths, opaline chert and volcanic ashes, among others, and the physical performance of construction materials made with these natural additives has been investigated to widen their applications [2,3]. Also, industrial byproducts such as fly ash and slags from metallurgy have been utilized for construction materials to reduce waste volumes [4]. Further, the performance of construction materials that utilize no cement but instead employ waste soils and industrial byproducts, such as mixtures of fly ash and diatomite have also been investigated [5]. This increase in the diversity of starting materials for mixing hardening mixtures suggests that construction can be conducted with economically optimal materials, derived from the surrounding nature and industries that can conform to desirable physical properties.

As one potential diversification of construction materials, steel slag-dredged soil mixtures is the focus of this study. Dredged soils are derived from the excavation of soil sediments beneath ports. The physical properties of soft dredged soils are difficult to improve as it contains a large fraction of fine particles and thus maintains the water content high. Therefore, they are treated with dumping after excavation that is costly and produces unwanted waste. Dredged soils are generated in Japan as well as in other countries where there is an inflow of water currents transporting soils that settle on sea floors and riverbeds

[6]. Further, the yield of the eroding soil particles is reported to be getting greater due to increases in the rate of soil erosion as a result of intensive agriculture and global warming [7]. The wider use of soil sediments would reduce the dumping of such materials in landfills and would enable the substitution of resources that would otherwise be excavated on land. Steel slag is one byproduct from ironworks that has the ability to alkali-activate. Although the utilization of steel slags has been investigated to increase volumes that are used [4,8], it is still difficult to utilize all steel slags that are produced. Recently, the utilization of dredged soils by modifying their physical properties with addition of alkaline activators has been investigated [4,8]. Improvements in the physical properties of dredged soils by mixing with steel slags would open up new areas of application in undersea construction by utilizing in constructions, such as reclamation and tideland. Simultaneously, it would replace cement utilized for ordinary undersea construction, which would contribute to reductions in the CO2 emissions and use of energy, as steel slag-dredged soil mixtures do not need preparatory calcination.

The mixtures made with various dredged soils and steel slags show differences in strength development, inhibiting the utilization of the steel slag-dredged soil mixtures in many engineering fields. It is because the hardening mechanisms, namely responsible components in the starting materials for the strength development and the secondary phase formation that is responsible for changes in physical properties, are both not immediately evident. Portlandite, $Ca(OH)_2$, in steel slags and soluble silica from dredged soils have been proposed to be the key components for the strength development because calcium silicate hydrate (C-S-H) is thought to be the cause of strength development [10]. Confirmation of the C-S-H formation and identifying factors that affect the formation of C-S-H would provide a methodology to predict its formation quantitatively, by analyzing the content of the critical phases in the starting materials. The effects of components such as humic acid in dredged soils are known to limit the strength development of cementitious materials [11] ,[12]. Considering these factors, the objective of this study is to identify the key components

affecting strength development, i.e., the formation of C-S-H, in steel slag-dredged soil mixtures. After determining the components that affect secondary phase formation, interaction of dredged soils and steel slags is simulated using geochemical modeling to provide insights into the possibility to predict the amounts of C-S-H needed to achieve specified strength development.

2.2. Materials and methods

2.2.1. Materials

2.2.1.1. Steel slags and dredged soils

The dredged soils used in this study were collected from four different bays in Japan, hereafter named soils A, B, C, and D. The physical properties of the dredged soils are detailed in **Table 2-1**. Humic acid was extracted from the dredged soils to quantify the content by the methodology described by Fukushima et al., (2009) [13]. The extracted samples of humic acid were purified by dialysis and freeze dried to quantify the content. Purified humic acid content was highest in soil D(0.30%) followed by B(0.20%), C(0.14%) and A(0.09%).

Steel slags were obtained from two ironworks in Japan and are hereafter named slag 1 and slag 2. The densities of slag 1 and slag 2 in surface-dry condition are 3.5 g/cm^3 and 3.8 g/cm^3, respectively. Particle size distributions of the steel slags and the dredged soils are shown in **Fig. 2-1**(a) and (b).
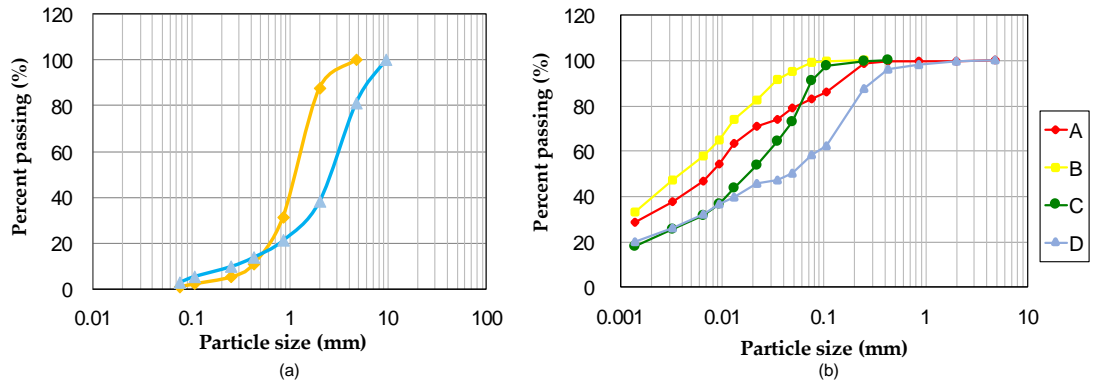
Fig. 2-1 Particle size distribution of (a) steel slags and (b) dredged soils of fraction smaller than 4.75 mm.

Table 2-1 Physical properties of the dredged soils.

	Soil particle density (g/cm^3)	Liquid limit	Plastic limit	Content of fine particles(<0.075mm) (%)
Soil A	2.777	73.4	28.4	83.2
Soil B	2.737	89.8	37.1	99.3
Soil C	2.709	44.1	29.1	91.1
Soil D	2.707	66.2	30.7	58.6

2.2.1.2. *Preparation of steel slag-dredged soil mixtures*

The steel slags were used in air-dried condition to make the experimental mixtures. Particles larger than 4.75 mm in the dredged soils such as marine shells were removed by sieving to eliminate inhomogeneity in the matrix of the mixtures for the measurement of strength. The water content was set to 1.5 times of the respective soil liquid limits (**Table 2-1**) by adding artificial seawater. This conditioning creates the soil slurries of a broadly similar consistency range.

The mixtures for measuring the strength development were made by mixing both steel slags with the four soils. The mixtures made with slag 1 and soils A, B, C, and D are termed 1A, 1B, 1C, and 1D, respectively, and the mixtures with slag 2 and soils A, B, C, and D are

termed 2A, 2B, 2C, and 2D, respectively. The steel slag-dredged soil mixtures for all analyses were prepared under the same conditions as the mixtures that were used for measuring strength development. The mixing ratio of steel slag to dredged soil was set to 3:7 by volume. As the dredged soils and the resulting mixtures were all saturated with water, the necessary weights of the surface-dried slag particles and saturated clay required for blending were calculated from the properties and the water content reported above. The measured bulk density of the mixture specimens was 97-100% of the theoretical values, indicating that very little air was entrapped in the process. The mixtures were thoroughly mixed with electrical mixer for about 5 minutes. The specimens for the strength tests were prepared by filling cylindrical plastic molds with a height of 100 mm and 50 mm in diameter. The mixtures to be used for cross sectional observations were prepared in a smaller container, made of PVC. When filling the molds, the mixtures were tapped to eliminate inclusions of air bubbles. The mixtures were cured hermetically in a plastic container at 25 ℃ under high humidity until testing. The pre- and post-curing weights of the specimens did not exhibit any statistically significant decreases in moisture content.

The specimens were cured for up to 91 days, and the mixtures at different curing times were selected for subsequent observations and analyses.

2.2.1.3. *Physical descriptions of steel slag-dredged soil mixtures*

The measurement of the unconfined compressive strength (q_u) was conducted for mixtures cured from 3 to 91 days, and the measurements of the shear modulus (G) were made for mixtures cured from 1 hour to 91 days. The strength at early curing ages, i.e. 1 hours to 3 days, which was too low to be measured by the conventional compression test, was also measured by a high-accuracy direct shear apparatus (see [14], for details). The shear modulus of 1A, 1B, 1C, 1D, 2A, 2B, 2C, and 2D were measured non-destructively in previous studies as an indicator for the physical strength at the early stage of curing, as it is known that the shear modulus and uniaxial compressive strength are positively correlated in

steel slag-dredged soil mixtures [15]. The modulus was calculated based on the mass density of the specimens and the shear wave velocity travelling between a pair of piezoelectric bender elements, which work as transmitter and receiver. Between 3 and 91 days of curing, the order of the magnitude of the relative strength of mixtures remained unchanged, for slag 1, the 1A showed the highest strength values followed by 1B, 1C, and 1D, and for slag 2 the 2A mixture had the highest values followed by 2B. The unconfined strength of mixtures made with slag 1 was much higher than those made with slag 2. The shear modulus indicated the significant increase at 3 days of curing especially in 1A and 1B and each G of 3 days was 209.0, 84.1, 12.1, and 1.2 MPa for mixtures 1A, 1B, 1C and 1D, respectively (**Fig. 2-2**).Therefore, investigation of the steel slag-dredged soil interaction at the early stage, namely at 3 days of curing, would provide sufficient information to determine the main reaction controlling the strength development.

(a)

(b)

(c)

(d)
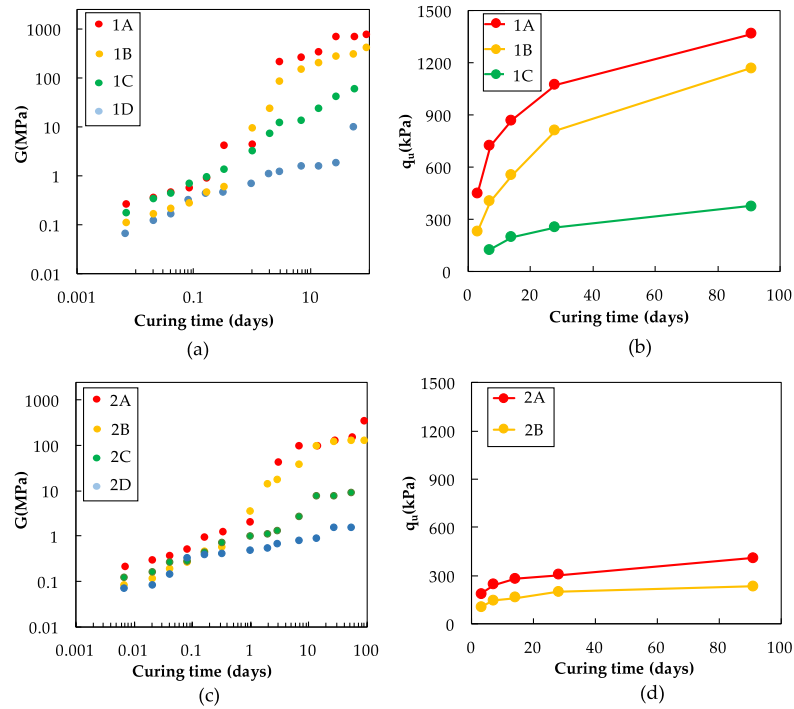
Fig. 2-2 Variation of mechanical properties of mixtures: (a) and (c) show the shear modulus (G) of the mixtures, and (b) and (d) show the unconfined compressive strength (q_u) of the mixtures.

2.2.2. Methods

2.2.2.1. Characterization of starting materials

The mineralogical composition of the steel slags and dredged soils was measured using randomly oriented samples by powder X-ray diffraction (XRD) with a Rigaku Multiflex Diffractometer operating at 30 kV and 20 mA, equipped with a Cu target. Steel slags and dredged soils were ground and pulverized, and powders with diameter of below 53 μm were used for the measurements.

Detailed characterization which covers various phases from minerals, and clay minerals to amorphous phases was made for the dredged soils. The clay minerals in the dredged soils were identified with XRD by the preferred orientation method. The dredged soil samples were washed with 10 % H_2O_2 to remove the organic matter and 1N HCl to remove carbonates that may interfere with the settlement of the clay sheets on the slide glass. After the treatment, suspended solutions were washed with deionized water to suppress the aggregation of clay particles. Particles with sizes below 2 μm were separated using a centrifuge and suspended clay particles were pipetted on slide glass and dried overnight to let clay minerals settle in the same orientation. After the first XRD measurement, ethylene glycol saturation was performed on the oriented samples to check for the existence of expandable clay minerals.

To observe the amorphous components in the dredged soils that were unidentifiable by XRD, optical microscope observations of the soil particles were made with transmitted light. After removal of organic matter and carbonates from 1 g of samples of dried dredged soils and dispersal in 50 mL of distilled water, 0.2 mL of the suspended solution was pipetted onto cover glass and heated until dry. Next, one drop of mountmedia (Wako Pure Chemical Industries) was applied and the sample was covered by slide glass to seal the samples for subsequent observations.

Selective dissolution experiments were conducted to quantify the amorphous biogenic silica and inorganic amorphous silica, following established methodologies [16] , [17]. The dredged soils were dried to equalize the soil particle quantities applied to dissolution

experiments. For the amorphous biogenic silica extraction, ground and dried soil particles were treated with 2 M Na_2CO_3 with solid to a liquid ratio (S/L) of 50 mg/40 mL and heated at 85 ℃ for 5 hours. For the inorganic amorphous silica extraction, 0.5M NaOH was added to the soil particles at an S/L ratio of 50 mg/50 mL and heated at 100 ℃ for 2.5 minutes. The dissolved Si concentration in the obtained supernatant was measured by an inductively coupled plasma atomic emission spectroscopy (ICP-AES; ICPE-9000, Shimadzu).

2.2.2.2.   *Analyses of steel slag-dredged soil mixtures*

The 3, 7, 28, and 91 day cured mixtures of all combinations of mixtures were freeze-dried to stop the hydration. The dried specimens were ground and pulverized to collect particle size of under 53μm for detecting changes in the mineralogical phases by XRD. For comparisons of the phase transitions from before curing, "0-day cured mixtures" were prepared by mixing pulverized, dry slag powder and dry soil powder. The mixing ratio was determined such that the weight/volume ratio of two solids, i.e. slag and clay particles, became identical to the specimens

described in Section 2.1. The mixtures were prepared for optical microscope (OM) and scanning electron microscope (SEM; SUPERSCAN SSX500, Shimadzu) analysis to observe the formation of secondary phases. Mixtures 1A and 1D at 3 days of curing were analyzed, as early strength development already displayed variance in the strength of the different combinations of dredged soils and steel slags. The 3 day cured mixtures were freeze dried and suspended in epoxy resin to preserve the structure of the mixture matrices. Cross sections of the resinated mixtures were polished to observe the formation of secondary phases.

2.2.2.3.   *Analyses of the solution chemistry of pore water*

The pH changes of the pore water of mixtures 1A, 1B, 1C, and 1D from 0 to 91 days and of mixture 2A from 0 to 14 days were measured directly with a pH meter employing pH probe (Hanna Instruments-1053B) that was an electrode for semi-solids and soils. Pore water

from mixtures 1A, 1B, 1C and 1D after 3 days of curing were extracted by compression and they were filtered by membrane filter with pore diameter of 0.2μm. The Ca concentration of the pore water samples were measured by ICP-AES. The dissolved Si concentration of the pore water in the dredged soils was measured by an Ultraviolet-Visible Absorption Spectroscope (UV-VIS; V-550, JASCO Corporation).

2.3. Results

2.3.1. Characterization of the starting materials

2.3.1.1. The steel slags

The mineralogical phases of slag 1 and slag 2 are similar to those of the reported ordinary steel slag [18], consisting of portlandite $Ca(OH)_2$, larnite C_2S, brownmillerite C_4AF, and others, as identified by XRD (**Fig. 2-3**). Slag 2 contains native iron which is not identified in slag 1. When we compare the intensity of the peaks corresponding to portlandite, its content is higher in slag 1 than in slag 2.
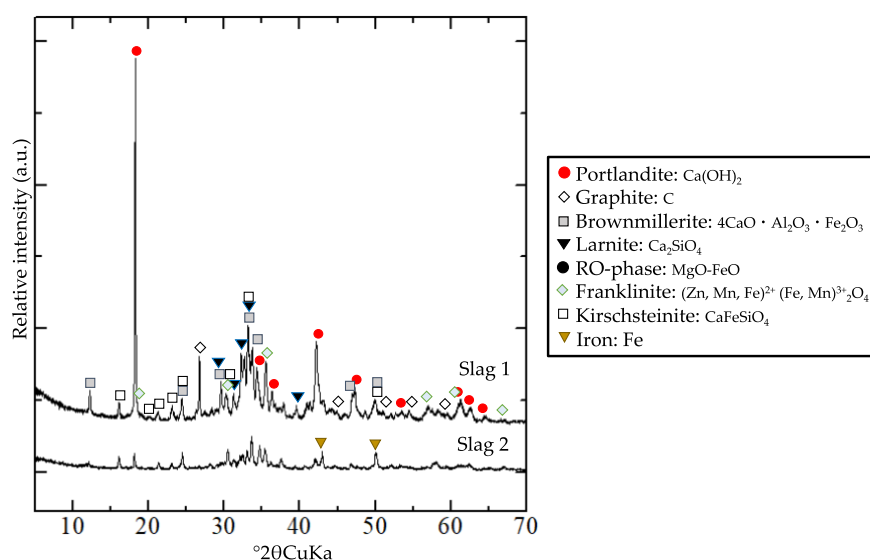
Fig. 2-3 XRD profiles of steel slag 1 and slag 2 prior to mixing with dredged soils.

2.3.1.2. Dredged soils

The XRD results show that all soils contained quartz, albite, halite, and pyrite (**Fig. 2-4**a); and clay minerals including smectite, kaolinite, chlorite, and illite (**Fig. 2-4**b). There are no significant differences between the soil samples in terms of mineralogy and clay mineralogy. The OM observation of particles in the dredged soils revealed that all soils contain amorphous silica phases, including diatom frustules originating from the growth of diatom algae (**Fig. 2-5**), and volcanic glass originating from erupted ejecta of volcanoes (**Fig. 2-6**).

Diatom frustules are a kind of biogenic silica, and volcanic glasses are a kind of inorganic silica. The genus of the diatoms varied among the four dredged soils, all containing both centric and pennate diatoms. The shapes of the volcanic glass did not differ significantly in these dredged soils. The dissolved mass of diatom frustules and volcanic glass by selective dissolution experiments showed that: both diatoms and volcanic glass content was highest in soil A, followed by soil B, C, and D (**Fig. 2-7**). The dissolved Si concentration of the pore water in the dredged soils was the highest in soil A, followed by soil B, C, and D (**Fig. 2-7**).
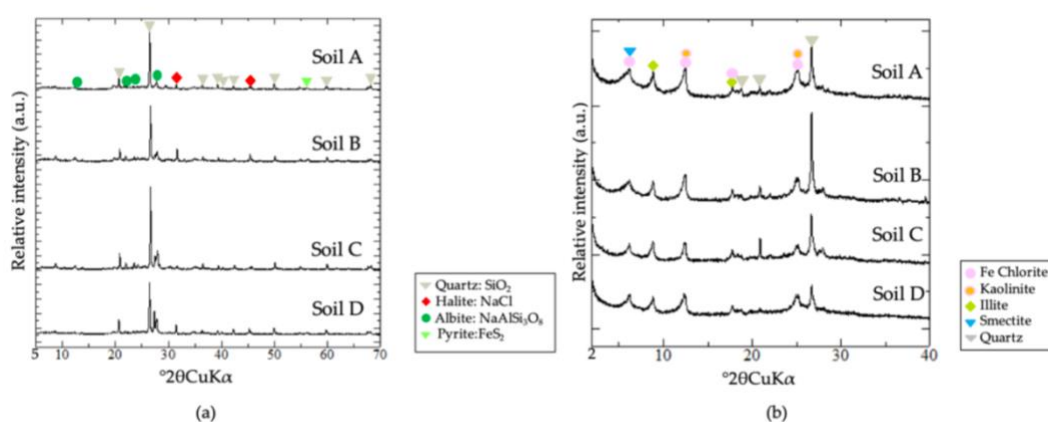
Fig. 2-4 XRD profiles of (a) randomly oriented dredged soil samples to detect mineralogical phases and (b) oriented dredged soil samples to detect clay mineralogical phases.
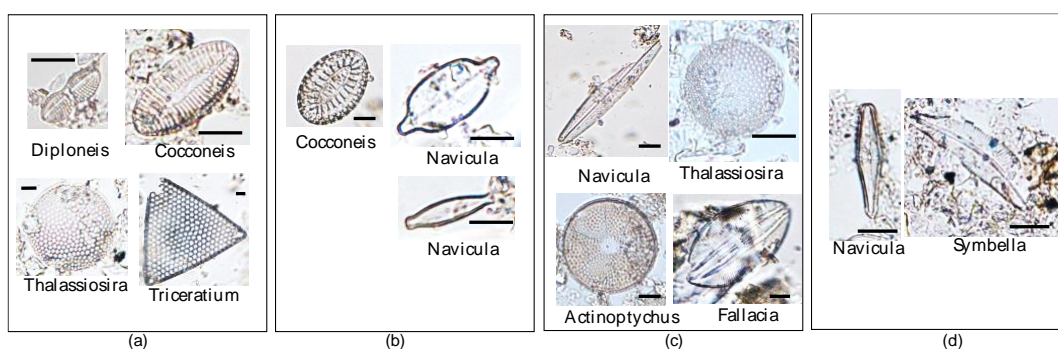
Fig. 2-5 Microscopic observations of diatom frustules incorporated in (a) soil A, (b) soil B, (c) soil C, and (d) soil D. Scale bars are 20μm.
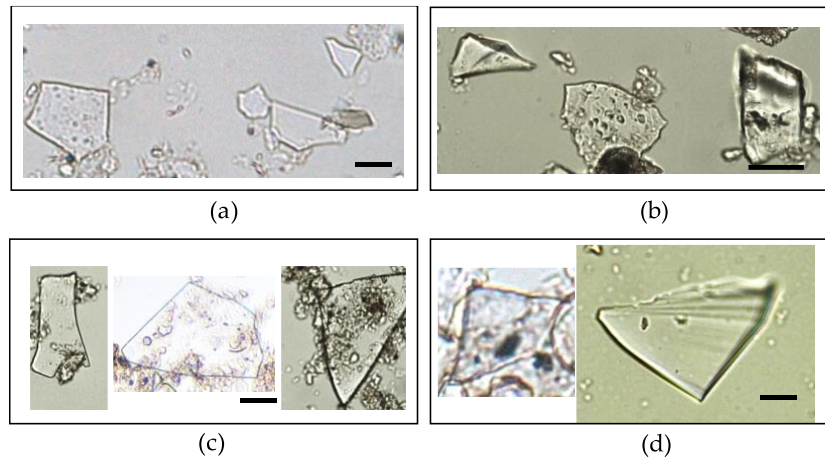
Fig. 2-6 Microscopic observations of volcanic glass particles incorporated in (a) soil A, (b) soil B, (c) soil C, and (d) soil D. Scale bars 20µm.
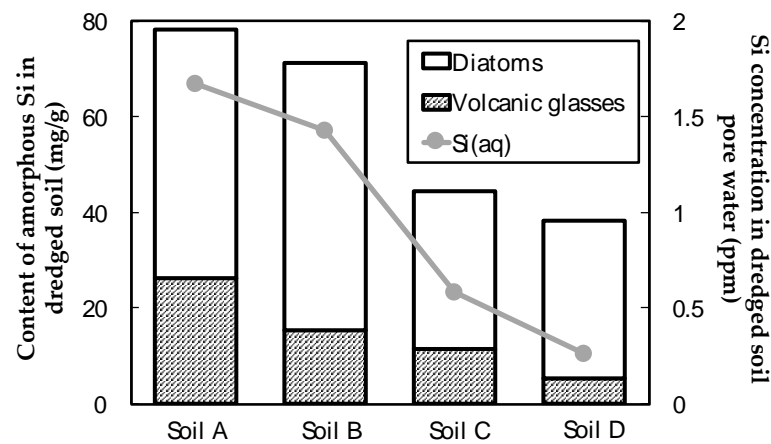
Fig. 2-7 Mass of diatoms and volcanic glasses by selective dissolution experiments, calculated as SiO_2.

2.3.2. Secondary phase formation in the mixtures

No newly formed crystalline mineralogical phases were detected in the XRD profiles of the cured mixtures **(Fig. 2-8** and **Fig. 2-9**). This leads to the conclusion that the secondary phase responsible for development of the strength of the mixtures is amorphous. Also, the peaks corresponding to portlandite were no longer detected in mixtures 1A and 1B after 7 days of curing, unlike the other components of the steel slag, such as larnite. The portlandite content of mixtures 1A and 1B after 7 days of curing was too low to be detected by XRD, but the peaks corresponding to portlandite was detected in mixtures 1C and 1D after 7 days of

curing (**Fig. 2-8**). In the XRD profiles of the mixtures with slag 2, the peaks corresponding to portlandite disappeared in all mixtures after 3 days of curing, showing that the portlandite content was much lower than that of the mixtures with slag 1 and that portlandite did not remain in the later curing stages.
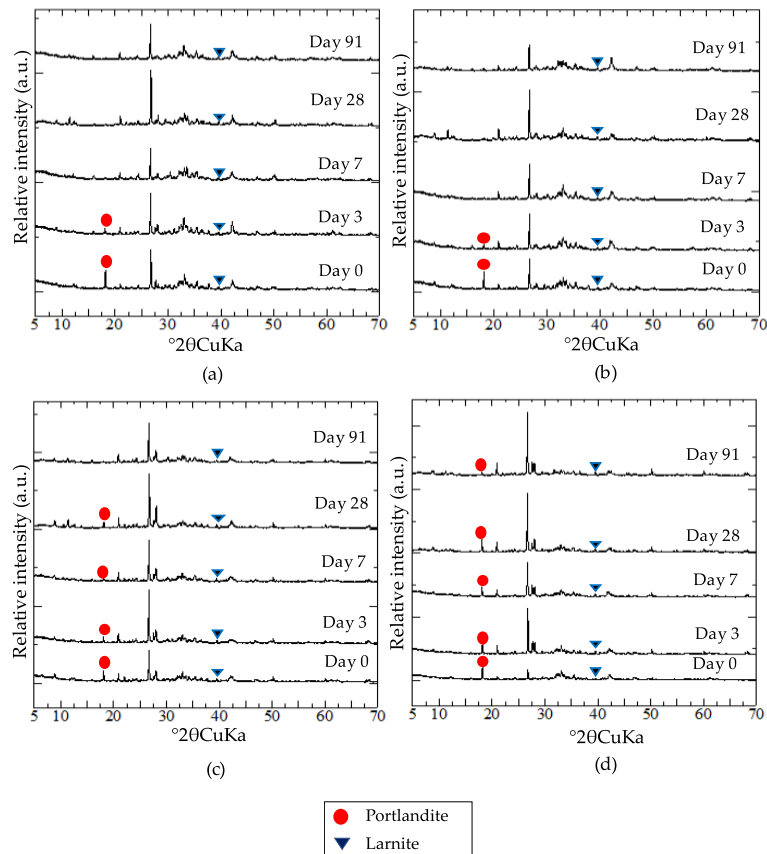
Fig. 2-8 XRD profiles of mixtures cured for 0, 3, 7, 28, and 91 days of (a) mixture 1A, (b) mixture 1B, (c) mixture 1C, and (d) mixture 1D.
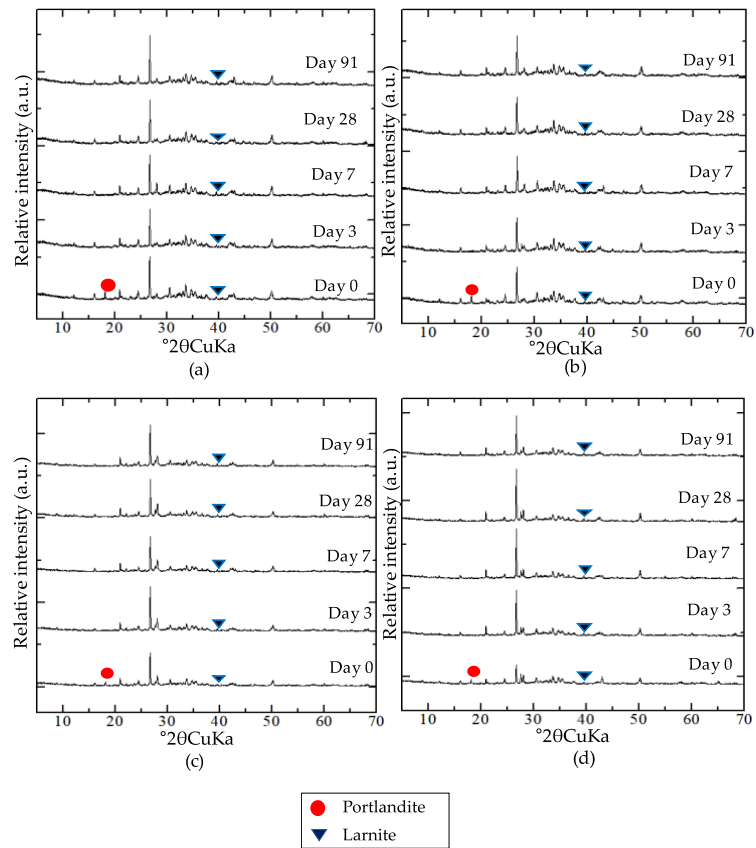
Fig. 2-9 XRD profiles of mixtures cured for 0, 3, 7, 28, and 91 days of (a) mixture 2A, (b) mixture 2B, (c) mixture 2C, and (d) mixture 2D.

Photos of the mixtures of soil 1A and 1D before curing and after 3 days of curing are shown in **Fig. 2-10**. Significant area of voids was observed in both specimens before curing. However, after 3 days, mixture 1A had fewer voids than before curing. In contrast to this, there was very little change in the void volume of mixture 1D after 3 days of curing. This suggests that the pores in mixture 1A were filled with secondary phases and caused the cementation of particles that were separate and unconnected before interaction of the steel slags dredged soils.
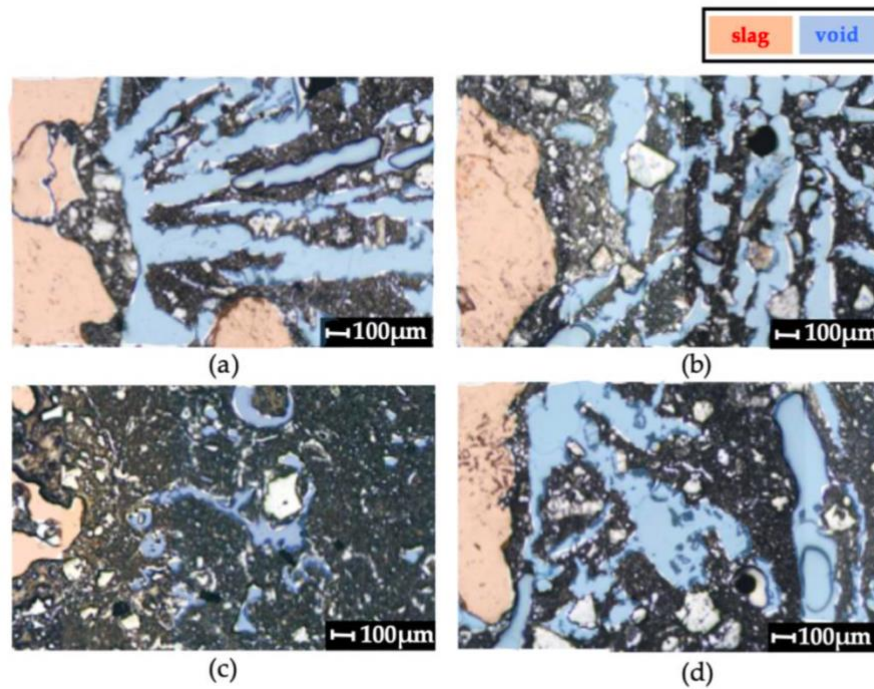
Fig. 2-10 Optical microscope observations of: (a) mixture 1A before curing, (b) mixture 1D before curing, (c) mixture 1A after 3 days of curing, and (d) mixture 1D after 3 days of curing. Areas that are shaded in orange correspond to slag particles, and the blue shaded areas corresponds to voids that were filled by epoxy resin.

From the SEM observations of the specimens after 3 days of curing, the formation of needle-like C-S-H in both mixture 1A and 1D was confirmed (**Fig. 2-11**); C-S-H is well known as the phase responsible for hardening in cementitious materials [19]. Based on the SEM observations, the C-S-H formed in mixture 1A appears denser than that in mixture 1D.
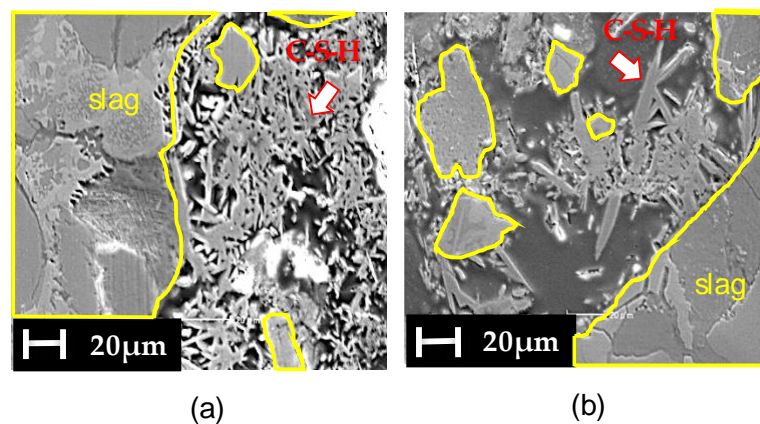
Fig. 2-11 C-S-H observed by SEM analysis of: (a) mixture 1A and (b) mixture 1D, after 3 days of curing.

2.3.3. pH and Ca concentrations of pore water in mixtures during curing

The pH of the pore water in the mixtures showed changes in the stronger mixtures, those with the higher unconfined strength, 1A and 1B, from 12 to 10. In mixtures 1C and 1D the pore water maintained pH values above 12 throughout the curing (**Fig. 2-12** (a)). Comparing the pH changes of mixtures 1A and 2A, the decrease in pH occurred earlier in 2A than in 1A. The dissolved Ca ion concentrations of the pore water obtained from mixtures 1A, 1B, 1C, and 1D after 3 days of curing, were 415 ppm, 54.5 ppm, 134 ppm, and 1140 ppm, respectively.
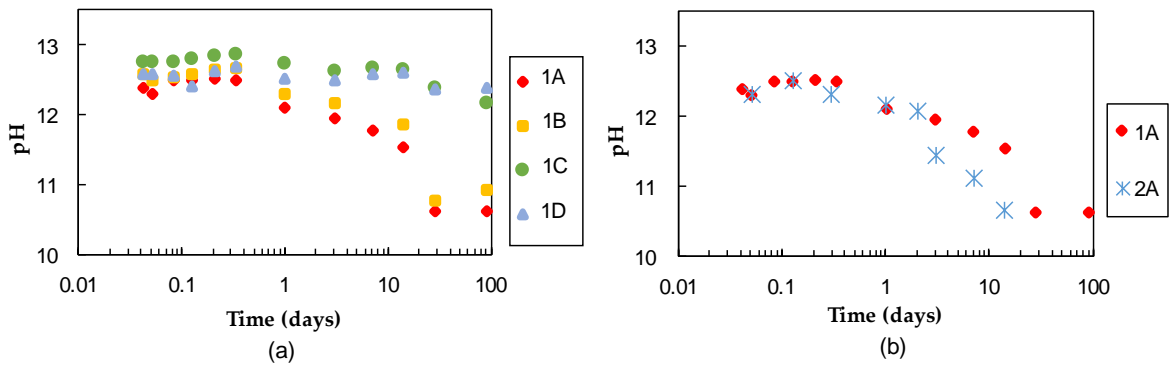
Fig. 2-12 pH changes of the pore water in (a)mixtures 1A, 1B, 1C, and 1D and (b) mixtures 1A and 2A during the curing.

2.4. Discussion

2.4.1. Possible candidates for factors affecting the formation of C-S-H

The chemical equation for C-S-H formation can be expressed as (1) [20].

$$1.6\ Ca^{2+} + 2.18H_2O + H_4SiO_{4(aq)} \rightarrow Ca_{1.6}SiO_{3.6}(OH)_{1.54}\cdot1.81H_2O_{(s)}+3.2H^+_{(aq)} \qquad (1)$$

Based on equation (1) and a previous study [10], the main factors determining the amount of C-S-H formation in steel slag-dredged soil mixtures can be considered as (a) the

supply of Ca ions, (b) pH increases that corresponds to increases in solubility of the silica-bearing phases, and (c) the supply of Si ions.

2.4.1.1. *Factor(a): Calcium ion supply*

The results of the XRD analyses of the mixtures made with slag 1 clearly show that portlandite was consumed after 7 days in only the stronger mixtures (mixture 1A and 1B; **Fig. 2-8**). This indicates that dissolved Ca ions were mainly supplied from the portlandite in the steel slags for the formation of C-S-H. Because portlandite easily reaches saturation in aqueous solutions at ambient temperatures [21], and Factor (a) here would be the limiting factor for C-S-H formation when there are limits to the portlandite quantity in the steel slags. The XRD analyses of the mixtures made with slag 2 show that the portlandite supply was much lower than in the mixtures with slag 1, indicating that the content of portlandite in the steel slags, is an important factor controlling the formation of C-S-H.

Here it is noteworthy that dredged soil D that formed the weakest mixture made with slag 1, contained the highest amount of humic acid amongst the other dredged soils used in this study. The presence of humic acid that bind with dissolved Ca ions [22], may limit the supply of Ca ions for C-S-H formation by forming insoluble compounds [23]. Ca complexing agents like humic acid may retain Ca in solution in form of complex, which cannot be filtered by 0.2µm filter, thus increasing its detected concentration in the pore water by ICP-AES. Such complexed Ca will however not be available for reactions with silica to produce C-S-H. Therefore, when Ca concentration of mixtures with different dredged soils are compared, the mixture with soil D may show the highest Ca concentration. Dissolved Ca ion concentration in the pore water of mixture D was the highest among these mixtures. This suggests that the presence of humic acids in the dredged soil may be inhibiting the supply of dissolved Ca ions to form C-S-H, at least in the mixtures studied here. Further, humic acid is known to inhibit the crystal growth of calcite by forming ligands with the surface of calcite [24] which may maintain the Ca ion concentration at high range, it is still not clarified if the same effect occurs

with C-S-H, that may inhibit C-S-H formation. Hence, the factors affecting the Ca ion supply can be assumed to be the portlandite content of steel slags, and the humic acid content may also be affecting the availability of Ca ion for C-S-H formation.

2.4.1.2. *Factor(b): pH of pore water in the mixtures*

Dissolution of portlandite in steel slags could also be responsible for factor (b), as achievement of increase in pH would cause increase in C-S-H formation due to increase in Si concentration and pH, causing C-S-H to become the phase that is thermodynamically stable. However, an additional factor is that the pH of the pore water may be buffered to values of weak bases by the humic acid as they are weak acids [15], [25]. The pH of the pore water of mixtures 1A, 1B, 1C, and 1D were maintained above 12 within the first day of curing, which can be explained by the dissolution equilibrium of portlandite, with a pH of 12.45 [18]. The effect of pH buffering by humic acid was not observed in the mixtures where pH was measured in this study. This suggests that the content of humic acids in soils A, B, C and D (0.09-0.30%) is not sufficient to act as a pH buffer.

A pH of above 12 was maintained after 91 days in the cured mixtures 1C and 1D. However, in mixtures 1A and 1B (**Fig. 2-12**), pH gradually decreased from 12.5 to 10.5. This period of decrease in pH of pore water overlaps with the period of portlandite consumption in the curing mixtures (**Fig. 2-8**). C-S-H formation is known to decrease the pH of the pore water to 10.5 [26]. This behavior of the pH here could indicate that the formation of C-S-H and consumption of portlandite are determining factors of the pH of the pore water of the mixtures.

2.4.1.3. *Factor(c): Silica supply*

Factor(c) here is likely dependent on the silica-bearing phases, originating in the dredged soils.   The kinetics of the reactive silica-bearing phases, are one of the components of the dredged soils, and may be critical for the formation of C-S-H.

The results of the XRD analysis indicate that the mineralogical compositions of soils A, B, C, and D are not significantly different (**Fig. 2-4**). The XRD results of the mixtures did not show the disappearance in the crystalline mineralogical phases including clay minerals, suggesting that they are not likely to be the source of Si ions due to their slow dissolution kinetics. Therefore, as other silica-bearing phases are suggested to be present in the dredged soils, these may be amorphous silica-bearing phases.

Amorphous silica that has a higher dissolution rate may be incorporated in the dredged soils, since they are sea sediments that could contain any particles that have settled on the sea floor. From OM observations, volcanic glass with angular plate-like shapes (**Fig. 2-6**) was a component of the dredged soils. In addition, diatom frustules with rounded, triangular, moon-like shapes (**Fig. 2-5**) were also observed in the dredged soils. Because both these components would be predominantly composed of amorphous silica, they are quite likely to be Si sources for C-S-H formation.

The amounts of diatom frustules and volcanic glass manifested by the dissolution experiment showed a strong positive correlation with the physical strength of the mixtures (**Fig. 2-2** and **Fig. 2-7**). To assess the ability of strength development of dredged soils, amorphous silica would be an important indicator for the strength development, and here the amount of amorphous silica is identified as the factor that contributes the most to the Si supply in the C-S-H formation. Further, the $H_4SiO_{4(aq)}$ concentration of pore water in the dredged soils correlate with the amorphous silica content, and this correlation could be used as a method to estimate the approximate potential for strength development namely by measuring the dissolved silica concentration of the pore water of newly sampled dredged soils (**Fig. 2-7**).

2.4.2. *Key factors for the successful iteration of the pozzolanic reaction*

Portlandite, which is the most likely phase in the steel slags that supplies Ca ions from the steel slag-dredged soil mixtures according to Kiso et al., (2008) [10] and in this study, is an important factor in the C-S-H formation (**Fig. 2-13**①). When reaching a pH of 12.45, the dissolution equilibrium with portlandite (**Fig. 2-13**②), amorphous silica in the dredged soil starts dissolving (**Fig. 2-13**③), forming C-S-H and consuming Ca and Si ions, and decreasing the pH (**Fig. 2-13**④). The decrease in the concentration of Ca ions and pH would make portlandite undersaturated in the sample, which would enable further the portlandite to dissolve, and to maintain a continuous chemical reaction to form C-S-H. A primary condition, a balance of the amount of portlandite and amorphous silica, will then be a sufficient reservoir among the components present at the start of the process, so that both components can readily be consumed to form C-S-H. This could be the condition of C-S-H formation, and the dissolution of amorphous silica could then be seen to be the rate-determining condition for the C-S-H formation. To understand the effect of the kinetics of different silica-bearing phases and the amount of amorphous silica on the formation of C-S-H, geochemical modeling of steel slag-dredged soil interactions was conducted using The Geochemist's Workbench, to understand and evaluate the quantitative effects of amorphous silica on C-S-H formation.

The Geochemist's Workbench thermodynamic database was loaded from Thermoddem provided by the French geological survey (BRGM). This database contains detailed thermodynamic properties of minerals forming at low temperatures, including hydrates like C-S-H that form in cements. The dissolution rate constants and the surface area of silica-bearing phases obtained from previous studies [27–31] were loaded in the model to understand and identify the phases responsible for the supply of dissolved Si to form C-S-H. The silica-bearing phases listed in **Table 2-2** and including portlandite were input in the model as reactants. Two models were calculated with these same reactants but with different quantities of amorphous silica. First, the system was adjusted to follow the measured pH changes in the pore water in mixtures 1A and 1B, by adding portlandite and amorphous silica with various surface areas as reactants, this is "run 1" (**Fig. 2-14**). The surface area and

dissolution rate constant of portlandite was set to fit the pH changes. Run 1 required 13 volume % of portlandite and 16 volume % of amorphous silica. For run 2, the quantity of amorphous silica was decreased to simulate the pH changes of mixtures 1C and 1D, to understand the quantitative effect of amorphous silica on the formation of C-S-H (**Fig. 2-14**).

Run 2 required a quarter amount of the amorphous silica input in run 1. Run 1 and Run 2 show that amorphous silica with the highest dissolution rate was the main phase that dissolved to supply dissolved Si ions to form C-S-H within 91 days of reaction time (**Fig. 2-15**), since it is the only phase among the silica-bearing phases that decreases in volume % as the reaction progresses.

The amount of amorphous silica that is simulated to dissolve, suggests how to determine the amount of C-S-H formation, and details the pH changes in the pore water of the mixtures.
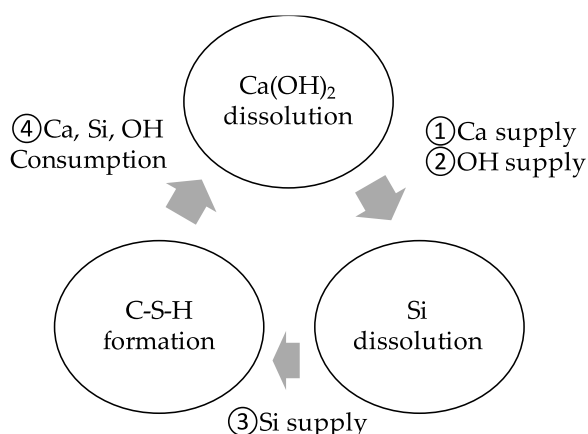
Fig. 2-13 Schematic mechanism of C-S-H formation cycle.

Table 2-2 Mineral dissolution rates and surface areas of reactants loaded in the geochemical modeling

	Mineral Dissolution Rate (mol/cm^2·s)	Surface Area (cm^2/g)	Reference	Vol %	
				Run 1	Run 2
Quartz	5.37×10^{-15}	1110	Brady and Walther (1990) [27]	10	10
Albite	4.17×10^{-15}	750	Chou and Wollast (1985) [28]	9	9
Smectite	1.97×10^{-16}	53,000	Sato et al. (2004) [29]	7	7
Kaolinite	3.31×10^{-16}	81,600	Huertas (1999) [30]	6	6
Amorphous Silica	9.40×10^{-12}	5000 (Adjusted)	Niibori et al. (2000) [31]	16	4
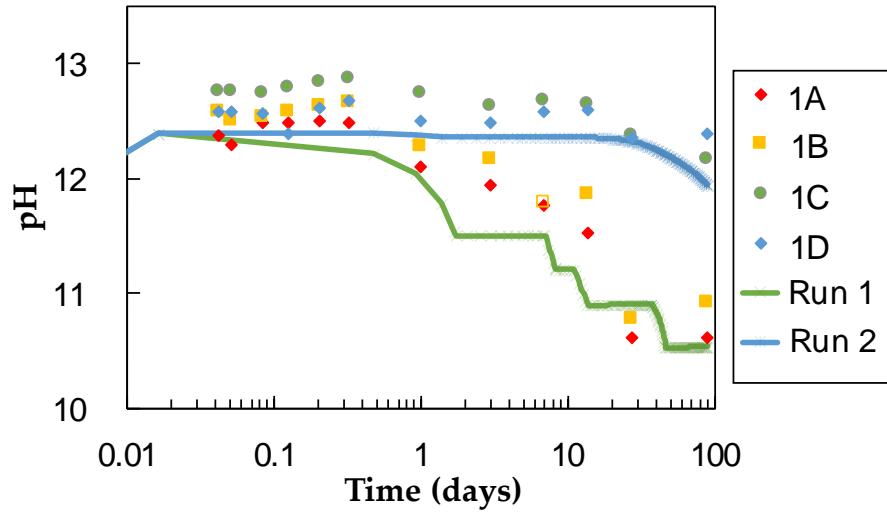
Fig. 2-14 pH changes of the pore water of the simulated mixtures, Run 1 with 16 volume % and Run 2 with 4 volume % of amorphous silica.

(a)   (b)
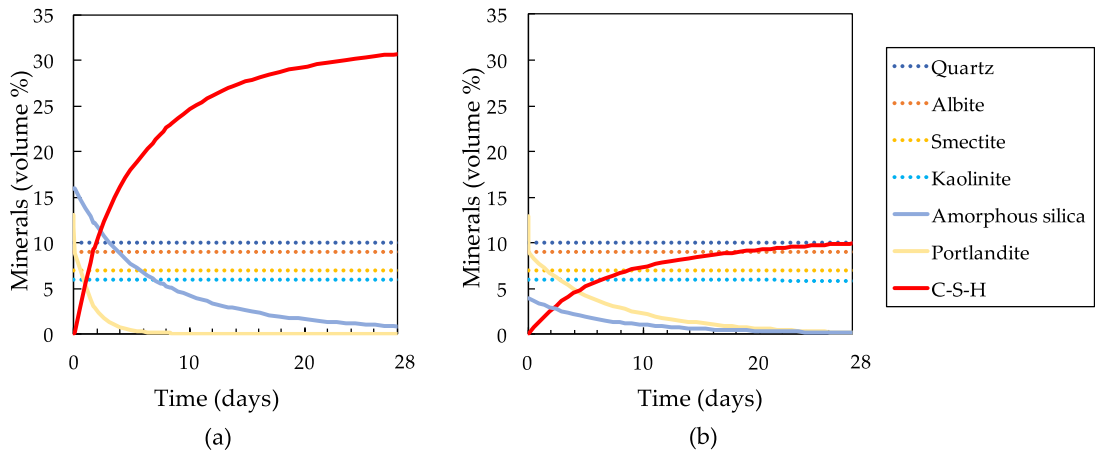
Fig. 2-15 Calculation of C-S-H formation by steel slag-dredged soil interactions in: (a) Run 1, with 16 volume % of amorphous silica as the reactant and (b) Run 2, with 4 volume % of amorphous silica as the reactant.

2.5. Conclusions

This research determined that the content of amorphous silica is one of the key factors affecting the C-S-H formation in dredged soil-steel slag mixtures.

The portlandite content in steel slags as the main factor for C-S-H formation is also suggested in the previous study [10] and was strongly supported. Here it is also possible to state that there is no effect owing to humic acid on pH buffering on the pore water of the mixtures. However, limitations of the Ca ion supply to form C-S-H or the crystal growth inhibition may arise by coexisting humic acids, indicating that these humic acids may play a role in suppressing C-S-H formation within the mixtures investigated in this study. The most significant discovery through this study is that, when focusing on controlling component in dredged soils for C-S-H formation, one of its determining factor was clarified to be the content of amorphous silica, which is the most reactive of the silica-bearing phases in dredged soils. Amorphous silica can be expected to establish an equilibrium with the dredged soils pore water as it has the highest solubility, higher than other silica-bearing phases, making it possible for the amount of amorphous silica to be estimated from the concentration of dissolved silica in the pore water of the dredged soils.

Presently, the strength development of mixtures is examined by actual destructive strength tests of the mixtures, which require laboratory work that is time consuming and labor intensive. If we apply the findings of the present research, estimates of the strength development based on the content of portlandite in steel slags and the dissolved Si concentration in dredged soil pore water would give a simple, easily attainable evaluation to determine whether newly sampled dredged soils and newly tested steel slags can be expected to develop sufficient strength for desired use.

The results of geochemical modeling that is adjusted to fit to the pH changes in the pore water of the mixtures shown here may make it possible to determine details of the starting components that contribute to the secondary phase formation, and a simulation of the

amount of its formation that would enable a precise prediction of strength development of mixtures made with wide variety of starting materials.

References

[1]   Standard specification for coal fly ash and raw or calcined natural pozzolan for use as a mineral admixture in concrete, in: Am. Soc. Test. Mater., 2008. https://doi.org/10.1520/B0783-10.2.

[2]   M. Davraz, L. Gunduz, Engineering properties of amorphous silica as a new natural pozzolan for use in concrete, Cem. Concr. Res. 35 (2005) 1251–1261. https://doi.org/10.1016/j.cemconres.2004.11.016.

[3]   T. Phoo-Ngernkham, P. Chindaprasirt, V. Sata, T. Sinsiri, High calcium fly ash geopolymer containing diatomite as additive, Indian J. Eng. Mater. Sci. 20 (2013) 310–318.

[4]   K. Horii, Overview of iron / steel slag application and development of new utilization technologies, (2015) 5–11.

[5]   S. Lirer, B. Liguori, I. Capasso, A. Flora, D. Caputo, Mechanical and chemical properties of composite materials made of dredged sediments in a fly-ash based geopolymer, J. Environ. Manage. 191 (2017) 1–7. https://doi.org/10.1016/j.jenvman.2017.01.001.

[6]   UNESCO International Sediment Initiative, Sediment issues & sediment management in large river basins interim case study synthesis report, 2011.

[7]   R. Amundson, A.A. Berhe, J.W. Hopmans, C. Olson, A.E. Sztein, D.L. Sparks, Soil and human security in the 21st century, Science. 348 (2015) 647–654. https://doi.org/10.1126/science.1261071.

[8]   H. Yi, G. Xu, H. Cheng, J. Wang, Y. Wan, H. Chen, An overview of utilization of steel slag, Procedia Environ. Sci. 16 (2012) 791–801. https://doi.org/10.1016/j.proenv.2012.10.108.

[9]   M. Miraoui, R. Zentar, N.E. Abriak, Road material basis in dredged sediment and basic oxygen furnace steel slag, Constr. Build. Mater. 30 (2012) 309–319. https://doi.org/10.1016/j.conbuildmat.2011.11.032.

[10]   E. Kiso, M. Tsujii, K. Ito, M. Nakagawa, M. Gomyo, T. Nagatome, Method of dredged soil improvement by mixing with converter steel-making slag, Proc. Civ. Eng. Ocean. 24 (2008) 327–332.

[11]   M. Kamon, S. Tomohisa, K. Sawa, On stabilization of hedoro by using cement group hardening materials, Zairyo. 432 (1989) 1092–1097.

[12]   G.-O. Kang, T. Tsuchida, Y.-S. Kim, W.-J. Baek, Influence of humic acid on the strength behavior of cement-treated clay during various curing stages, J. Mater. Civ. Eng. 29 (2017) 1–18. https://doi.org/10.1061/(ASCE)MT.1943-5533.0001919.

[13]   M. Fukushima, M. Yamamoto, T. Komai, K. Yamamoto, Studies of structural alterations of humic acids from conifer bark residue during composting by pyrolysis-gas chromatography/mass spectrometry using tetramethylammonium hydroxide (TMAH-py-GC/MS), J. Anal. Appl. Pyrolysis. 86 (2009) 200–206. https://doi.org/10.1016/j.jaap.2009.06.005.

[14]   N. Weerakoon, S. Nishimura, H. Sato, K. Toda, T. Sato, Y. Arai, Laboratory estimation of stiffness and strength mobilization in steel slag-mixed dredged clays with curing time, in: Proc. 3rd Int. Conf. Gr. Improv. Gr. Control, Hangzou, 2017: p. in print.

[15]   H. Sato, S. Nishimura, T. Sato, K. Toda, Y. Arai, Characteristics and interpretation of development of strength and stiffness for early-age Calcia-stabilized dredged soils, in: Japanese Geotech. Soc. Hokkaido Branch, 2016: pp. 4–5.

[16]   R.A. Mortlock, P.N. Froelich, A simple method for the rapid determination of biogenic opal in pelagic marine sediments, Deep Sea Res. Part A. Oceanogr. Res. Pap. 36 (1989) 1415–1426. https://doi.org/10.1016/0198-0149(89)90092-7.

[17]   H. Kodama, Identification and quantification of non-crystalline inorganic minerals in soils by selective chemical dissolution method, Chisitsu News No.496. (1995) 26–35.

[18]   J. Vlcek, V. Tomkova, H. Ovcacikova, F. Ovcacik, M. Topinkova, V. Matejka, Slags from steel production: Properties and their utilization, Metallurgy. 52 (2013) 329–333. http://hrcak.srce.hr/index.php?show=clanak&id_clanak_jezik=141044.

[19]   I.G. Richardson, Nature of C-S-H in hardened cements, Cem. Concr. Res. 29 (1999) 1131–1147. https://doi.org/10.1016/S0008-8846(99)00168-4.

[20]   P. Blanc, X. Bourbon, A. Lassin, E.C. Gaucher, Chemical model for cement-based materials: Temperature dependence of thermodynamic functions for nanocrystalline and crystalline C–S–H phases, Cem. Concr. Res. 40 (2010) 851–866. https://doi.org/10.1016/j.cemconres.2009.12.004.

[21]   R.G. Bates, V.E. Bower, E.R. Smith, Calcium hydroxide as a highly alkaline pH standard, J. Res. Natl. Bur. Stand. (1934). 56 (1956) 305–312. https://doi.org/10.6028/jres.056.040.

[22]   E. Tipping, M.A. Hurley, A unifying model of cation binding by humic substances, Geochim. Cosmochim. Acta. 56 (1992) 3627–3641. https://doi.org/10.1016/0016-7037(92)90158-F.

[23]   W. Zhu, C.F. Chiu, C.-L. Zhang, K.-L. Zeng, Effect of humic acid on the behaviour of solidified dredged material, Can. Geotech. J. 46 (2009) 1093–1099. https://doi.org/10.1139/T09-045.

[24]   A.R. Hoch, M.M. Reddy, G.R. Aiken, Calcite crystal growth inhibition by humic substances with emphasis on hydrophobic acids from the Florida Everglades, Geochim. Cosmochim. Acta. 64 (2000) 61–72. https://doi.org/10.1016/S0016-7037(99)00179-9.

[25]   H. Tremblay, J. Duchesne, J. Locat, S. Leroueil, Influence of the nature of organic compounds on fine soil stabilization with cement, Can. Geotech. J. 39 (2002) 535–546. https://doi.org/10.1139/t02-002.

[26]   A. Atkinson, N. Everitt, R. Guppy, Evolution of pH in a radwaste repository: internal reactions between concrete constituents, Harwell, U.K. 20 (1988).

[27]   P.V. Brady, J.. V. Walther, Kinetics of quartz dissolution at low temperatures, Chem. Geol. 82 (1990) 253–264.

[28]   L. Chou, R. Wollast, Steady-state kinetics and dissolution mechanisms of albite., Am. J. Sci. 285 (1985) 963–993. https://doi.org/10.2475/ajs.285.10.963.

[29]   T. Sato, K. Masato, Y. Shingo, M. Tsutsui, K. Fukushi, T. Tanaka, S. Nakayama, Dissolution mechanism and kinetics of smectite under alkaline condition, in: Proc. Int. Work. Bentonite-Cement Interact. Repos. Environ., 2004: pp. A3-38 to A3-41.

[30]   F.J. Huertas, L. Chou, R. Wollast, Mechanism of kaolinite dissolution at room temperature and pressure Part II: Kinetic study, Geochim. Cosmochim. Acta. 63 (1999) 3261–3275. https://doi.org/10.1016/S0016-7037(99)00249-5.

[31]   Y. Niibori, M. Kunita, O. Tochiyama, T. Chida, Dissolution rates of amorphous silica in highly alkaline solution, J. Nucl. Sci. Technol. 37 (2000) 349–357. https://doi.org/10.1080/18811248.2000.9714905.

3. Characteristics of soil organic matters in dredged soils which form soft mixtures

Abstract

Dredged soils have been used as construction materials by alkaline activation with steel slag (steel slag-dredged soil mixtures) at harbors. Such mixtures develop strength chiefly by calcium silicate hydrate (C-S-H) formation by the pozzolanic reaction. However, the strength of such mixtures is unpredictable, and in some cases, mixtures have been too soft for the intended engineering application. An identification of strength development indicators would accelerate evaluation processes for strength development to facilitate and promote the utilization of such materials. This paper focuses on the relationship between the characteristics of soil organic matters in dredged soils and the strength development of the mixtures by a comparison of eight dredged soils collected from eight different Japanese harbors. The characteristics of the soil organic matters were identified to determine as indicators of mixtures with weak strength development, i.e., enriched sulfur content in extracted soil organic matter (humic acid) fraction, and the N/C ratio of humic acid similar to land humic acid standards. Increases in the validated fraction of dredged soils and steel slag by replacing fractions disadvantageous to construction resources would contribute to reduce waste production, which would lower the environmental impact of the use, aiming to achieve sustainable utilization of such materials.

3.1. Introduction

Chapter 2 investigated four dredged soils obtained from different Japanese harbors and their mixtures with two steel slags [1,2]. These studies showed that the inorganic amorphous silica content of dredged soils, comprising diatom frustules and volcanic glasses, is a key factor affecting the extent of silica supply to form C-S-H. Furthermore, as discussed in Kiso et al. [3], portlandite content in steel slag is confirmed as another key factor, which is a major supplier of dissolved calcium and achieves alkaline conditions, which enables the dissolution of silicate phases and the precipitation of C-S-H.

However, some mixtures made with the dredged soils and steel slag with sufficient amorphous silica and portlandite showed no strength development in unconfined compressive strength tests. This potentially indicated the existence of other factors that affect the strength development of these mixtures. Some organic matter including humic acid, an extractable fraction of soil organic matters, are known to inhibit the strength development of cementitious materials [4,5]. Toda et al. [1] have shown that the strength of the mixtures was not determined by the bulk content of humic acids. Furthermore, that quantification of humic acids may not indicate the effect of soil organic matters on the strength of the mixtures. Since soil organic matter has an indefinite macromolecular structure with variety in elemental compositions and functional groups [6–9], specific components in the soil organic matters could affect the strength of the mixtures that was not quantified by the evaluation of bulk humic acid content. In addition, in the previous studies, the effects of specific components of soil organic matters on the strength development of the mixtures are not comprehensively understood.

The objective of this study is to determine whether particulars such as the elemental composition of humic acid in dredged soils can be used as a parameter that indicates dredged soils that form soft mixtures after mixing with a steel slag, in addition to known factors that work as indicators such as amorphous silica and portlandite content in dredged soils and steel slag, respectively. In addition, the results of this study could underpin

whether soil organic matters in dredged soils does or does not affect the strength development of the mixtures. Tests of unconfined compressive strength of the mixtures made with eight dredged soils collected from eight different Japanese harbors and a steel slag are carried out with characterization of the humic acids of the dredged soils to compare the characteristics of hard and soft mixtures. The characterization of mineralogical phase compositions and solution compositions of the mixtures are carried out to address the possibility of how soil organic matters may affect the strength development of the mixtures.

3.2. Materials and methods

3.2.1. Materials

3.2.1.1. Dredged soils

Eight dredged soil samples from different Japanese harbors were studied. Four dredged soil samples named soils A, B, C, and D also employed in Toda et al. [1] were used for further study of their soil organic matters. Four other dredged soil samples named soils E, F, G, and H were newly collected from different Japanese harbors for this study. The characterization of soils A, B, C, and D and analyses of their mixtures with steel slag were carried out in Toda et al. [1]. The results of characterization of soils A, B, C, and D and analyses of their mixtures was also reported in Toda et al. [1]. The characterization of soils E, F, G, and H and subsequent formation of mixtures followed the methodology of Toda et al. [1] to compare the characteristics of eight soil organic matters and strength development of the eight mixtures.

The physical properties of the dredged soils are summarized in **Table 3-1**. The soil particle density, liquid limit, and the content of fine particles were obtained following Japanese Industrial Standards A 1202, A 1205, and A 1204, respectively. The accuracy of soil particle density and liquid limit measurements were all in the range of ±0.01 g/cm^3 and ±0.1%. The content of fine particles was obtained using sufficient amounts of sample, and

the data accuracy typically is in the range of ±5%. All dredged soils were clay and silt rich, with common soil particle densities of soils (2.55 to 2.75 g/cm^3) except soil G, which was slightly less dense than the other soils likely caused by soil organic matters [10].

Liquid limits of the dredged soils A, B, C, and D were 73.4, 89.8, 44.1, and 66.2% [1], respectively. Liquid limits of the dredged soil E, F, G, and H were 80.0, 54.5, 96.1, and 66.1%, respectively, which the liquid limit was used to adjust the water content of the dredged soils prior to mixing with steel slag.

Table 3-1 Physical properties of dredged soils.

Samples	Soil Particle Density (g/cm^3)	Liquid Limit	Content of Fine Particle (<0.075 mm) (%)
Soil A [1]	2.777	73.4	83.2
Soil B [1]	2.737	89.8	99.3
Soil C [1]	2.709	44.1	91.1
Soil D [1]	2.707	66.2	58.6
Soil E	2.721	80.0	75.5
Soil F	2.655	54.5	86.3
Soil G	2.544	96.1	99.3
Soil H	2.629	66.1	63.5

[1] From Toda et al. [1].

The characterization of soils E, F, G, and H followed the methodology described in Toda et al. [1]. The bulk mineralogy and clay mineralogy of the dredged soils were characterized with powdered samples pulverized to finer than 53 μm in diameter and oriented samples of particles below 2 μm in diameter prepared by elutriation by X-ray diffraction analysis (XRD; RINT2100, Rigaku, Tokyo, Japan). Inorganic amorphous silica contents were quantified by selective dissolution methods, where diatom frustules were dissolved by heating 50 mg of dried soil per 40 mL of 2M Na_2CO_3 at 85 °C for 5 hours [11] and volcanic glass were dissolved by heating 50 mg of dried soil per 50 mL of 0.5 M NaOH at 100 °C for 2.5 minutes [12]. Dissolution experiments were repeated three times to calculate the average and standard errors of the results. Subsequently, the silica concentration of supernatants was measured by inductively coupled plasma-atomic emission spectroscopy (ICP-AES; ICPE-9000, Shimadzu, Kyoto, Japan) to quantify

inorganic amorphous silica contents in the dredged soils. The bulk and clay mineralogy of soils E, F, G, and H (**Fig. 3-1**) were virtually identical, and they were also very similar to soils A, B, C, and D [1] (**Fig. 3-2**), containing quartz, cristobalite, albite, pyrite, kaolinite, illite, chlorite, and smectite. The total inorganic amorphous silica contents of soils E, F, G, and H, which were calculated as the sum of quantified diatom frustules and volcanic glass, were 79.6 ± 4.2, 64.3 ± 1.7, 90.0 ± 2.2, and 75.3 ± 3.1 mg/g respectively, while the inorganic amorphous silica content of soils A, B, C, and D reported in Toda et al. [1] were 78.2 ± 5.9, 71.4 ± 2.8, 44.4 ± 3.4, and 38.2 ± 1.5 mg/g, respectively.

(a)

(b)
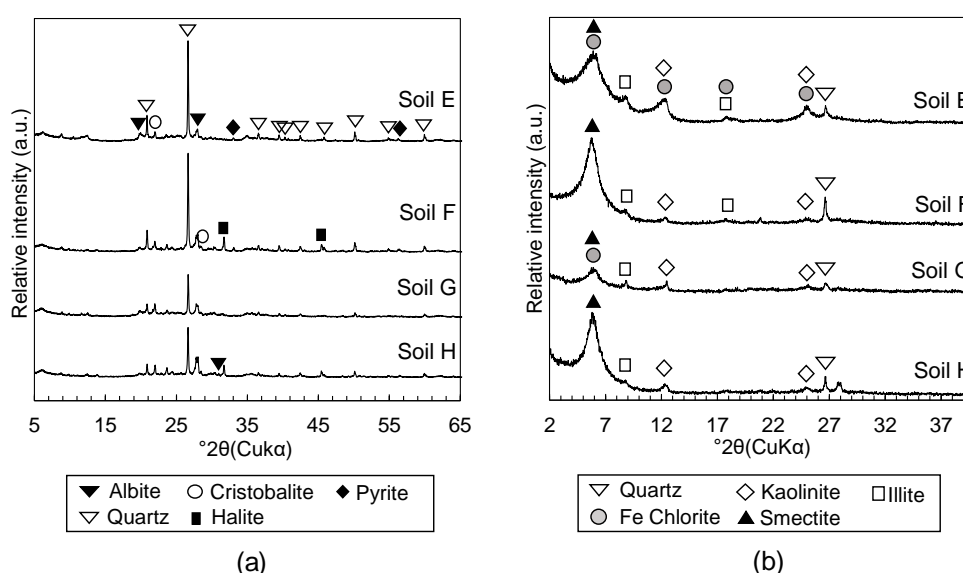
Fig. 3-1 X-ray diffraction (XRD) patterns of (a) powdered dredged soil to detect bulk mineralogical phases and (b) oriented particles of dredged soils to detect clay mineralogical phases. Names of dredged soil samples are labeled on the upper right of each XRD pattern.
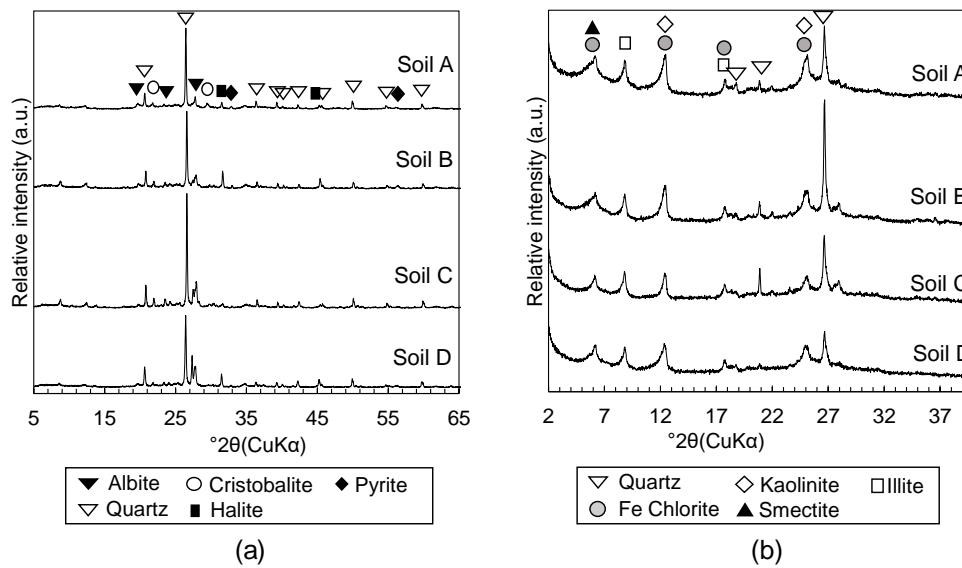
Fig. 3-2 XRD patterns of (a) powdered dredged soil to detect bulk mineralogical phases and (b) oriented particles of dredged soils to detect clay mineralogical phases. Names of dredged soil samples are labeled on the upper right of each XRD pattern. From Toda et al. [1].

3.2.1.2. Steel slag

Steel slag 1, employed in Toda et al. [1], was used to form the steel slag-dredged soil mixtures in this study. Its mineralogical composition was confirmed to be similar to those of ordinary steel slag, containing larnite, brownmillerite, RO phase, calcite, and portlandite with other oxide phases, based on the XRD analysis (Multiflex Diffractometer, Rigaku, Tokyo, Japan) of powdered samples pulverized to finer than 53 μm in diameter [1] (**Fig. 3-3**).
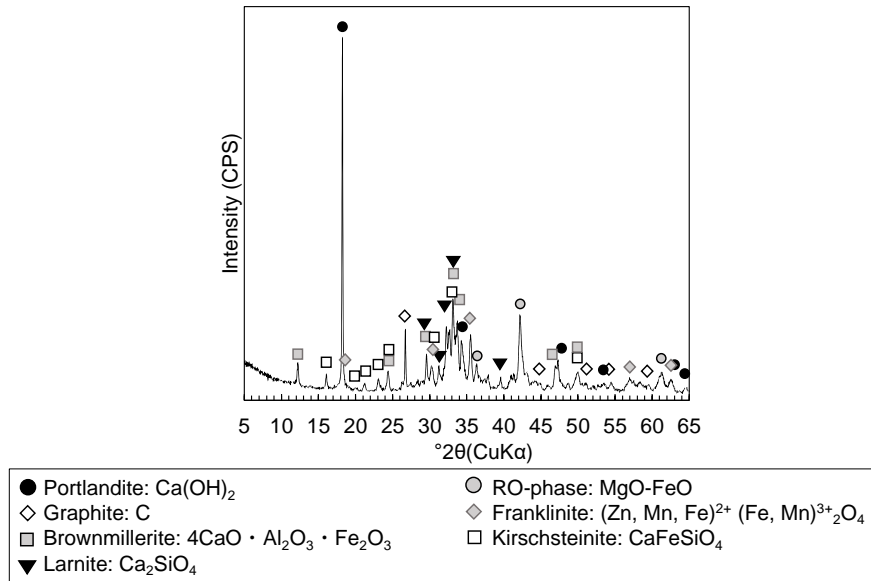
Fig. 3-3 XRD pattern of powdered steel slag 1 showing mineralogical
phases. From Toda et al. [1].

3.2.2. Methods

A schematic diagram of the experimental methodology is shown in **Fig. 3-4**. The
framed words are the samples, and below the frames are the measurements conducted for
each state of samples. Procedures for sample preparations are described between the
connecting lines of the frames. Numbers in brackets refer to subsections of methods that
describe each methodology.
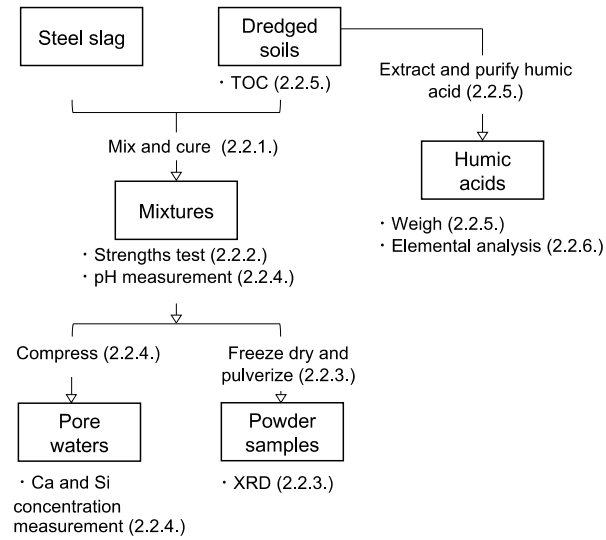
Fig. 3-4 Diagram of experimental procedures.

3.2.2.1. *Preparation of steel slag-dredged soil mixtures*

The steel slag-dredged soil mixture specimens were prepared with steel slag 1 and soils E, F, G, and H by the method described in Toda et al. [1]. The mixtures of steel slag 1 and soils E, F, G, and H were termed mixtures 1E, 1F, 1G, and 1H, respectively. They were prepared by mixing steel slag into dredged soil in the volume ratio 3:7. Air-dried steel slag was used to make the mixtures. The water content of the dredged soils was conditioned to 1.5 times the liquid limit using artificial sea water to equalize the physical properties before mixing. The mixing was performed by an electronic mixer for 5 minutes; then, the mixture was packed into cylindrical plastic molds, of height of 100 mm and diameter of 50 mm, and covered with plastic film. Then, it was cured to conduct the subsequent tests of unconfined compressive strength. The mixtures were cured in a sealed plastic container in saturated humidity at 25 °C for the duration of the tests to eliminate reduction in the water content.

3.2.2.2. *Unconfined Compressive Strength Tests*

The unconfined compressive strength (q_u) was measured for mixtures 1E, 1F, 1G, and 1H cured for 3, 7, 14, and 28 days after demolding from the cylindrical plastic molds. The unconfined compressive strength tests were performed in triplicate for each condition and the average values and standard errors were calculated. The q_u values of mixtures made with steel slag 1 and soils A, B, C, and D were cured for 3, 7, 14, and 28 days were from Toda et al. [1]; these mixtures were termed 1A, 1B, 1C and 1D, respectively.

3.2.2.3. *Mineralogical phases assemblage*

The XRD analysis (Multiflex Diffractometer, Rigaku, Tokyo, Japan) of mixtures 1E, 1F, 1G, and 1H for 1, 3, 7, and 28 days of curing were carried out with powdered samples. About 5 g of freeze-dried mixture was used for preparing powdered sample to reduce the effect of heterogeneity in the mixtures on the evaluation of the mineralogical compositions. Samples were pulverized to the grain size below 53 μm. The XRD patterns of mixtures 1A, 1B, 1C, and 1D for 0, 3, 7, and 28 days of curing were from Toda et al. [1]. The peak assignment was selectively carried out for phases that play a role in the pozzolanic reaction.

3.2.2.4. *Chemistry of the pore waters*

The pH of the pore water in mixtures 1E, 1F, 1G, and 1H cured from 1 to 28 days were measured directly from the mixtures using a pH meter employing a pH probe (1053B, Hanna Instruments, Woonsocket, RI, USA) with an electrode for semi-solids and soils. The pH measurements were performed three times, and average values and standard errors were calculated. The calcium and silica concentrations of the pore waters of the 1E, 1F, 1G, and 1H mixtures cured from 1 to 28 days and mixtures 1A, 1B, 1C, and 1D cured from 1 to 7 days were measured with pore waters collected by compressing one entire cylinder of the mixture specimens prepared by the plastic mold used for the unconfined compressive strength tests. One pore water sample was prepared for each condition, due

to limitations in the amount of mixture sample. The collected pore waters were filtered by 0.2 μm membrane filters; then, calcium and silica concentrations were measured using inductively coupled plasma-atomic emission spectroscopy (ICP-AES; ICPE-9000, Shimadzu, Kyoto, Japan). The pH data of mixtures 1A, 1B, 1C, and 1D and calcium concentration data of mixtures 1A, 1B, 1C, and 1D from the 3-day cured samples were measured in Toda et al. [1] by the same method, which is shown in this study.

3.2.2.5. Quantification of soil organic matter and humic acids in the dredged soils

The total organic carbon (TOC) content in the dredged soils A, B, C, D, E, F, G, and H were measured in a TOC analyzer (TOC-L, Shimadzu, Kyoto, Japan) with 0.4 to 0.5 g of freeze-dried soils. The TOC content was calculated by subtracting the total inorganic carbon (TIC) content from the total carbon (TC) content. The measurements of TIC and TC were conducted twice, and average values and standard errors were calculated.

The humic acids of soils E, F, G, and H were extracted from the dredged soils to quantify the humic acid content following the methodology in Fukushima et al. [13,14], which was the same to the humic acid extraction from soils A, B, C, and D in Toda et al. [1]. The humic acid extraction was not repeated, assuming the dredged soils to contain humic acid homogenously from the result of TOC measurement repetition. A schematic diagram of the humic acid extraction and purification method is shown on **Fig. 3-5**. A 10 g of freeze-dried dredged soil and 100 mL of aqueous alkaline solution (1.0 M NaOH and 0.1 M $Na_4P_2O_7$ mixed in volume ratio 1:1) were mixed and shaken under an N_2 atmosphere for 24 hours to solubilize soil organic matter. The condition of the extraction procedure is known to affect the recovery ratio of humic acids, and it must be kept the same between each soil samples to make comparisons of their humic acid content. Solubilized soil organic matter was collected after centrifugation of the mixture at 10,000 rpm for 15 minutes, and the supernatant was filtered using an A5 filter. Then, the filtrate was acidified to pH 1 by

concentrated HCl (approximately 1 mL), which was stirred for 24 hours. Then, the resulting precipitate was collected by centrifugation at 10,000 rpm for 15 minutes and filtration with a 0.20 μm filter. The precipitate was the soil organic matter that classifies to humic acid. Then, the purification of humic acid was carried out to remove coexistent inorganic phases. The re-dissolution of humic acid in 100 mL of aqueous 0.1 M NaOH was followed by the addition of concentrated HCl (1 mL) and HF (3 mL) to re-precipitate the humic acid. The slurry was stirred for 24 hours and then centrifuged at 10,000 rpm for 15 minutes to collect the precipitate. Subsequently, the precipitate was dialyzed to remove coexisting ions such as Na. The precipitate was transferred to a dialysis tube (SpectraPore, nominal molecular weight cut-off of 1 kDa) and dialyzed against water for two weeks. The dialyzed slurry was freeze-dried in order to obtain a powder sample, which was weighed to quantify the humic acid content in the dredged soils. The weighing accuracy of the precision balance was ±0.0001 g, which gave the error range of ±0.001% in the calculation of humic acid content in the dredged soils.

The difference in TOC and humic acid content of common land soils and dredged soil samples could depict the characteristics of dredged soil samples. Hence, the TOC and humic acid content of standard land soils of the Japan Humic Substance Society (JHSS), Inogashira (Andosols) and Dando (Brown Forest Soils) soils, which are the two soil types that cover 61% of Japanese land [15], were used for the comparison of the soil organic matter contents [16].
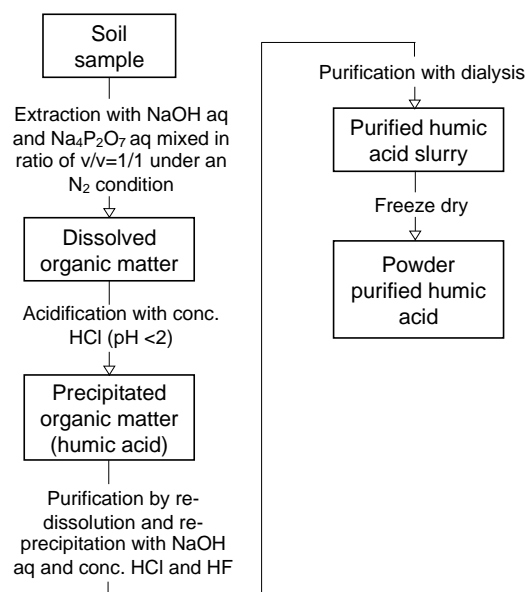
Fig. 3-5 Diagram of humic acid extraction and purification procedures from the dredged soils.

3.2.2.6.   Elemental compositions of humic acids

Analyses of C, H, N, and S contents of purified humic acid powder of soils A, B, C, D, E, F, G, and H were carried out at the Center for Instrumental Analysis at Hokkaido University. Prior to the analyses, the powdered humic acids were dehydrated under reduced pressure for at least 24 hours. The C, H, and N contents were measured by an elemental analyzer (CE440, Exeter Analyzer, Warwickshire, UK). About 2 mg of sample was used for the measurement and WO_3 was added as a combustion aid for the C, H, and N analysis. The maximum permissive error of measurement of C, H, and N contents was ±0.3%. The S contents were measured by an ion chromatography (Dionex ICS-1600, Thermo Fischer Scientific, Waltham, MA, US). About 2 mg of sample was used for a measurement. The maximum permissive error of measurement of S content was ±0.3%. The content of oxygen was calculated by subtracting the sum of the quantified percentage of C, H, N, and S from 100%. The elemental compositions of JHSS standards [17], Dando,

and Inogashira humic acids were referred in the results to make a comparison between humic acids of common land soils and dredged soil samples.

3.3. Results

3.3.1. *Characterization of the mixtures*

3.3.1.1. *Unconfined compressive strength*

The average q_u values of the mixtures is shown in **Fig. 3-6**. Error bars are omitted, as they typically fell within the range of the plot size, and they do not affect the interpretation on coordinates of the plots on the figure. Mixtures 1D and 1H did not develop sufficient strength to undergo unconfined compressive strength tests and the plots are not presented in **Fig. 3-6**. The q_u value of mixture 1G was low throughout the 28 days of the curing period (18 to 28 kPa). Mixtures 1D, 1H, and 1F were classified as soft mixtures, which did not qualify for use as construction works with lower strength than the target strength of 250 kPa at 28 days of curing, calculated from required strength of 100 kPa with safety factor [18]. Mixtures 1A, 1B, 1C, 1E, and 1F with q_u values above 250 kPa at 28 days of curing were classified as hard mixtures, making them acceptable for use in construction work. Mixtures 1A, 1B, 1C, 1E, and 1F developed strength (increases in q_u value) during the curing period; mixture 1A showed the highest strength at 28 days of curing, followed by mixtures 1B, 1E, 1F, and 1C.
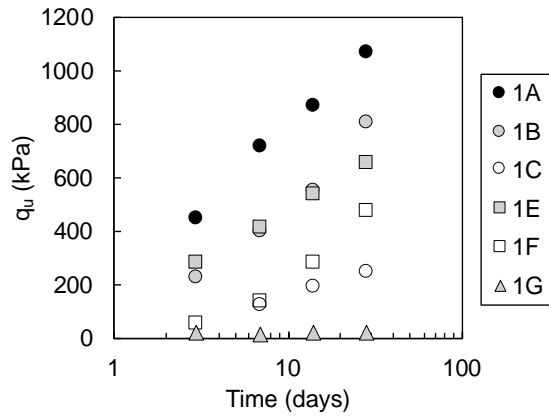
Fig. 3-6 Unconfined compressive strength (q$_u$) values of mixtures 1A, 1B, 1C, 1E, 1F, and 1G with curing time (data for mixtures 1A, 1B, and 1C are from Toda et al. [1]).

3.3.1.2. *Mineralogical phase assemblages*

The XRD patterns of mixtures 1A, 1B, 1C, 1D, 1E, 1F, 1G, and 1H are shown in **Fig. 3-7**. The XRD patterns of mixtures 1A, 1B, 1C, and 1D are from Toda et al. [1]. The consumption of portlandite was the major change in the mineralogical phase assemblage in some mixtures as a function of curing time. Mixture 1E showed the consumption of portlandite after 7 days of curing with disappearance of the peak intensity corresponding to portlandite (**Fig. 3-7**e). This tendency of the portlandite peak disappearance in mixtures exhibiting a q$_u$ value above 600 kPa at 28 days of curing were also observed in mixtures 1A and 1B (**Fig. 3-7**a,b). In mixtures 1F, 1G, and 1H, the portlandite still remained after 28 days of curing (**Fig. 3-7**f,g,h) as did mixtures 1C and 1D (**Fig. 3-7**c,d). Amorphous silica and C-S-H were not detected with XRD, due to their amorphous and poorly crystalline characteristics [19,20].
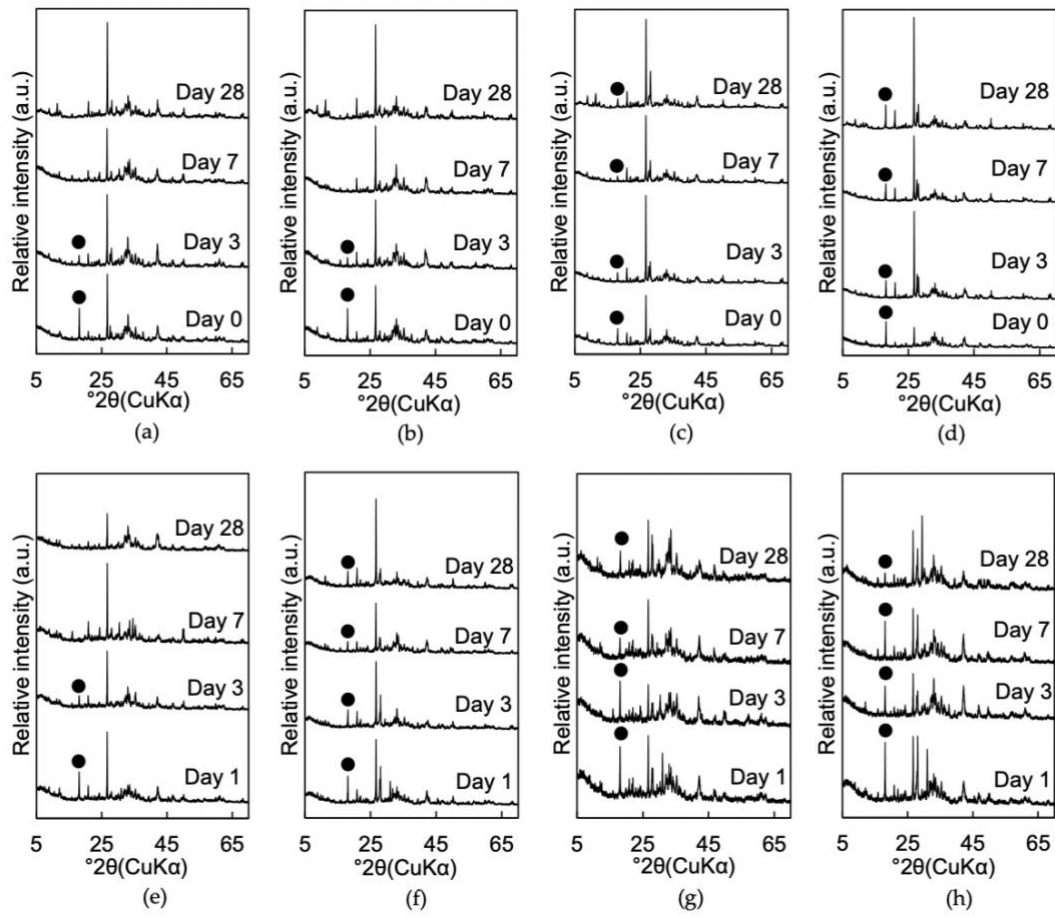
Fig. 3-7 XRD patterns of (a) mixtures 1A, (b) 1B, (c) 1C, (d) 1D, (e) 1E, (f) 1F, (g) 1G, and (h) 1H cured for 1, 3, 7, and 28 days. XRD patterns (a–d) are from Toda et al. [1]. Black dot (●): Portlandite (Ca(OH)$_2$).

3.3.1.3. Solution chemistry of pore water

Fig. 3-8 shows the solution chemistry of the pore water collected from the mixtures. Standard errors of pH, Ca, and Si measurements were mostly smaller than the size of the plots in the figures. In addition to data collected in this study, pH data of mixtures 1A, 1B, 1C, and 1D and calcium concentration data of mixtures 1A, 1B, 1C, and 1D at 3 days of curing time are cited from Toda et al. [1] and plotted in **Fig. 3-8**a,b, respectively. The pH of pore water of mixtures 1E and 1F decreased from the order of 12 to lower pH values throughout the 28 days of curing, which was similar to mixtures 1A and 1B (**Fig. 3-8**a). Mixtures 1G and 1H maintained pH around 12, which was similarly observed in mixtures

1C and 1D. The calcium concentration of mixtures 1D and 1H were around 30 mmol/L at least until 7 days of curing (**Fig. 3-8**b). The calcium concentration of the pore water of mixtures 1A, 1B, 1E, 1F, and 1G gradually decreased from over 15 to below 10 mmol/L with curing time. Calcium concentrations of pore water of mixture 1C between 1 and 7 days of curing were maintained at around 5 mmol/L. Silica concentrations of pore waters of all mixtures were between 0.07 and 0.38 mmol/L during 28 days of curing (**Fig. 3-8**c).
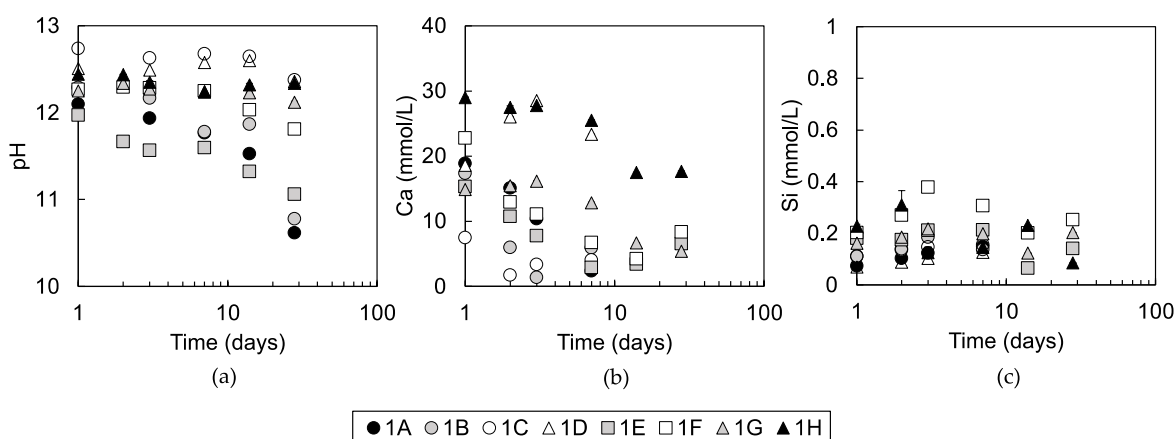
●1A ○1B ○1C △1D ■1E □1F △1G ▲1H

Fig. 3-8 (a) pH of pore waters of mixtures 1A, 1B, 1C, 1D, 1E, 1F, 1G, and 1H at 1 to 28 days of curing, (b) calcium concentrations, and (c) silica concentrations of the pore waters of mixtures 1A, 1B, 1C, and 1D of 1 to 7 days of curing and of mixtures 1E, 1F, 1G, and 1H of 1 to 28 days of curing are plotted as a function of curing time. Standard errors of the measurements are plotted on the figures.

3.3.1.4. Characterization of soil organic matter in dredged soils

The TOC and humic acid content of the dredged soils and JHSS standard soils are shown in **Table 3-2** with elemental compositions of the corresponding humic acids. The TOC contents of the dredged soil samples were lower than Inogashira and Dando soils. The humic acid contents in the dredged soils were lower than those in the JHSS standards, except for soil G. The TOC and humic acid contents of soils A, B, C, D, E, F, G, and H varied from 0.60 ± 0.01% to 3.86 ± 0.01% and 0.09% to 0.93%, respectively. Soil G had higher TOC and humic acid content than that of the other dredged soils, as could be

expected from it having the lightest soil particle density among the dredged soils (**Table 3-1**).

Table 3-2 Total organic carbon (TOC), humic acid content and humic acid elemental compositions of soils A, B, C, D, E, F, G, and H. The values of Inogashira and Dando soils, Japan Humic Substance Society (JHSS) standards, are also listed for comparison.

Samples	TOC	Humic Acid Content	Humic Acid Elemental Composition (wt.%) [1]				
	(wt. %)	(wt. %)	C	H	N	S	O [3]
Soil A	0.60 ± 0.01	0.09 [2]	45.55	3.61	2.39	3.14	45.31
Soil B	1.20 ± 0.01	0.20 [2]	47.26	4.22	2.73	2.72	43.07
Soil C	1.97 ± 0.01	0.14 [2]	52.03	4.46	2.53	2.20	38.78
Soil D	1.21 ± 0.10	0.30 [2]	41.12	3.57	3.25	7.23	44.83
Soil E	0.68 ± 0.01	0.16	43.33	3.15	2.13	1.14	50.25
Soil F	1.46 ± 0.04	0.24	46.17	3.92	2.86	0.99	46.06
Soil G	3.86 ± 0.01	0.93	51.76	4.12	3.93	1.62	38.57
Soil H	1.50 ± 0.08	0.24	47.88	4.70	3.92	7.04	36.46
Inogashira [4]	16.7	5.10	54.83	4.27	4.01	0.26	36.63
Dando [4]	6.19	0.69	53.04	5.25	4.49	0.29	36.93

[1] Maximum permissive error of elemental analysis was ±0.3%. [2] From Toda et al. [1]. [3] Calculated by subtraction from 100%. [4] TOC and humic acid content from Kuwatsuka et al. [16] and elemental composition from Watanabe et al. [17].

Humic acids in the dredged soils were mostly nitrogen-poor and sulfur-rich in comparison with the humic acids of JHSS standards. Inogashira humic acid contained 4.01% of nitrogen and 0.26% of sulfur, while Dando humic acid contained 4.49% of nitrogen and 0.29% of sulfur. Among humic acids of dredged soils, humic acids of soils D and H, with 7.23% and 7.04% of sulfur, respectively, contained much more sulfur than the other humic acids. Humic acids of soils D, G, and H were not as poor in nitrogen content as other humic acids of dredged soils in comparison with JHSS standards; they contained 3.25%, 3.93%, and 3.92% of nitrogen, respectively.

3.4. Discussion

3.4.1. *Indicators for strength development of the steel slag-dredged soil mixtures*

Inorganic amorphous silica content in the dredged soils and portlandite content in steel slag have been pointed out as important factors for the strength development of steel slag-dredged soil mixtures [1]. Amorphous silica supplies dissolved silica and portlandite supplies dissolved calcium and establish alkaline condition for C-S-H formation via the pozzolanic reaction. The amorphous silica content of dredged soils was linearly correlated to q_u values of the mixtures, i.e., at 28 days of curing, except in soils G and H (**Fig. 3-9**a). Soils G and H were two of the dredged soils classified as resulting in soft mixtures, with remaining portlandite after curing (**Fig. 3-7**g,h), regardless of the similar content of amorphous silica to the soils, which formed hard mixtures (**Fig. 3-9**a) with portlandite consumption (soils A, B, and E) (**Fig. 3-7**a,b,e). This suggests that soils G and H contain components that may inhibit the pozzolanic reaction.
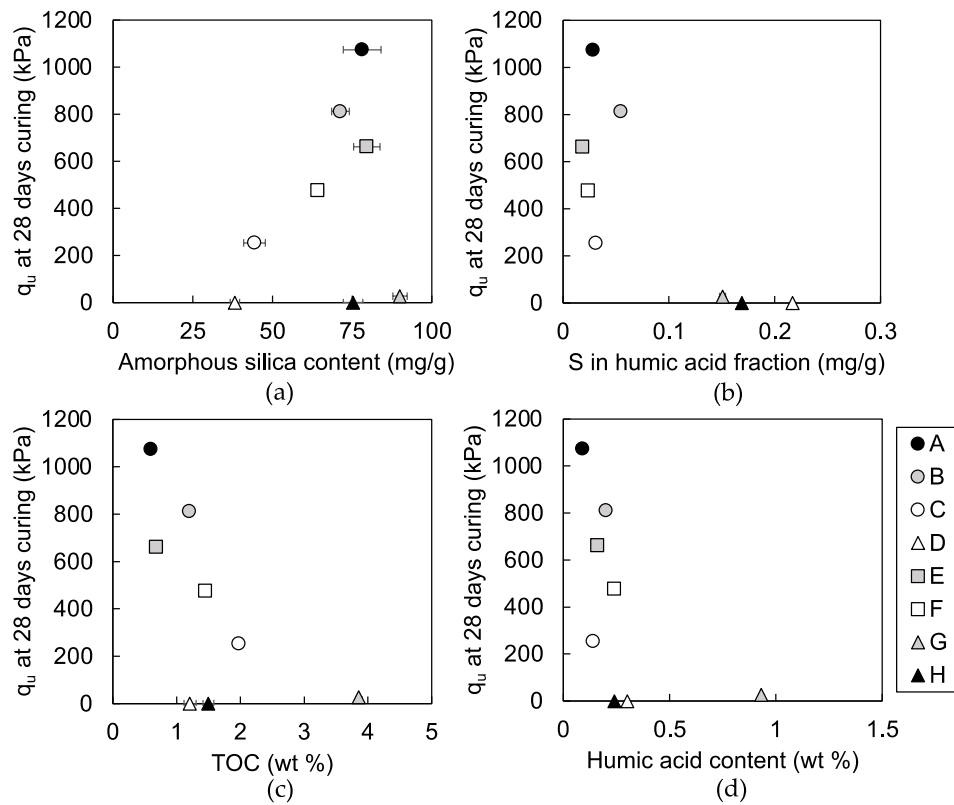
Fig. 3-9 Relationship of (a) amorphous silica, (b) sulfur in the humic acid fraction, (c) TOC and (d) humic acid content per gram of dried dredged soil with q_u values of each steel slag-dredged soil mixtures at 28 days of curing. The q_u values for mixtures 1D and 1H are plotted as 0 kPa in order to include their plots in the diagram; they did not undergo unconfined compressive strength tests. The amorphous silica content of soils A, B, C, and D and the q_u values of mixtures 1A, 1B, 1C, and 1D are cited from Toda et al. [1]. Error bars of figure (a,c) show standard errors of data collected from repeated experiments and error bars of figure (b,d) show accuracy of the measurements.

The sulfur content in the humic acid fraction distinguished soils G and H, and also soil D from soils A, B, C, E, and F (**Fig. 3-9**b). Soils G, H, and D contained over 0.151 mg of sulfur per gram of soil in the humic acid fraction (**Fig. 3-9**b), whereas soils A, B, C, E, and F contained sulfur below 0.05 mg/g. Therefore, the sulfur in humic acid fraction could suggest the occurrence of inhibition in the pozzolanic reaction and the subsequent strength development of the mixtures. Inhibition in the pozzolanic reaction of mixtures 1G and 1H was suggested to result from the effect of soil organic matters because soils G and H were rich in sulfur in the humic acid fraction and had sufficient dissolved silica supply similar to

soils that formed hard mixtures: soil A, B, and E. Furthermore, inhibition in the pozzolanic reaction of the mixture 1D may result from the effect of soil organic matters, together with the limitation of dissolved silica supply because soil D was rich in sulfur in the humic acid fraction but had minimal amorphous silica content among the studied dredged soil samples.

In addition, as expected from Toda et al. [1], the TOC (**Fig. 3-9**c) or humic acid content (**Fig. 3-9**d) showed no relationship with q_u values of the mixtures, which emphasized the importance of interpreting the content of specific components of soil organic matters for the indication of dredged soils, which form soft mixtures.

3.4.2. *Characteristics of humic acids that inhibit strength development of the mixtures*

From the results in **Fig. 3-9**b, it is clear that the inhibition of the strength development of the 1G, 1H, and 1D mixtures were indicated by the content of sulfur-bearing components in the humic acids. These may be directly attributed to the inhibition in the pozzolanic reaction of the mixtures, as well as there may be unquantified components in the soil organic matters that correlate positively to the sulfur-bearing components and may contribute to the inhibition of the pozzolanic reaction.

Intrinsic characteristics of humic acids of the soils G, H, and D were further investigated with a comparison of their elemental ratios, which have been used to evaluate the average properties, sources, and alterations of humic acids [8,21,22].

The S/C of humic acids in all of the studied dredged soils was higher than that of the JHSS standards (**Fig. 3-10**a). This may result from differences in the following: (1) the inclusions of sulfur-bearing organic compounds; (2) degree of abiotic reaction of reduced sulfur with organic matter [23], which increases the preservation of sulfur in sedimentary soils [24]; and/or (3) the redox state of the sedimentary soils [21] where reducing conditions

are favorable to conserve sulfur in the sediments. Factors affected S/C of humic acids of dredged soils is not conclusive, though it could be further discussed with analysis of sulfur redox states of humic acids, which may indicate the redox condition of sedimentary soils. In addition, if sulfur-bearing components play a role in the inhibition of the pozzolanic reaction, their redox state would be critical for a full understanding of the inhibition mechanism of the pozzolanic reaction. The speciation of sulfur in humic acids of sedimentary soils is commonly assumed to be disulfides, thiols, sulfonates, or ester-bonded sulfates [24,25]; however, these various chemical properties would act differently on the pozzolanic reaction.
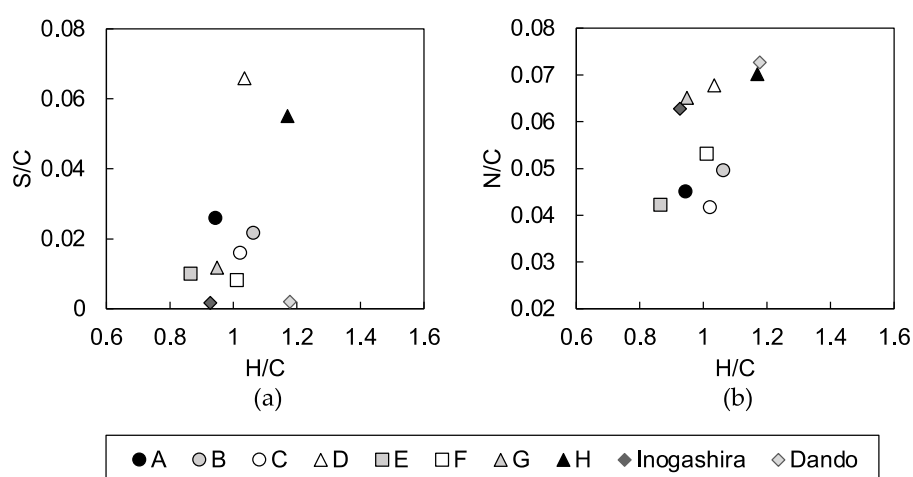
Fig. 3-10 (a) S/C versus H/C atomic ratios and (b) N/C versus H/C atomic ratios of humic acids extracted from the dredged soils (A, B, C, D, E, F, G, and H), Dando humic acid and Inogashira humic acid.

Furthermore, **Fig. 3-10**a shows that the S/C ratio of humic acid of soils D and H were almost twice as large as the S/C ratio of humic acids of other dredged soils and JHSS standards. The sulfur content in the humic acid fraction of dredged soils could indicate the inhibition of a pozzolanic reaction of the mixtures made with soils D and H (**Fig. 3-9**b), because their humic acids had a high S/C ratio. The inhibition of pozzolanic reaction of the mixture made with soil G, whose humic acid had a similar S/C ratio to the humic acids of dredged soils that formed hard mixtures, was also indicated by the sulfur content in the humic acid fraction of dredged soils (**Fig. 3-9**b) because the content of humic acid in soil G

was high. Characteristics of humic acids are suggested to vary between dredged soils that form soft mixtures. The input of organic matters to the sedimentary soils and sulfur enrichment in the soil organic matter structure shape the sulfur content in the humic acid fraction of dredged soils as an indicator of dredged soils that form soft mixtures.

The nitrogen content in the humic acid fraction of the dredged soils did not clearly indicate dredged soils that form soft mixtures as sulfur did; hence, nitrogen-bearing functional groups are not likely a candidate of soil organic matters that inhibit the pozzolanic reaction. However, the N/C versus H/C plot suggested that the N/C ratio of the humic acid could be a characteristic of the dredged soils that form soft mixtures (**Fig. 3-10**b). The humic acids of soils D, G, and H plot between the two JHSS standards of N/C of 0.062 to 0.073. The higher N/C of soil organic matter has been suggested to result from the sedimentation of marine organic matter rich in amides, and/or as a result of low aeration, which could conserve the compositions of the sedimented organic matter [8]. Stuermer et al. [21] supported the former factor when they observed that algal sources, rather than highland plant sources, caused N/C enrichment.

The causes of sulfur and nitrogen enrichment of humic acids in dredged soils are not determined due to several possible causes of the enrichment. Despite the requirement of further investigations to clarify specific components in soil organic matters that may contribute to the inhibition of the pozzolanic reaction, the discussion here highlights that: (1) the content of such organic components in dredged soils is suggested to be affected by the input of organic matters to sedimentary soils and the sedimentary environment; (2) the N/C of humic acids also indicate the dredged soils that form soft mixtures as the sulfur content in the humic acid fraction of dredged soils does. Overall, these newly discovered indicators of dredged soils that form soft mixtures when mixed with a steel slag, together with quantification of their inorganic amorphous silica content, would enhance the utilization of dredged soils by accelerating the evaluation processes of their strength development.

3.4.3. Effects of soil organic matters on pozzolanic reaction

The factors that affect the pozzolanic reaction are calcium and silica sources, or other coexisting components such as soil organic matters that inhibit the reaction, as emphasized by mixtures 1D, 1G, and 1H. Soil organic matters in soils D, G, and H could interact with the pozzolanic reaction by pH buffers to the weak alkaline region [4]; the formation of calcium-organic matter complexation [26], and mineral surface coverage [27–29]. Such reactions would cause the solution chemistry to be undersaturated vis-a-vis C-S-H, which disables its precipitation, decreases calcium supply to C-S-H formation, and inhibits phase dissolution or precipitation, which could inhibit the pozzolanic reaction.

Among these possibilities, the effect of a pH buffer by soil organic matters was not significant in any of the mixtures as discussed in Toda et al. [1]. The pH of the pore water in the mixtures was above 12 after 1 day of curing in all mixtures (**Fig. 3-8**a). From the comparisons of calcium concentrations of pore water in cement-treated soils of Tremblay et al. [4], which showed organic reagents to cause one to two order higher concentrations of calcium in solution with the control sample of Tremblay et al. [4] and our data, it is speculated that the formation of calcium complexation may not be significant in the mixtures 1D, 1G, and 1H. The occurrence of surface coverage by soil organic matters could not be clarified, yet it is clear that the dissolution of portlandite was not inhibited, as shown by the pH and calcium concentrations of pore water in mixtures 1D, 1G, and 1H at saturation of portlandite with pH around 12.5 and calcium concentration above 20 mmol/L (**Fig. 3-8**a,b). In addition, silica concentrations of all mixtures at all curing times were similar (**Fig. 3-8**c), so the soil organic matters in soils D, G, and H may not inhibit the dissolution of amorphous silica either, which leaves precipitation sites of C-S-H as possible surface-covering sites for soil organic matters. It was confirmed that a pH buffering effect does not play a role in the inhibition of the pozzolanic reaction in steel slag-dredged soil mixtures. The calcium complexation ability of soil organic matters in soils D, G, and H, and its ability

to cover the mineral surface will be investigated to determine how pozzolanic reaction

inhibition occurs in the mixtures made with soils D, G, and H in future research.

3.5. Conclusions

The inhibition of strength development in steel slag-dredged soil mixtures by soil

organic matters is detailed. Our data especially highlight the importance of the

quantification of specific components among soil organic matter in evaluating the effect on

the strength development of such mixtures. Dredged soils with enriched sulfur content in

the humic acid fraction, and/or N/C ratio of extracted humic acids similar to that of land

humic acids, resulted in the formation of soft mixtures. These characteristics could be used

as indicators of dredged soils that form soft mixtures, together with the inorganic

amorphous silica content in the dredged soils. Also, the TOC and humic acid content in

dredged soils are not suggested as indicators of soft mixture formation. Our findings clarify

that the strength development indicators have significant implications for the utilization of

steel slag-dredged soil mixtures. The discovery of indicators of strength development of

steel slag-dredged soil mixtures will accelerate evaluation processes for the strength

development of mixtures made with newly sampled dredged soils by making the estimation

of their strength development possible, which would facilitate and promote the utilization of

steel slags and dredged soils.

Subsequently, the inhibition of the pozzolanic reaction by soil organic matters that form

soft mixtures was not due to the pH-buffering capacity of soil organic matters but may be

occurring because of calcium complexation or mineral surface coverage by soil organic

matters. An understanding of the inhibition mechanism of the strength development

requires further studies, clarification of what component in the soil organic matters to

attribute to the inhibition of the pozzolanic reaction, and how this component inhibits it;

however, the results show the potential of this study for further investigations to facilitate

the validation of dredged soils by mixing with cementing additives that form C-S-H as the

major binding phase via the pozzolanic reaction. Overall, the findings should contribute to an increased utilized fraction of dredged soils and industrial by-products that act as alkaline activators that replaces the destination of such materials from disposal wastes to construction resources, which would promote their utilization in the construction industry.

References

[1]   K. Toda, H. Sato, N. Weerakoon, T. Otake, S. Nishimura, T. Sato, Key factors affecting strength development of steel slag-dredged soil mixtures, Minerals. 8 (2018). https://doi.org/10.3390/min8050174.

[2]   K. Toda, H. Sato, N. Weerakoon, T. Otake, S. Nishimura, T. Sato, Correction: Toda, K., et al. Key factors affecting streng th development of steel slag-dredged soil mixtures. Minerals 2018, 8(5), 174, Minerals. 8 (2018). https://doi.org/10.3390/min8050174.

[3]   E. Kiso, M. Tsujii, K. Ito, M. Nakagawa, M. Gomyo, T. Nagatome, Method of dredged soil improvement by mixing with converter steel-making slag, Proc. Civ. Eng. Ocean. 24 (2008) 327–332.

[4]   H. Tremblay, J. Duchesne, J. Locat, S. Leroueil, Influence of the nature of organic compounds on fine soil stabilization with cement, Can. Geotech. J. 39 (2002) 535–546. https://doi.org/10.1139/t02-002.

[5]   G.-O. Kang, T. Tsuchida, Y.-S. Kim, W.-J. Baek, Influence of humic acid on the strength behavior of cement-treated clay during various curing stages, J. Mater. Civ. Eng. 29 (2017) 1–18. https://doi.org/10.1061/(ASCE)MT.1943-5533.0001919.

[6]   H.R. Schulten, M. Schnitzer, Three-dimensional models for humic acids and soil organic matter, Naturwissenschaften. 82 (1995) 487–498. https://doi.org/10.1007/BF01134484.

[7]   R. Sutton, G. Sposito, Molecular structure in soil humic substances: The new view, Environ. Sci. Technol. 39 (2005) 9009–9015. https://doi.org/10.1021/es050778q.

[8]   J.A. Rice, P. MacCarthy, Statistical evaluation of the elemental composition of humic substances, Org. Geochem. 17 (1991) 635–648. https://doi.org/10.1016/0146-6380(91)90006-6.

[9]   M.J. Avena, L.K. Koopal, W.H. Van Riemsdijk, Proton binding to humic acids: Electrostatic and intrinsic interactions, J. Colloid Interface Sci. 217 (1999) 37–48. https://doi.org/10.1006/jcis.1999.6317.

[10]   G.R. Blake, Particle density, in: W. Chesworth (Ed.), Encycl. Soil Sci., Springer Netherlands, Dordrecht, 2008: pp. 504–505. https://doi.org/10.1007/978-1-4020-3995-9_406.

[11]   R.A. Mortlock, P.N. Froelich, A simple method for the rapid determination of biogenic opal in pelagic marine sediments, Deep Sea Res. Part A. Oceanogr. Res. Pap. 36 (1989) 1415–1426. https://doi.org/10.1016/0198-0149(89)90092-7.

[12]   H. Kodama, Identification and quantification of non-crystalline inorganic minerals in soils by selective chemical dissolution method, Chisitsu News No.496. (1995) 26–35.

[13]   M. Fukushima, M. Yamamoto, T. Komai, K. Yamamoto, Studies of structural alterations of humic acids from conifer bark residue during composting by pyrolysis-gas chromatography/mass spectrometry using tetramethylammonium hydroxide (TMAH-py-GC/MS), J. Anal. Appl. Pyrolysis. 86 (2009) 200–206. https://doi.org/10.1016/j.jaap.2009.06.005.

[14]   M. Fukushima, K. Yamamoto, K. Ootsuka, T. Komai, T. Aramaki, S. Ueda, S. Horiya, Effects of the maturity of wood waste compost on the structural features of humic acids, Bioresour. Technol. 100 (2009) 791–797. https://doi.org/10.1016/j.biortech.2008.06.030.

[15]   H. Obara, Y. Takata, K. Kohyama, T. Ohkura, Y. Maejima, S. Watabayashi, T. Kanda, A new soil map of Japan based on comprehensive soil classification system of Japan First Approximation, Bull. Natl. Inst. Agro-Environmental Sci. 37 (2016) 133–148.

[16]   S. Kuwatsuka, A. Watanabe, K. Itoh, S. Arai, Comparision of Two Methods of Preparation of Humic and Fulvic Acids, IHSS Method and NAGOYA Method, Soil Sci. Plant Nutr. 38 (1992) 23–30. https://doi.org/10.1080/00380768.1992.10416948.

[17]   A. Watanabe, K. Itoh, S. Arai, S. Kuwatsuka, Comparison of the composition of humic and fulvic acids prepared by the IHSS method and NAGOYA method, Soil Sci. Plant Nutr. 40 (1994) 601–608. https://doi.org/10.1080/00380768.1994.10414299.

[18]   Coastal development institute of technology, Technical manual for utilizing Calcia modified soil at ports, airports and coasts (in Japanese), 2017.

[19]   S. Grangeon, F. Claret, C. Roosz, T. Sato, S. Gaboreau, Y. Linard, Structure of nanocrystalline calcium silicate hydrates : insights from X-ray diffraction , synchrotron X-ray absorption and nuclear magnetic resonance research papers, J. Appl. Crystallogr. 49 (2016) 1–14. https://doi.org/10.1107/S1600576716003885.

[20]   B. Lothenbach, A. Nonat, Calcium silicate hydrates: Solid and liquid phase composition, Cem. Concr. Res. 78 (2015) 57–70. https://doi.org/10.1016/j.cemconres.2015.03.019.

[21]   D.H. Stuermer, K.E. Peters, I.R. Kaplan, Source indicators of humic substances and
        proto-kerogen. Stable isotope ratios, elemental compositions and electron spin
        resonance spectra, Geochim. Cosmochim. Acta. 42 (1978) 989–997.
        https://doi.org/10.1016/0016-7037(78)90288-0.

[22]   M. Giovanela, E. Parlanti, E.J. Soriano-Sierra, M.S. Soldi, M.M.D. Sierra, Elemental
        compositions, FT-IR spectral and thermal behavior of sedimentary fulvic and humic acids
        from aquatic and terrestrial environments, Geochem. J. 38 (2004) 255–264.
        https://doi.org/10.2343/geochemj.38.255.

[23]   A. Vairavamurthy, K. Mopper, Geochemical formation of organosulphur compounds
        (thiols) by addition of H2S to sedimentary organic matter, Nature. 329 (1987) 623–625.
        https://doi.org/10.1038/329623a0.

[24]   T.G. Ferdelman, T.M. Church, G.W. Luther, Sulfur enrichment of humic substances in a
        Delaware salt marsh sediment core, Geochim. Cosmochim. Acta. 55 (1991) 979–988.
        https://doi.org/10.1016/0016-7037(91)90156-Y.

[25]   M.A. Vairavamurthy, D. Maletic, S. Wang, B. Manowitz, T. Eglinton, T. Lyons,
        Characterization of sulfur-containing functional groups in sedimentary humic substances
        by X-ray absorption near-edge structure spectroscopy, Energy and Fuels. 11 (1997)
        546–553. https://doi.org/10.1021/ef960212a.

[26]   C. J. Milne, D. Kinningburgh, J. C.M. De Wit, W. H. Van Riemsduk, L. K. Koopal,
        Analysis of metal-ion binding by a peat humic acid using a simple electrostatic model, J.
        Colloid Interface Sci. 175 (1995) 448–460. https://doi.org/10.1016/j.jcis.2008.12.029.

[27]   J. Plank, M. Gretz, Study on the interaction between anionic and cationic latex particles
        and Portland cement, Colloids Surfaces A Physicochem. Eng. Asp. 330 (2008) 227–233.
        https://doi.org/10.1016/j.colsurfa.2008.08.005.

[28]   N.L. Thomas, J.D. Birchall, The retarding action of sugars on cement hydration, Cem.
        Concr. Res. 13 (1983) 830–842.

[29]   J. Plank, C. Hirsch, Impact of zeta potential of early cement hydration phases on
        superplasticizer adsorption, Cem. Concr. Res. 37 (2007) 537–542.
        https://doi.org/10.1016/j.cemconres.2007.01.007.

4. Effects of lignosulfonate on synthesis products of the pozzolanic reaction

Abstract

Soil organic matters affect the pozzolanic reaction that may determine the strength development of soil-employed construction materials. The effect of lignosulfonate, a model soil organic matter, on the pozzolanic reaction with initial Ca/Si ratio of 1.6, 1.0 and 0.8 ($C_{1.6}$-S-H, $C_{1.0}$-S-H and $C_{0.8}$-S-H) was investigated.

At equal synthesis period but escalation in the amount of lignosulfonate addition, $C_{1.6}$-S-H, $C_{1.0}$-S-H, and $C_{0.8}$-S-H formation was inhibited explicitly with a threshold. Below thresholds, lignosulfonate caused C-S-H formation with modification to an uniform structure regardless to initial Ca/Si ratio. Inhibition of C-S-H formation is suggested to occur by formation of secondary phases that occur when lignosulfonate dosage exceeds the limit of C-S-H formation.

Keywords: C-S-H, pozzolanic reaction, lignosulfonate, reaction inhibition

4.1.   Introduction

Industrial byproducts and waste soils are environmentally low-impact resources for the construction industry. The industry has been actively receiving such materials that validates wastes. Construction materials made with such resources are particularly attractive for regional use close to the material sources because of the feasibility in the transport and application associated with cost savings.

Dredged soils are one of the candidates for civil construction engineering among those raw materials. Dredged soils harden by alkaline activation of cement [1,2] but also by

industrial byproducts such as steel slags [3] or geopolymer with fly ash [4] which latter mixtures also contribute to validation of industrial byproducts. Yet, utilization of such mixtures are limited majorly due to unclarified cause of strength development variation affected by compositions of soil samples collected at different ports [3,5].

For cases where steel slag is used as alkaline activator to dredged soils, calcium silicate hydrates (C-S-H) forms by the pozzolanic reaction and majorly cause strength to develop [5,6]. Portlandite in steel slags and amorphous silicate phases in dredged soils are proposed as the reactants, which those contents were suggested as key factors that determine strength development of the mixtures [6]. Recently, dredged soils that contain specific type of soil organic matters (i.e., enriched in sulfur) are discussed to inhibit the strength development of the mixtures, supported by insignificant consumption of portlandite after curing, regardless to coexisting portlandite and amorphous silicate phases in abundancy [7]. Therefore, the inhibition may be triggered by an exceeding amount of specific soil organic matters which is speculated to exist in some dredged soils. However, while mechanical properties of construction materials in coexistence of soil organic matters [8–11] and the effect of organic admixtures to retard cement hydration [12–16] have been extensively studied, little is known about how soil organic matters totally inhibits cementation reaction.

Utilization of such soils may be possible if the mechanism of the inhibition of the pozzolanic reaction is clarified, for example by discovering an effective admixture to make soil organic matters inert to pozzolanic reaction. To do so, clarification of: (1) the effect of soil organic matters to the pozzolanic reaction products as a function of its dosage and (2) specific soil organic matters that function to inhibit the pozzolanic reaction are required. This study focuses to understand the former topic as a starting point to clarify inhibition of the pozzolanic reaction by soil organic matters. This study aims to characterize and discuss how a well-known organic admixture in cement chemistry, lignosulfonate, affects the products of the pozzolanic reaction with escalation of its dosage. It was expected to form C-S-H at lower dosage of lignosulfonate and inhibit C-S-H formation at higher dosages. This paper presents

the result of an investigation on the mineralogical and microstructural characterization of the products of the pozzolanic reactions formed in coexistence of lignosulfonate, and their compositions in solution chemistry, which the results are integrated to interpret the interactions of lignosulfonate with the pozzolanic reaction and how it may cause the inhibition of the pozzolanic reaction.

4.2. Materials and methods

4.2.1. Lignosulfonate

Lignosulfonate was selected regarding to its similarities with natural soil organic matters among other organic admixtures in manufacture of constructions, which mostly are synthetic polymers [17–19]. Lignosulfonate is a commonly used cement hydration retarder [15,20] that originates from natural plant sources which compose variety of carbon structure and functional groups, similar to soil organic matters. Additionally, soil organic matters and lignosulfonate bear sulfur in the structure, that was an indicator of dredged soil samples which inhibited the pozzolanic reaction. Lignosulfonate is suggested to form semipermeable layers around cement minerals by their electrostatic interaction with Ca ion and mineral surfaces to retards hydration [12,13]. This cause of the retardation will be compared to the effect of lignosulfonate to synthesized products of the pozzolanic reaction.

4.2.2. C-S-H syntheses

The pozzolanic reaction with three initial Ca/Si ratios were conducted to comprehensively understand the effect of lignosulfonate. That is because, variation of amorphous silica content between dredged soil samples and portlandite content between steel slag samples can cause Ca/Si ratio of C-S-H to vary. C-S-H have a range of Ca/Si ratio that it can form [21], determined by the amount of soluble Ca and Si sources. If an electrostatic interaction mostly determines the effect of lignosulfonate to the pozzolanic

reaction, electrostatic property of C-S-H, known to differ between Ca/Si ratios [22], may cause difference in the effect.

C-S-H with initial Ca/Si ratio of 1.6, 1.0 and 0.8 were synthesized with Aerosil 200 (Nippon Aerosil Co. Ltd.) and portlandite (Wako Pure Chemicals Inc.) for Si and Ca sources, respectively. Sodium lignosulfonate (lignosulfonate) (Tokyo Chemical Industry Co. Ltd.) was used as lignosulfonate reagent. As received lignosulfonate was used for the C-S-H syntheses. C-S-H syntheses with initial Ca/Si of 1.6, 1.0 and 0.8 are hereafter called as $C_{1.6}$-S-H, $C_{1.0}$-S-H, and $C_{0.8}$-S-H series.

C-S-H syntheses were carried out with solid to liquid ratio of 1:20, at 50 ℃, on 100 rpm shaker with synthesis duration of 10 days. C-S-Hs were synthesized in the presence of 0 to 65 wt.% of lignosulfonate by mass ratio, in steps of ca. 10 wt.%, against total mass of amorphous silica and portlandite used in the syntheses in order to interpret how lignosulfonate influence the pozzolanic reaction as a function of its dosage. The maximum dosage was set below the calculated maximum ratio of soil organic matters against amorphous silica content in dredged soil samples studied in [7].

Initially, amorphous silica, lignosulfonate and deionized water were weighed into a polyethylene container and mixed until homogenous. After, weighed portlandite was added to the container then mixed. Subsequently, the samples were set onto the shaker. After synthesis, solid products were collected by centrifugation at 3000 rpm for 40 minutes, then freeze-dried and grinded thoroughly to obtain powder samples. Supernatant solutions were filtrated by 0.2 μm filter before conducting subsequent analyses.

4.2.3. Characterization of solid products and analysis of solution composition

4.2.3.1. XRD

X-ray diffraction (XRD) was conducted to powdered solid samples after synthesis to determine the mineralogical compositions, using RINT2100 X-ray diffractometer (Rigaku)

equipped for CuKα radiation at 30 kV and 20 mA. Randomly oriented powder samples were scanned from 2 to 70° 2θ at a scanning speed of 0.02°/s.

4.2.3.2. ^{29} Si MAS NMR

The single-pulse ^{29} Si Magic-Angle Spinning Nuclear Magnetic Resonance (^{29} Si MAS NMR) of $C_{1.6}$-S-H, $C_{1.0}$-S-H and $C_{0.8}$-S-H series products were acquired on JNM-ECA 500II spectrometer (Japan Electron Optics Laboratory) equipped with a 4 mm probe. Samples were packed into a 4 mm zirconium rotor. The acquisition parameters were as follows: spectral frequency, 99.4 MHz; contact time, 34.3 ms; relaxation delay, 40 s; scan times, 6400; spinning rate, 12 kHz; and 90° excitation pulse of 3 μs. Q^0, Q^1, Q^{2b}, Q^{2Ca}, Q^3, and Q^4 state of ^{29}Si were assigned to peaks at ca. -70, -79, -82, -85, -96, and -110 ppm, respectively [23][24][25]. Superscript letters on Q refer to number of coordinated silicon-oxygen tetrahedra. Q^0 corresponds to monomer tetrahedra without coordination to other tetrahedras. Q^1 and Q^2 are found on C-S-H [26][24] at isolated pairs of the tetrahedra, i.e., dimers or the end of silicate chains and at bridging dimers, respectively. Q^{2b} and Q^{2Ca} corresponds to classification of Q^2 silicates that coordinates to Ca layer or bridges between silicate dimers, respectively [27]. Q^3 and Q^4 are found in amorphous silica [28][29][30] at hydrated amorphous silica framework with coordination of three tetrahedra and amorphous silica framework with coordination of four tetrahedra, respectively.

The ratio of peak areas of Q^1 and Q^2 (sum of Q^{2b} and Q^{2Ca}) confirms the silicate structure of C-S-H which is well studied to correspond with Ca/Si ratio of C-S-H. C-S-H with lower Ca/Si ratio are known to have more of bridging tetrahedra (Q^2) and less of isolated pairs of tetrahedra (Q^1) compared to that of C-S-H with a higher Ca/Si ratio [31]. The Ca/Si ratio of synthesized C-S-H was calculated using (4-1) [32]

$$\frac{Ca}{Si} = \frac{\frac{3}{2}Q^1 + \frac{2}{3}Q^2}{Q^1 + Q^2}, (4\text{-}1)$$

where Q^1 and Q^2 are corresponding peak areas calculated through deconvolutions of the ^{29}Si MAS NMR spectra by gaussian fitting.

Ca and Si concentrations in the supernatant solutions were measured by inductively coupled plasma-atomic emission spectroscopy (ICP-AES; ICPE-9000, Shimadzu). Solutions for ICP-AES analysis were diluted and stored in fridge right after the sample collection to eliminate precipitation of dissolved species. pH was also recorded for the same solutions. Dissolved organic carbon (DOC) was measured by total organic carbon analyzer (TOC; TOC-L, Shimadzu). Ca and Si concentrations of solutions after synthesis were used to calculate Ca/Si ratio of solid phases by subtraction of Ca and Si distributed in solution phase from total Ca and Si in reaction.

4.3. Results

4.3.1. Phase compositions

XRD patterns of synthesized products are shown in **Fig. 4-1**. C-S-H formed in the range of lignosulfonate dosage between 0 to 29 wt.%, 0 to 47 wt.% and 0 to 56 wt.%, in the $C_{1.6}$-S-H, $C_{1.0}$-S-H and $C_{0.8}$-S-H series, respectively. In all C-S-H series, intensity of basal reflection for C-S-H [33], which appears at 11.2-13.5Å (6.5-7.9°2θ(CuKa)) in the XRD patterns, decreases and disappears as the lignosulfonate dosage increased. Larger dosage of lignosulfonate form C-S-H without ordered stacking of C-S-H layers. Those C-S-H formed without basal reflection consisted of reflections from C-S-H layer shown with maxima at ~1.8Å (49.8 °2θ(CuKa)) and 2.7-3.2Å (28.2-33.2 °2θ(CuKa)), indicated that the formation of C-S-H layer was not inhibited. Inhibition of the C-S-H formation occurred at the dosage of lignosulfonate over 38, 56 and 65 wt.% of $C_{1.6}$-S-H, $C_{1.0}$-S-H and $C_{0.8}$-S-H series, respectively. Inhibition of C-S-H formation is confirmed by XRD patterns consisting of portlandite peaks and broad diffraction of amorphous silica around 2.6-5.9Å (15-35 °2θ(CuKa)). Because of the abrupt change in the XRD patterns from C-S-H to portlandite

and amorphous silica, there appear to be the thresholds for the lignosulfonate dosage in which to inhibit the pozzolanic reaction.
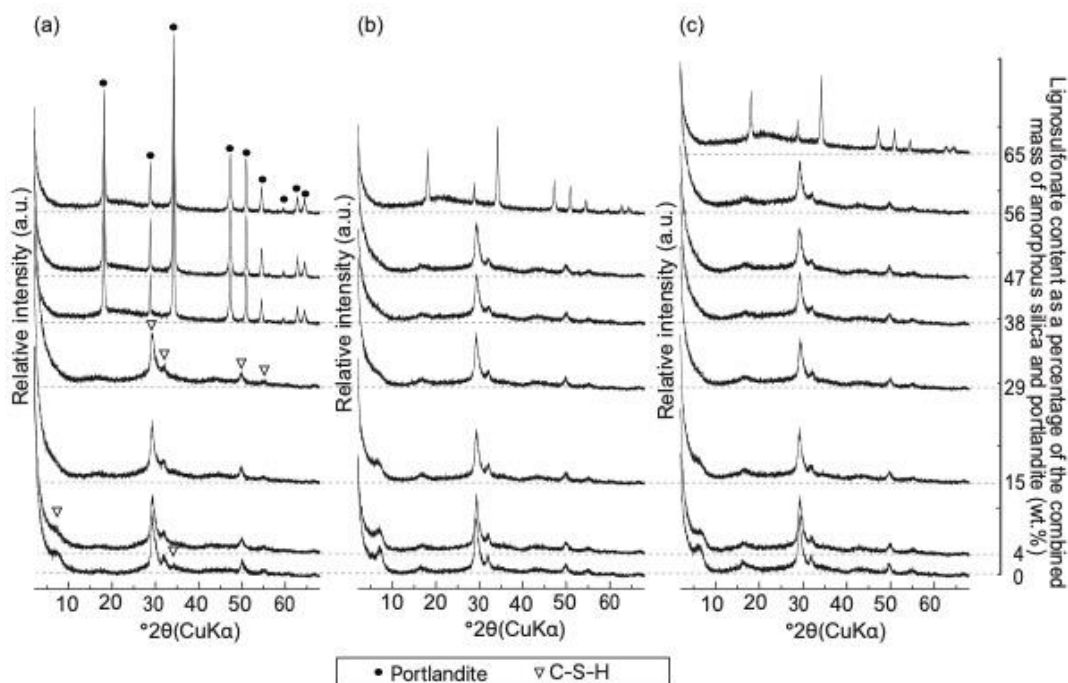
Fig. 4-1 XRD profiles of synthesized products, with initial Ca/Si of (a) 1.6, (b) 1.0 and (c) 0.8 with increment in the dosage of lignosulfonate. Vertical axis shows the weight percentage of lignosulfonate against the sum of amorphous silica and portlandite added in the systems.

4.3.2. Polymerization state of silicates

^{29}Si MAS NMR spectra of synthesized products are shown in Fig. **4-2**. Samples that the formation of C-S-H was confirmed by XRD, showed Q^1 and Q^2 peaks that corresponds to C-S-H [24,26]. The intensities of Q^1 peak decreased and Q^2 peak increased with escalation of lignosulfonate dosage in $C_{1.6}$-S-H and $C_{1.0}$-S-H series. In reverse, Q^2 peak intensity decreased with escalation of lignosulfonate dosage in $C_{0.8}$-S-H series.

Ca/Si ratio calculated from NMR spectra is shown in **Fig. 4-3**. The Ca/Si ratio of C-S-H changed as a function of lignosulfonate dosage. Increase in lignosulfonate dosage caused

decrease in Ca/Si ratio of $C_{1.6}$-S-H and $C_{1.0}$-S-H series, from 1.17 to 0.99 and 0.99 to 0.95, respectively. In reverse, Ca/Si of $C_{0.8}$-S-H series increased from 0.77 to 0.85. The addition of lignosulfonate caused the Ca/Si ratio of C-S-H to converge towards a value regardless to the initial Ca/Si ratio.

The ^{29}Si MAS NMR spectra of synthesized products in which the pozzolanic reaction was inhibited (38 wt.%, 56 wt.%, and 65 wt.% of the added amount of lignosulfonate in the $C_{1.6}$-S-H, $C_{1.0}$-S-H and $C_{0.8}$-S-H series, respectively) showed broad peaks consisted of Q^0, Q^1, Q^2, Q^3 and Q^4 peaks. Among these peaks, Q^3 and Q^4 peaks likely correspond to unreacted amorphous silica added as a reactant [28–30]. The appearance of Q^0, Q^1 and Q^2 peaks in these synthesized products suggests that amorphous silica was depolymerized to secondary products consisting of Q^0, Q^1 and Q^2 polymerized states.
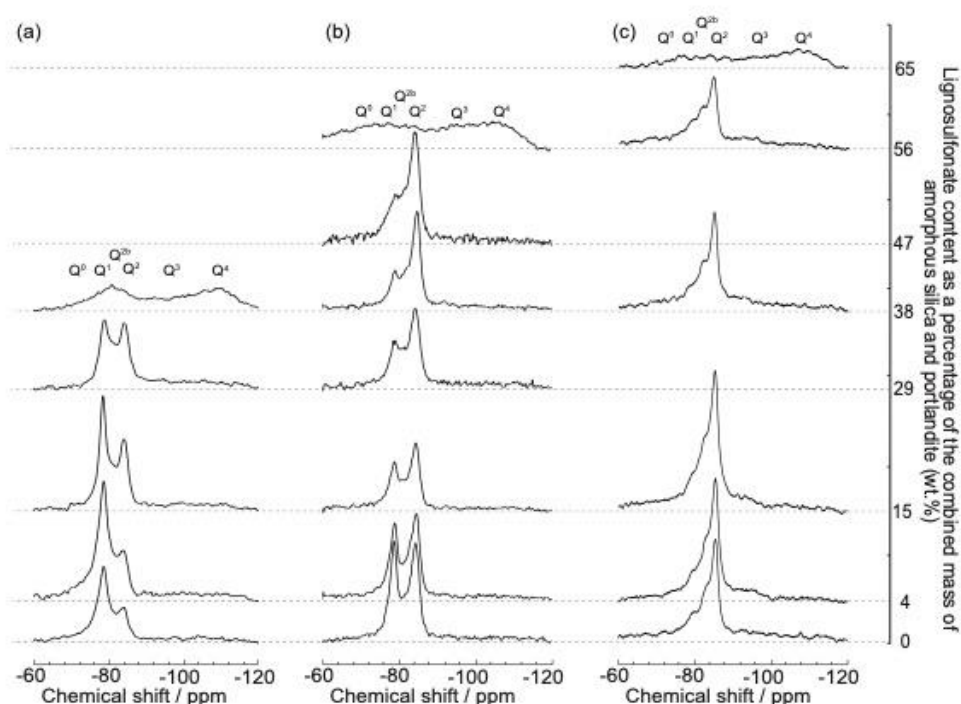
Fig. 4-2 29Si MAS NMR spectra of synthesized products in the (a) $C_{1.6}$-S-H, (b) $C_{1.0}$-S-H and (c) $C_{0.8}$-S-H series. Vertical axis shows the weight percentage of lignosulfonate against amorphous silica and portlandite added in the systems.
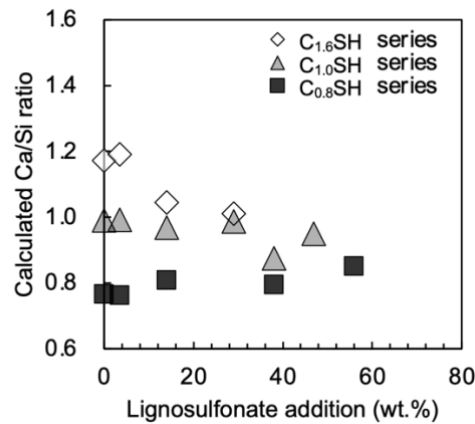
Fig. 4-3 Ca/Si ratio of calcium silicate hydrate (C-S-H) calculated from ^{29}Si MAS NMR spectra as a function of the weight percentage of lignosulfonate against the sum of amorphous silica and portlandite added in the systems.

4.3.3. Solution composition

Calcium, silica and DOC concentrations and pH of solutions after synthesis are shown on **Fig. 4-4**.

pH of the solutions in the $C_{1.6}$-S-H series was in the range between 12.24 and 12.42, which slightly decreased as lignosulfonate dosage increased (**Fig. 4-4**a). In the $C_{1.0}$-S-H and $C_{0.8}$-S-H synthesis series, pH decreased more significantly as lignosulfonate dosage increased in the samples where C-S-H formation was successful. pH decreased from 12.30 to 11.31, and from 10.75 to 9.68 in the $C_{1.0}$-S-H and $C_{0.8}$-S-H series, respectively. On the other hand, in the samples where C-S-H was not formed, pH of the pore waters was above 12.00 which is likely buffered by portlandite (**Fig. 4-4**a; i.e., pH 12.45 at 56 wt.% of lignosulfonate addition in the $C_{1.0}$-S-H series, pH 12.10 at 65 wt.% of lignosulfonate addition in the $C_{0.8}$-S-H series).

DOC in the solutions increased as lignosulfonate addition increased in all the C-S-H series (**Fig. 4-4**b). However, slope of DOC increase as a function of lignosulfonate dosage was steeper in the $C_{0.8}$-S-H synthesis series than $C_{1.0}$-S-H series. In the $C_{1.6}$-S-H series,

slope of the DOC increase was consistent with that in the $C_{1.0}$-S-H series under the conditions where C-S-H was formed, but abruptly increased after the C-S-H formation was inhibited (i.e., 47 wt.% of lignosulfonate addition). Then, the slope became more consistent with that in the $C_{0.8}$-S-H series.

Dissolved Ca concentrations were 18.5, 2.97 and 0.67 mmol/L without lignosulfonate addition in the $C_{1.6}$-S-H, $C_{1.0}$-S-H and $C_{0.8}$-S-H series, respectively (**Fig. 4-4**c). Dissolved Ca concentration increased as a function of lignosulfonate addition in all the C-S-H series, except for the conditions where C-S-H was formed (0 to 29 wt.% of lignosulfonate addition) in the $C_{1.6}$-S-H series that slightly decreased in its concentration from 18.5 to 15.2 mmol/L.

Dissolved Si concentrations were 0.02, 0.12 and 1.25 mmol/L without lignosulfonate addition in the $C_{1.6}$-S-H, $C_{1.0}$-S-H and $C_{0.8}$-S-H series, respectively (**Fig. 4-4**d). In all the series, dissolved Si concentration increased with increasing lignosulfonate dosage, while C-S-H formation was successful. Over the threshold of inhibition of C-S-H formation, Si concentration was constrained in the range of 0.20 to 0.94 mmol/L in all series.

Ca/Si ratio of solid phase after synthesis was calculated by subtraction of Ca and Si distributed to solution phase from total Ca and Si in experiment batches, which is plotted as a function of the added weight percentage of lignosulfonate against the sum of amorphous silica and portlandite used in synthesis (**Fig. 4-5**). Solid Ca/Si ratio of $C_{1.6}$-S-H series was almost constant around 1.57 regardless to lignosulfonate dosage. $C_{1.0}$-S-H and $C_{0.8}$-S-H series showed slight decrement of Ca/Si ratio as a function of lignosulfonate dosage, from 1.0 to 0.95 and 0.80 to 0.74, respectively.
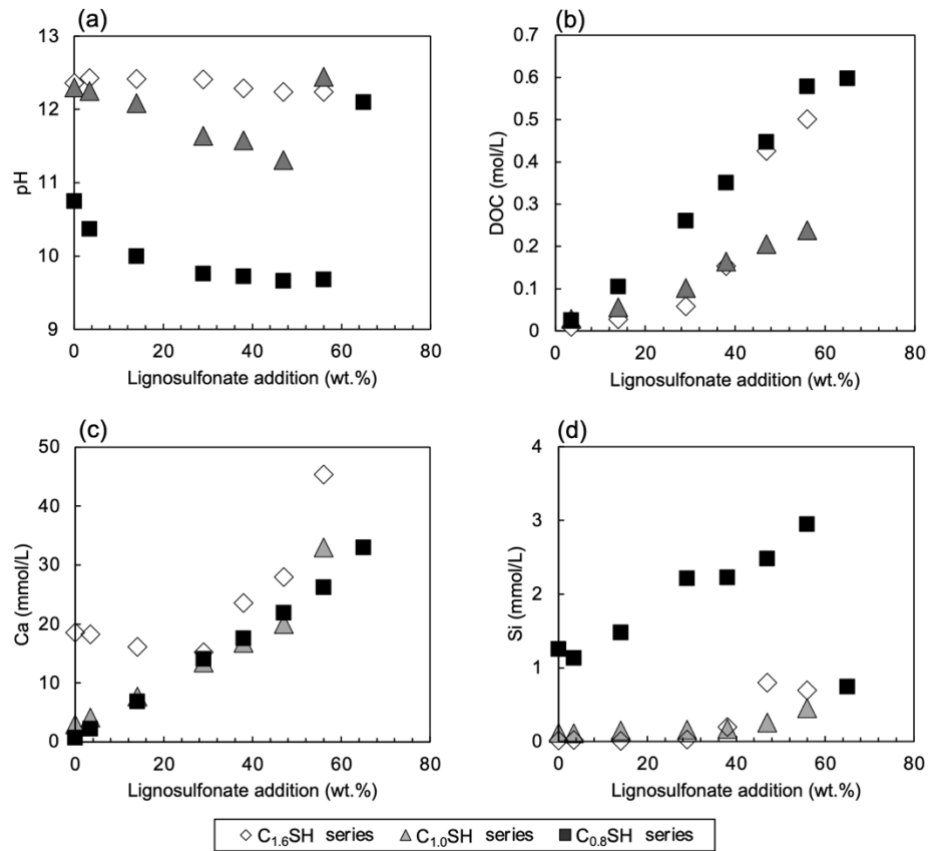
Fig. 4-4 Changes in solution chemistry as a function added weight percentage of lignosulfonate against amorphous silica and portlandite used in the synthesis (wt.%). Each graph shows (a) pH, (b) Dissolved organic carbon (DOC), (c) calcium concentration and (d) silica concentration of solutions collected after C-S-H synthesis.
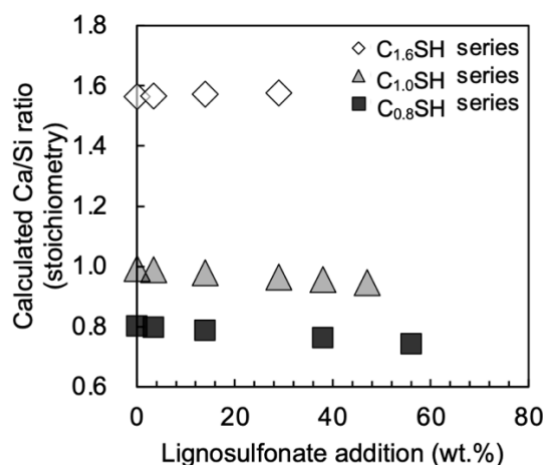
Fig. 4-5 Ca/Si ratio of solid phase calculated by subtraction of Ca and Si distributed to solution after synthesis from total Ca and Si in experiment, is plotted as a function of the added weight percentage of lignosulfonate against the sum of amorphous silica and portlandite used in the experiment.

4.4. Discussion

4.4.1. Lignosulfonate modifies C-S-H structure

Lignosulfonate may modify the structure of C-S-H synthesized in this study. Basal reflection of C-S-H disappeared (**Fig. 4-1**), which suggests the interference of lignosulfonate on stacking of C-S-H layers, similar to intercalation of organic polymers in C-S-H [34]. The changes of Ca/Si ratio of C-S-H as a function of lignosulfonate dosage, calculated from ^{29}Si MAS NMR spectra (**Fig. 4-3**), confirmed modification of bridging state of silicate chains in C-S-H, which was similarly observed in the effect of polyacrylic acid to C-S-H structure [35]. It was found the Ca/Si ratio of C-S-H to converge to a value regardless to initial Ca/Si ratio by addition of lignosulfonate (**Fig. 4-3**). Overall, components of lignosulfonate, similar to studied organic polymers or other components original in lignosulfonate may intercalate in between C-S-H layers and modify the Ca/Si ratio simultaneously, where the effect of the lignosulfonate to the structure of C-S-H are uniform regardless to initial Ca/Si of synthesis experiments.

The causes of modification in C-S-H structure may be from electrostatic interaction in solid phases [12,20] or Ca complexation reaction by lignosulfonate in solution phase, which

latter cause was speculated from positive correlation of DOC and Ca concentration in solution phase (i.e., $C_{1.0}$-S-H and $C_{0.8}$-S-H series in which C-S-H had formed, **Fig. 4-7**). The causes are discussed by the comparison of Ca/Si ratio of C-S-H calculated from ^{29}Si MAS NMR spectra (**Fig. 4-3**) and Ca/Si ratio of solid phase calculated by subtraction of Ca and Si in solution after the synthesis from total Ca and Si in each system (**Fig. 4-5**).

$C_{1.6}$-S-H series showed discrepancy in two calculated Ca/Si ratios (**Fig. 4-3,Fig. 4-5**). Undetected remnant portlandite in XRD analysis may be counted in calculation of Ca/Si ratio from solution partitioning but not by ^{29}Si MAS NMR spectra, where 1.57 and 1.17 was respective calculated Ca/Si ratio of the lignosulfonate-free C-S-H. Also, the decrease of Ca/Si ratio calculated from ^{29}Si MAS NMR spectra as a function of lignosulfonate dosage, that was not explanatory by constant Ca/Si ratio of C-S-H calculated from solution partitioning of Ca and Si, suggested lignosulfonate to affect C-S-H structure by the fraction partitioned to solid phase.

$C_{0.8}$-S-H series also showed discrepancy in two calculated Ca/Si ratios (**Fig. 4-3,Fig. 4-5**). Ca/Si ratio calculated from ^{29}Si MAS NMR spectra increased as a function of lignosulfonate dosage. Whereas Ca/Si calculation from solution partitioning showed the opposite trend. These opposing trends indicated that Ca distribution to solution phase did not explain the Ca/Si ratio modification of C-S-H by increase in lignosulfonate dosage. Therefore, the tendency of lignosulfonate to modify Ca/Si ratio of C-S-H towards a value in $C_{1.6}$-S-H and $C_{0.8}$-S-H series, calculated from ^{29}Si MAS NMR spectra, may be caused by incorporated lignosulfonate in C-S-H structure, rather than Ca partitioning to solution by complex formation with lignosulfonate.

$C_{1.0}$-S-H series did not show significant discrepancy in the calculated Ca/Si values, where both values decreased as a function of lignosulfonate dosage (**Fig. 4-3,Fig. 4-5**). Hence, decrease in Ca/Si ratio of C-S-H confirmed by ^{29}Si MAS NMR spectra may be caused by the distribution of Ca to solution phase (**Fig. 4-4**c) that was increased by lignosulfonate addition, presumably by forming Ca-lignosulfonate complexation. Simultaneously,

incorporation of lignosulfonate in C-S-H structure formed in $C_{1.0}$-S-H series maybe occurring as suggested in $C_{1.6}$-S-H and $C_{0.8}$-S-H series, as increase of lignosulfonate dosage cause Ca/Si ratio of C-S-H to modify towards a similar value of $C_{1.6}$-S-H and $C_{0.8}$-S-H series.

Although the interaction of lignosulfonate with pozzolanic reaction that determines C-S-H structure was not conclusive, incorporation of lignosulfonate to C-S-H structure and Ca-lignosulfonate complex formation was suggested to occur when C-S-H formed in coexistence of lignosulfonate via the pozzolanic reaction. It was also found that difference in initial Ca/Si ratio to cause variation in how lignosulfonate interacts with pozzolanic reaction. The interaction in $C_{1.6}$-S-H and $C_{0.8}$-S-H series was suggested to occur in solid phase, that may be caused by electrostatic interaction of C-S-H and lignosulfonate. The interaction in $C_{1.0}$-S-H series is suggested to occur similarly in solid phase, but also by Ca-lignosulfonate complex formation.
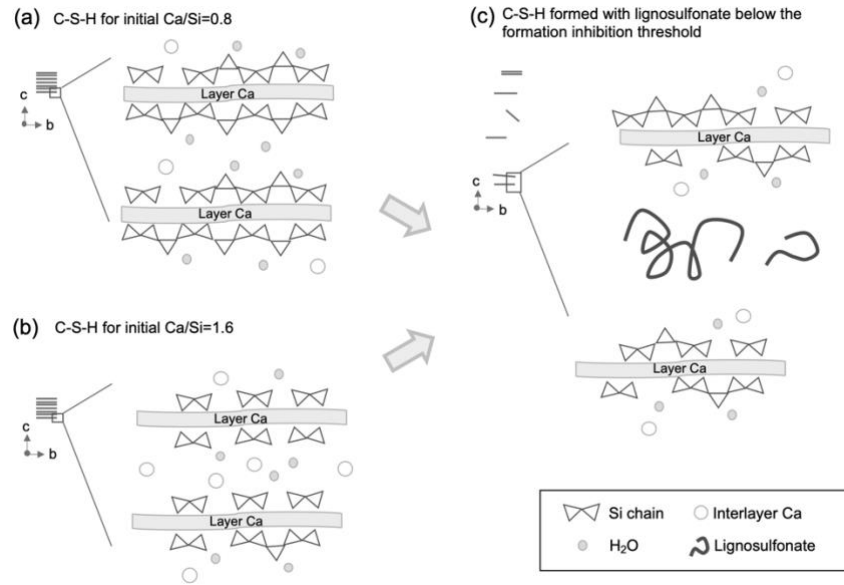
Fig. 4-6 Schematic diagram of C-S-H structure change by lignosulfonate. Stacking layers of C-S-H on upper left of each figure(a), (b) and (c) show the structure of C-S-H viewed along the a axis, and the magnification of the area enclosed by rectangle show the schematic structure of C-S-H. Figure (a) and (b) show C-S-H synthesized without lignosulfonate, and figure (c) shows the C-S-H synthesized with lignosulfonate, below the C-S-H formation thresholds. Regardless to initial Ca/Si ratio, addition of lignosulfonate was suggested to modify C-S-H to a uniform structure.
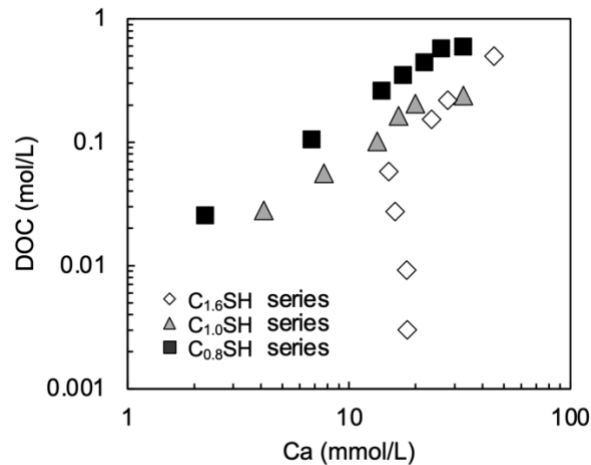
Fig. 4-7 Relationship of DOC and calcium concentrations of solutions after C-S-H synthesis

4.4.2. Lignosulfonate inhibits pozzolanic reaction

Inhibition of the pozzolanic reaction occurred with a threshold in lignosulfonate dosage, which was illustrated by the explicit change in mineralogical phases assemblage of the products composed of C-S-H to reactants, below and over the threshold (**Fig. 4-1**). Lignosulfonate must function to inhibit the forward pozzolanic reaction to have reactants conserved. Also, lignosulfonate is speculated to disable the polymerization of C-S-H layer itself, from XRD patterns below the threshold composing of diffractions from C-S-H layer that suddenly discontinues over the threshold. The thresholds of C-S-H synthesis series with lower initial Ca/Si ratio showed requirement of a larger amount of lignosulfonate to inhibit the pozzolanic reaction. Hence, the abundancy of lignosulfonate against amorphous silica may be critical to trigger the inhibition of the pozzolanic reaction.

The inhibition of the pozzolanic reaction occurred with following phenomena in all C-S-H synthesis series: (1) formation of minor and unidentifiable secondary phase with Q^0, Q^1, and Q^2 polymerized states of silicates; (2) constraint on Si concentration of solution composition; and (3) constraint on pH values. Such secondary phase form in solution composition of somewhat disproportioned to ordinary C-S-Hs [21]. Si concentration constraint may be the secondary phase, as amorphous silica at equilibrium possess Si concentration ca. 5 mmol/L under pH 12.0 in ambient condition [36,37]. The phase for constraint of pH may be portlandite, that possesses pH around 12.5 in equilibrium at ambient condition. Ca concentration constraint did not exist since Ca-lignosulfonate complexation influenced its concentration.

Such secondary phases maybe composed majorly of Si and lignosulfonate, as it forms at higher dosage of lignosulfonate, that constrains Si concentration, and lower initial Ca/Si ratio requiring more lignosulfonate to form the phase. It is hereafter named as lignosulfonate-silica phase.

Lignosulfonate-silica phase may work as the "impermeable layer" that limits the access of water to mineral surfaces, hence inhibit dissolution of primary phases [12,13] and

formation of C-S-H. Alternatively, constraints of solution chemistry may inhibit the pozzolanic reaction. Pozzolanic reaction is considered as an iterating reaction (**Fig. 4-8**a), that starts from portlandite dissolution until its equilibrium that supplies dissolved Ca and increases pH to alkaline region (**Fig. 4-8**a(i,ii)). Consequently, amorphous silica dissolves as it has high solubility under higher alkaline condition (**Fig. 4-8**a(iii)). Such dissolution of initial phases results in saturation of C-S-H. Formation of C-S-H links silica with Ca ion, that releases proton (decreases pH) in silanol groups with consumption of Ca and silica in solution (**Fig. 4-8**a(iv)). Hence C-S-H formation undersaturates the solution against portlandite which initiates the next iteration of the pozzolanic reaction (**Fig. 4-8**a(i,ii)). If the pozzolanic reaction occur in coexistence of lignosulfonate that inhibits the reaction (**Fig. 4-8**b), the iteration may not iterate. After the dissolution of portlandite and amorphous silica (**Fig. 4-8**b(i,ii)), formation of the secondary phases with silica and lignosulfonate (**Fig. 4-8**(iv)) is speculated. It would not release proton and may also not consume Ca ion (**Fig. 4-8**b(iv)), hence portlandite remains saturated and insignificantly consumed, with a unique solution composition. This reaction may explain the observations of the samples which the pozzolanic reaction was inhibited. Interaction of lignosulfonate in solid phase may cause such reaction, rather than Ca-lignosulfonate complexation formation that must consume portlandite as a Ca source. Overall, what determines the success of the iteration of the pozzolanic reaction could regard on the choices between Ca (**Fig. 4-6**) or lignosulfonate (**Fig. 4-9**) for silica to precipitate with.

In conclusion, the effect of lignosulfonate on the products over the thresholds of the C-S-H formation, is speculated to be similar regardless to initial Ca/Si ratio, that may form the secondary phases that at least form from lignosulfonate and amorphous silica. It may compose the impermeable layer or constrain the solution composition and inhibit the pozzolanic reaction. The silicate structure of the lignosulfonate-silica phase may resemble the silicate chains of ordinary C-S-H, but their polymerization may not develop as a C-S-H layer, since the phase contain variety of polymerized states of silica tetrahedra, and the

pozzolanic reaction inhibition is speculated to start when C-S-H layers are no longer possible

to form.
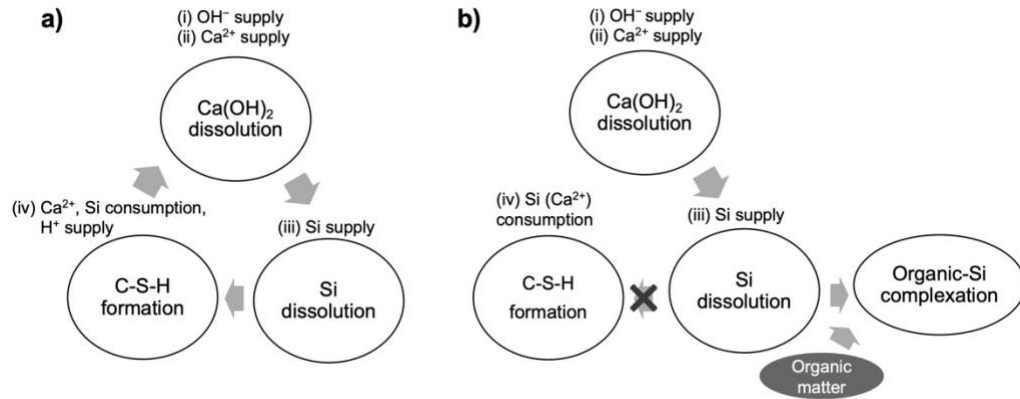
Fig. 4-8 Schematic diagrams of pozzolanic reaction a) without soil organic matters and b) with soil organic matters that inhibit formation of C-S-H (after [6]).
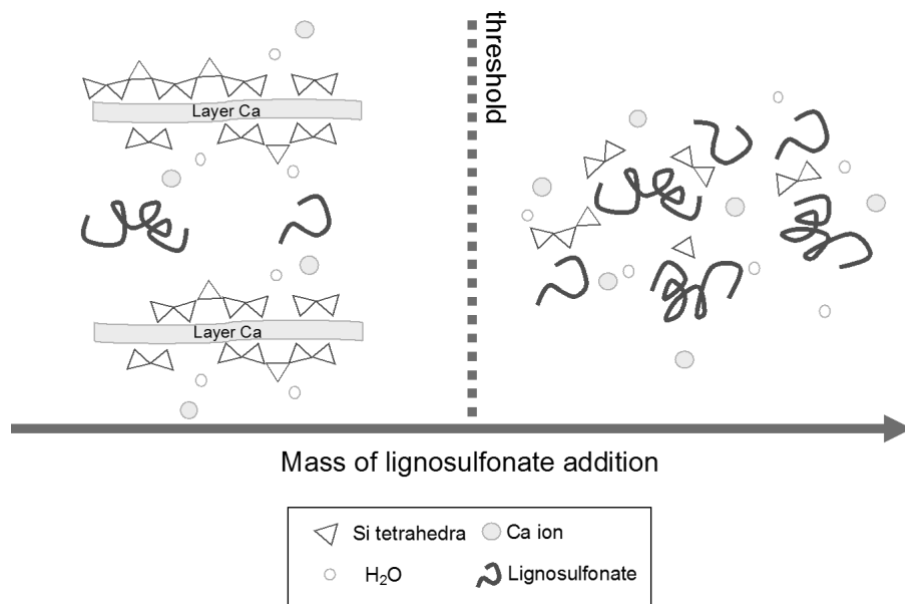
Fig. 4-9 Schematic diagram of the lignosulfonate-silica phase, that may occur when lignosulfonate inhibits the pozzolanic reaction. Polymerized state of silica would be similar to that of C-S-H, and it would form a composite with lignosulfonate.

4.4.3. Implication to the dredged soil utilization

The C-S-H synthesis with lignosulfonate explicitly illustrated that soil organic matters could inhibit the pozzolanic reaction. Also, a specific amount of soil organic matters was proved to trigger the inhibition of the pozzolanic reaction, which was speculated from the common high sulfur content of soil organic matters in dredged soils, that formed soft mixtures [7]. The existence of portlandite in samples which the pozzolanic reaction was inhibited, simulated the phases compositions of steel slag-dredged soil mixtures after curing, that formed soft mixtures. Although further study is needed to clarify what components in soil organic matters and lignosulfonate cause the inhibition of the pozzolanic reaction, both organic matters may contain common specific components that inhibit the pozzolanic reaction, such as sulfur-bearing components.

In addition, the investigation on the effect of lignosulfonate to the structure of C-S-H suggests the possibility of lignosulfonate, soil organic matters, to influence the strength development of construction materials, even they do not inhibit the pozzolanic reaction. It is because, Ca/Si ratio of C-S-H is known to affect the strength development of construction materials [38], hence incorporation of soil organic matters to C-S-H may similarly affect the strengths.

4.5. Conclusions

C-S-H synthesis via the pozzolanic reaction with lignosulfonate at escalating dosages, illustrated the existence of a threshold of the dosage that inhibits the pozzolanic reaction. The lower initial Ca/Si ratio of C-S-H needed higher amount of lignosulfonate to reach the threshold. The inhibition of the pozzolanic reaction with a model organic matter was experimentally illustrated. Below the threshold, C-S-H formed and increment in lignosulfonate dosage converged Ca/Si ratio of C-S-H to a value regardless to initial Ca/Si ratio. Increase in lignosulfonate dosage is speculated to uniformly modify the secondary

phases formation. Also, structural stacking of C-S-H layers disappeared by addition of lignosulfonate.

Over the threshold, C-S-H did not form, with remaining portlandite and amorphous silica. Undefined secondary phase, here named as lignosulfonate-silica phase, consisting of Q^0, Q^1, and Q^2 states of silica formed when the pozzolanic reaction was inhibited. A secondary phases that consist of lignosulfonate and silica may cause the inhibition of the pozzolanic reaction, which may be the impermeable layer that inhibit the hydration of starting materials, or it may inhibit the pozzolanic reaction by constraining the solution composition to oversaturation of portlandite, as it may not consume Ca nor decreases pH that hinder the iteration of the pozzolanic reaction.

The C-S-H synthesis via the pozzolanic reaction well simulated the mineralogical phases assemblage of the steel slag-dredged soil mixtures that did and did not develop strength. Dredged soils that forms soft mixtures must contain specific soil organic matters that inhibit the pozzolanic reaction. The successful simulation suggests the possible existence of common key organic components to inhibit the pozzolanic reaction in soil organic matters in dredged soils and lignosulfonate, such as sulfur-bearing components. In addition, the effect of lignosulfonate to C-S-H structure may imply that even soil organic matters do not inhibit the pozzolanic reaction, they may affect the strength development of soil-employed construction materials by affecting the C-S-H structure.

In conclusion, the investigation on the interaction of soil organic matters with pozzolanic reaction was proved to have a significant implication in utilization of soil wastes as construction materials. We propose that with further studies on clarification of interaction between the soil organic matters and the pozzolanic reaction, the validation of waste soils would be enhanced, which will increase the sustainability of the construction industry.

References

[1]   T. Tsuchida, Y.X. Tang, Estimation of compressive strength of cement-treated marine clays with different initial water contents, Soils Found. 55 (2015) 359–374. https://doi.org/10.1016/j.sandf.2015.02.011.

[2]   Y.T. Kim, J. Ahn, W.J. Han, M.A. Gabr, Experimental evaluation of strength characteristics of stabilized dredged soil, J. Mater. Civ. Eng. 22 (2010) 539–544. https://doi.org/10.1061/(ASCE)MT.1943-5533.0000052.

[3]   N.R. Weerakoon, S. Nishimura, H. Sato, K. Toda, T. Sato, Y. Arai, Stiffness and strength mobilisation in steel-slag-mixed dredged clays in early curing, Proc. Inst. Civ. Eng. - Gr. Improv. (2018) 1–17. https://doi.org/10.1680/jgrim.17.00083.

[4]   S. Lirer, B. Liguori, I. Capasso, A. Flora, D. Caputo, Mechanical and chemical properties of composite materials made of dredged sediments in a fly-ash based geopolymer, J. Environ. Manage. 191 (2017) 1–7. https://doi.org/10.1016/j.jenvman.2017.01.001.

[5]   E. Kiso, M. Tsujii, K. Ito, M. Nakagawa, M. Gomyo, T. Nagatome, Method of dredged soil improvement by mixing with converter steel-making slag, Proc. Civ. Eng. Ocean. 24 (2008) 327–332.

[6]   K. Toda, H. Sato, N. Weerakoon, T. Otake, S. Nishimura, T. Sato, Key factors affecting strength development of steel slag-dredged soil mixtures, Minerals. 8 (2018). https://doi.org/10.3390/min8050174.

[7]   K. Toda, R. Kikuchi, T. Otake, S. Nishimura, Y. Akashi, A. Michihiro, K. Takeshi, T. Sato, Effect of Soil Organic Matters in Dredged Soils to Utilization of their Mixtures Made with a Steel Slag, Materials (Basel). 13 (2020).

[8]   W. Zhu, C.F. Chiu, C.-L. Zhang, K.-L. Zeng, Effect of humic acid on the behaviour of solidified dredged material, Can. Geotech. J. 46 (2009) 1093–1099. https://doi.org/10.1139/T09-045.

[9]   H. Tremblay, J. Duchesne, J. Locat, S. Leroueil, Influence of the nature of organic compounds on fine soil stabilization with cement, Can. Geotech. J. 39 (2002) 535–546. https://doi.org/10.1139/t02-002.

[10] G.-O. Kang, T. Tsuchida, Y.-S. Kim, W.-J. Baek, Influence of humic acid on the strength behavior of cement-treated clay during various curing stages, J. Mater. Civ. Eng. 29 (2017) 1–18. https://doi.org/10.1061/(ASCE)MT.1943-5533.0001919.

[11] M. Kamon, S. Tomohisa, K. Sawa, On stabilization of hedoro by using cement group hardening materials, Zairyo. 432 (1989) 1092–1097.

[12] N.R. Lummer, J. Plank, Combination of lignosulfonate and AMPS ® - co -NNDMA water retention agent — An example for dual synergistic interaction between admixtures in cement, Cem. Concr. Res. 42 (2012) 728–735. https://doi.org/10.1016/j.cemconres.2012.02.009.

[13] M. Bishop, A.R. Barron, Cement hydration inhibition with sucrose, tartaric acid, and lignosulfonate: Analytical and spectroscopic study, Ind. Eng. Chem. Res. 45 (2006) 7042–7049. https://doi.org/10.1021/ie060806t.

[14] N.L. Thomas, J.D. Birchall, The retarding action of sugars on cement hydration, Cem. Concr. Res. 13 (1983) 830–842.

[15] V.S. Ramachandran, Interaction of calcium lignosulfonate with tricalcium silicate, hydrated tricalcium silicate, and calcium hydroxide, Cem. Concr. Res. 2 (1972) 179–194. https://doi.org/10.1016/0008-8846(72)90040-3.

[16] V.S. Ramachandran, M.S. Lowery, Conduction calorimetric investigation of the effect of retarders on the hydration of Portland cement, Thermochim. Acta. 195 (1992) 373–387. https://doi.org/10.1016/0040-6031(92)80081-7.

[17] Y.F. Houst, P. Bowen, F. Perche, A. Kauppi, P. Borget, L. Galmiche, J. Le Meins, F. Lafuma, R.J. Flatt, I. Schober, P.F.G. Ban, D.S. Swift, B.O. Myrvold, B.G. Petersen, K. Reknes, Design and function of novel superplasticizers for more durable high performance concrete (superplast project), 38 (2008) 1197–1209. https://doi.org/10.1016/j.cemconres.2008.04.007.

[18] K. Yoshioka, E.I. Tazawa, K. Kawai, T. Enohata, Adsorption characteristics of superplasticizers on cement component minerals, Cem. Concr. Res. 32 (2002) 1507–1513. https://doi.org/10.1016/S0008-8846(02)00782-2.

[19] L. Ferrari, J. Kaufmann, F. Winnefeld, J. Plank, Interaction of cement model systems with superplasticizers investigated by atomic force microscopy , zeta potential , and adsorption measurements, J. Colloid Interface Sci. 347 (2010) 15–24. https://doi.org/10.1016/j.jcis.2010.03.005.

[20] M.Y.A. Mollah, W. Yu, R. Schennach, D.L. Cocke, Fourier transform infrared spectroscopic investigation of the early hydration of Portland cement and the influence of sodium lignosulfonate, Cem. Concr. Res. 30 (2000) 267–273. https://doi.org/10.1007/978-3-030-00937-3_18.

[21] B. Lothenbach, A. Nonat, Calcium silicate hydrates: Solid and liquid phase composition, Cem. Concr. Res. 78 (2015) 57–70. https://doi.org/10.1016/j.cemconres.2015.03.019.

[22] H. Viallis-Terrisse, A. Nonat, J.C. Petit, Zeta-potential study of calcium silicate hydrates interacting with alkaline cations, J. Colloid Interface Sci. 244 (2001) 58–65. https://doi.org/10.1006/jcis.2001.7897.

[23] F. Matsushita, Y. Aono, S. Shibata, Calcium silicate structure and carbonation shrinkage of a tobermorite-based material, Cem. Concr. Res. 34 (2004) 1251–1257. https://doi.org/10.1016/j.cemconres.2003.12.016.

[24] M.D. Andersen, H.J. Jakobsen, J. Skibsted, Characterization of white Portland cement hydration and the C-S-H structure in the presence of sodium aluminate by 27Al and 29Si MAS NMR spectroscopy, Cem. Concr. Res. 34 (2004) 857–868. https://doi.org/10.1016/j.cemconres.2003.10.009.

[25] E. Lippmaa, M. Magi, A. Samoson, G. Engelhard, A.R. Grimmer, Structural Studies of Silicates by Solid-State High-Resolution 29Si NMR, J. Am. Chem. Soc. 102 (1980) 4889–4893. https://doi.org/10.1021/ja00535a008.

[26] M. Mägi, E. Lippmaa, A. Samoson, G. Engelhardt, A.R. Grimmer, Solid-state high-resolution silicon-29 chemical shifts in silicates, J. Phys. Chem. 88 (1984) 1518–1522. https://doi.org/10.1021/j150652a015.

[27] I. Klur, B. Pollet, J. Virlet, A. Nonat, C-S-H Structure Evolution with Calcium Content by Multinuclear NMR, in: P. Colombet, H. Zanni, A.-R. Grimmer, P. Sozzani (Eds.), Nucl.

Magn. Reson. Spectrosc. Cem. Mater., Springer Berlin Heidelberg, Berlin, Heidelberg, 1998: pp. 119–141.

[28]   X.D. Cong, R.J. Kirkpatrick, S. Diamond, 29Si MAS NMR spectroscopic investigation of alkali silica reaction product gels, Cem. Concr. Res. 23 (1993) 811–823. https://doi.org/10.1016/0008-8846(93)90035-8.

[29]   G.E. Maciel, D.W. Sindorf, Silicon-29 Nuclear Magnetic Resonance Study of the Surface of Silica Gel by Cross Polarization and Magic-Angle Spinning, J. Am. Chem. Soc. 102 (1980) 7606–7607. https://doi.org/10.1021/ja00545a056.

[30]   W. Lutz, D. Täschner, R. Kurzhals, D. Heidemann, W. Lutz, D. Täschner, R. Kurzhals, D. Heidemann, C.H. Characterization, Characterization of Silica Gels by 29Si MAS NMR and IR Spectroscopic Measurements To cite this version : HAL Id : hal-00509231, J. Inorg. Gen. Chem. 635 (2009) 2191–2196.

[31]   X. Cong, R.J. Kirkpatrick, 29Si MAS NMR study of the structure of calcium silicate hydrate, Adv. Cem. Based Mater. 3 (1996) 144–156. https://doi.org/10.1016/s1065-7355(96)90046-2.

[32]   I.G. Richardson, Model structures for C- (A) -S-H (I), Arta Crystallogr. Sect. B Struct. Sci. Cryst. Eng. Mater. B70 (2014) 903–923. https://doi.org/10.1107/S2052520614021982.

[33]   S. Grangeon, F. Claret, Y. Linard, C. Chiaberge, X-ray diffraction: A powerful tool to probe and understand the structure of nanocrystalline calcium silicate hydrates, Acta Crystallogr. Sect. B Struct. Sci. Cryst. Eng. Mater. 69 (2013) 465–473. https://doi.org/10.1107/S2052519213021155.

[34]   H. Matsuyama, J.F. Young, Intercalation of Polymers in Calcium Silicate Hydrate: A New Synthetic Approach to Biocomposites?, Chem. Mater. 11 (1999) 16–19. https://doi.org/10.1021/cm980549l.

[35]   H. Matsuyama, J.F. Young, Synthesis of calcium silicate hydrate/polymer complexes: Part I. Anionic and nonionic polymers, J. Mater. Res. 14 (1999) 3379–3388.

[36]   G.B. Alexander, W.M. Heston, R.K. Iler, The solubility of amorphous silica in water, J. Phys. Chem. 58 (1954) 453–455. https://doi.org/10.1021/j150516a002.

[37]   M.S. Tang, H. Su-Fen, Effect of Ca(OH)2 on Alkali-Silica Reaction, in: Proc. Eight Int. Congr. Cem. Chem., 1980: pp. 94–99.

[38]   W. Kunther, S. Ferreiro, J. Skibsted, Influence of the Ca/Si ratio on the compressive strength of cementitious calcium-silicate-hydrate binders, J. Mater. Chem. A. 5 (2017) 17401–17412. https://doi.org/10.1039/c7ta06104h.

5. Key components in organic reagents on the inhibition of the pozzolanic reaction

Abstract

Soil organic matters are suggested to inhibit the pozzolanic reaction, that determine the strength development of soil-employed construction materials. The effect of four organic reagents, Aldrich humic acid (HA), lignosulfonate, lignin, and Wako HA on the pozzolanic reaction with initial Ca/Si ratio of 1.6 is investigated, by characterization of organic reagents and synthesized products.

At equal synthesis period but escalation in the amount of organic reagents addition, from 0 to 56 wt.% with increment of ca. 10 wt.%, C-S-H formation was inhibited explicitly with thresholds, except Wako HA added series that had low solubility. The organic reagent dosage at the thresholds were different between three organic reagents, that indicated the specific organic components that play a key role in the inhibition of the pozzolanic reaction, undeterminable from the total dosage of organic reagents. At the thresholds, the abundancy of reduced sulfur was at similar values. Reduced sulfur was speculated to trigger the inhibition of the pozzolanic reaction, when organic reagents are soluble in the system, that let key components such as reduced sulfur to interact with the pozzolanic reaction.

Keywords: pozzolanic reaction, soil organic matters, C-S-H, formation threshold

5.1. Introduction

Soil organic matters inhibit hardening of soil-employed construction materials. Steel slag-dredged soil mixtures are an example of such materials. The strength development of steel slag-dredged soil mixtures is caused by the formation of calcium silicate hydrates (C-S-H) as a major secondary phase via the pozzolanic reaction. Soil organic matters are known

to inhibit the pozzolanic reaction, that was revealed in Chapter 4. The inhibition of the pozzolanic reaction results in soft mixtures, disadvantageous to utilize as construction materials. From comparison of the elemental composition of the extracted soil organic matters from dredged soils, difference in its composition, such as sulfur content, was able to distinguish dredged soils that form soft mixtures. Therefore, content of specific soil organic matters in dredged soils was speculated to determine their effect on the pozzolanic reaction. However, the key components in soil organic matters that plays a key role on the inhibition of the pozzolanic reaction was not clarified.

This study aims to clarify the key components, by comparing the effectiveness of four organic reagents, Aldrich humic acid (HA), lignosulfonate, lignin, and Wako HA, on the inhibition of the pozzolanic reaction. It is evaluated through C-S-H synthesis via the pozzolanic reaction in coexistence of each organic reagents with escalation in the dosage. The Ca/Si ratio of C-S-H synthesis was fixed at 1.6, to compare the effect of organic reagents to the pozzolanic reaction. The Ca/Si ratio of 1.6 was chosen as C-S-H with high Ca/Si is expected to form at early stage of curing in steel slag-dredged soil mixtures, like cementitious composites [1]. Organic reagents are expected to inhibit the C-S-H formation at different dosages, which would lead to the interpretation of the effectiveness of each reagent to the inhibition of the pozzolanic reaction. Organic reagents were characterized in terms of elemental composition, carbon speciation, oxidation state of sulfur, and the content of acidic functional groups. Those characteristics were compared between organic reagents regarding to their ability to inhibit the pozzolanic reaction. The key component in soil organic matters that play a key role in the inhibition of the pozzolanic reaction was interpreted.

5.2. Materials and methods

5.2.1. C-S-H synthesis

C-S-H with Ca/Si of 1.6 was synthesized with Aerosil 200 (Nippon Aerosil Co. Ltd.) and portlandite (Wako Pure Chemicals Inc.) for Si and Ca sources, respectively. As received Aldrich humic acid (Aldrich HA) (Sigma-Aldrich Corp.), Lignin alkali (lignin) (Tokyo Chemical Industry Co. Ltd.), and Wako humic acid (Wako HA) (Wako Pure Chemicals Inc.) were used for the C-S-H synthesis. Sodium lignosulfonate (lignosulfonate) (Tokyo Chemical Industry Co. Ltd.) used in C-S-H synthesis experiment in Chapter 4, with initial Ca/Si ration of 1.6 are shown on this chapter, to make comparison of the effectiveness of four organic reagents to the pozzolanic reaction. The selection of soil organic reagents was chosen based on their compositional similarity to the soil organic matters, where Aldrich HA and Wako HA are the humic acids extracted from soils and lignosulfonate and lignin are organic reagents derived from natural woods.

C-S-H syntheses were carried out with solid to liquid ratio of 1:20, at 50 ℃, on 100 rpm shaker with synthesis duration of 10 days. Initially, amorphous silica, an organic reagent and deionized water were weighed into a polyethylene container and mixed until homogenous. After, weighed portlandite was added to the container then mixed, then the samples were set onto the shaker.

C-S-H was synthesized in the presence of 0 to 56 wt.% of organic reagents, in steps of ca. 10 wt.%, by mass ratio against total mass of amorphous silica and portlandite. Solid products were collected by centrifugation at 3000 rpm for 40 minutes, then freeze-dried and grinded to obtain powder samples. Supernatant solutions were filtrated by 0.2 μm filter before conducting subsequent analyses.

5.2.2. Characterization of solid synthesized products and their solution chemistry

X-ray diffraction (XRD) was conducted to solid samples after synthesis to determine the mineralogical compositions, using RINT2100 X-ray diffractometer (Rigaku) equipped for CuKα radiation at 30 kV and 20 mA. Randomly oriented powder samples pulverized under 53μm were scanned from 2 to 70° 2θ at a scanning speed of 0.02°/s.

Ca and Si concentrations in the supernatant solutions were measured by inductively coupled plasma-atomic emission spectroscopy (ICP-AES; ICPE-9000, Shimadzu). pH was also recorded for the same solutions. Dissolved organic carbon (DOC) was measured by total organic carbon analyzer (TOC; TOC-L, Shimadzu).

5.2.3. Characterization of organic reagents

5.2.3.1. Elemental composition

Analyses of C, H, N, and S contents of purified Aldrich HA, lignosulfonate, and lignin, and as received Wako HA were carried out at the Center for Instrumental Analysis at Hokkaido University. Prior to the analyses, the powdered organic reagents were dehydrated under reduced pressure for at least 24 hours. The C, H, and N contents were measured by an elemental analyzer (CE440, Exeter Analyzer, Warwickshire, UK). About 2 mg of sample was used for the measurement and WO_3 was added as a combustion aid for the C, H, and N analysis. The maximum permissive error for measurement of C, H, and N contents was ±0.3%. S in organic reagent was oxidized by the combustion flask method [2]. Those sulfate ions, which were absorbed to aqueous H_2O_2, were analyzed using ion chromatography (Dionex ICS-1600, Thermo Fischer Scientific, Waltham, MA, US). About 2 mg of organic reagent was used for a measurement. The maximum permissive error of measurement of S content was ±0.3%. The content of oxygen was calculated by subtracting the sum of the quantified percentage of C, H, N, and S from 100%.

5.2.3.2. Solid-state ^{13}C Cross-Polarization/Magic-Angle Spinning Nuclear Magnetic Resonance (CP/MAS NMR)

Solid-state ^{13}C CP/MAS NMR spectra were obtained with Bruker DCX-300 spectrometer at a field strength corresponding to 75.5 MHz using a 4-mm CPMAS probe. Samples were packed into 4 mm rotor. The acquisition parameters were as follows: spectral frequency, 99.4 MHz; contact time, 1 ms; pulse delay, 4 s; scan times, 16000; spinning rate, 8 kHz; line-

broadening, 50 Hz. Peak assignment and integration of spectra were carried out following chemical shift regions [3–5] as alkyl carbon (alkyl-C):0–45 ppm, alkyl carbon attached to N,O (N,O-alkyl C): 45–60 ppm, alkyl carbon attached to oxygen derived from polysaccharide (polysaccharide-C):60–110 ppm, aromatic and/or olefinic carbon attached to hydrogen or carbon (aromatic-C-H, C-C):110–140 ppm, aromatic and/or olefinic carbon attached to oxygen (aromatic-(C-O):140–160 ppm, and carboxyl and ketones (carbonyl-C): 160–220 ppm. Aliphaticity to aromaticity ratio was also calculated with classification of chemical shift region of 0 to 110 ppm and 110 to 160 ppm, respectively.

5.2.3.3. *Sulfur K-edge X-ray Adsorption Near Edge Structure (XANES)*

XANES measurement was carried out at Beamline BL-11B at the Photon Factory in Tsukuba, Japan. Ni-coated focus mirror and Si (111) double-crystal monochromator were used to produce a monochromatic X-ray. Aldrich HA, lignosulfonate, lignin, and Wako HA were measured in total electron yield mode. The reference materials, pyrite, cysteine, L-cystine, methionine sulfoxide, cysteic acid, and Na_2SO_4 were measured in total electron yield mode. Reference materials were obtained from FUJIFILM Wako Pure Chemical Corp. (Osaka, Japan), Kanto Chemical Co., Inc. (Tokyo, Japan), or Tokyo Chemical Industries, Co.,Ltd. (Tokyo, Japan). Organic reagents and reference materials were ground thoroughly and mounted on nickel plate by spreading the sample thinly on carbon tape to set in vacuum chamber (~1×10^{-7} Bar.) at ambient temperature for the measurement. The data were collected in the energy range of 2460 to 2510 eV, which 2460 to 2465 eV was measured in step width of 0.5 eV, 2465 to 2490 eV with step width of 0.1 eV and 2490 to 2510 eV with step width of 0.5 eV, with duration of data acquisition at each step of 1 second. The S K-edge XANES data analysis was done with program Athena Version 0.9.26. Energy calibration of acquired XANES spectra were done by setting the whiteline maximum of Na_2SO_4 to 2480.0 eV which then the data were processed for background correction. Subsequently, linear combination fitting was carried out to quantify the abundancy of sulfur

oxidation species of organic reagents. All reference materials were set as fitting components at the process of linear combination fitting.

5.2.3.4. Acidic functional groups

Total acidity and carboxylic group contents were measured using the $Ba(OH)_2$ and $Ca(CH_3COO)_2$ methods, respectively [6]. The phenolic hydroxyl group content was calculated by subtracting the carboxyl group content from total acidity.

Total acidity measurement was conducted as follows. An aliquot (20–50 mg) of dialyzed organic reagent was placed in an round-bottom flask and 20 mL of 0.1 N $Ba(OH)_2$ solution was added. A blank sample in the absence of organic reagents was set up simultaneously. The air in each flask was displaced by N_2 and a soda lime tube was used as cap of flask to prevent CO_2 contamination. After shaking for 24 h at 25 °C, the solution was filtered through a membrane filter with filter size of 0.45 μ m. The residue on the filter was washed with CO_2-free water, and the filtrate was titrated with 0.25 N HCl solution to pH 8.4 under N_2 by using a pH meter connecting to a glass electrode. The total acidity can be calculated by (5-1):

$$Total\ acidity\ (meqg^{-1}\ of\ C) =$$

$$\{(V_{blank} - V_{sample}) * [HCl])\}/\{(organic\ reagent, mg) * \%C/100\} * 1000\ \text{(5-1)},$$

where V_{blank} and V_{sample} represent titers for blank and sample, respectively.

Carboxylic group content was measured as follows. An aliquot (20–50 mg) of organic reagent was placed to an round-bottom flask and 10 mL of 0.5 N $Ca(CH_3COO)_2$ solution was added. A blank sample in the absence of HS was set up simultaneously. As described above, the sample was shaken under CO_2-free conditions. After the filtration step, the filtrate was titrated with 0.05 N NaOH solution to pH 9.8 under N_2 by using a pH meter connecting to a glass electrode. The COOH content can be calculated with (5-2):

$$COOH\ content\ (meqg^{-1}\ of\ C) =$$

$$\{(V_{blank} - V_{sample}) * [NaOH])\}/\{(organic\ reagent, mg) * \%C/100\} * 1000\ \text{(5-2)}$$

The measurement of total acidity and carboxylic groups were repeated four times to calculate average values and standard errors of the measurements. The total acidity and carboxylic group content of Aldrich HA reported on [7,8] were used for the comparison which the average value was calculated with standard errors.

5.3. Results

5.3.1. XRD of C-S-H synthesis products

XRD patterns of synthesized products are shown in **Fig.** 5-1. C-S-H formed in the range of organic reagents dosage between 0 to 15 wt.%, 0 to 29 wt.% and, 0 to 47 wt.%, in the Aldrich HA, lignosulfonate, and lignin added series, respectively. Wako HA did not inhibit the formation of C-S-H in the dosage between 0 to 56 wt.%. Inhibition of C-S-H formation is confirmed by XRD patterns consisting of portlandite peaks with broad diffraction of amorphous silica around 2.6-5.9Å (15-35 °2θ(CuKa)). Because of the abrupt change in the XRD patterns from C-S-H to portlandite and amorphous silica, there appear to be the thresholds for the organic reagents dosage in which to inhibit the pozzolanic reaction. Aldrich HA was most effective in inhibiting the pozzolanic reaction, followed by lignosulfonate, lignin, and Wako HA.
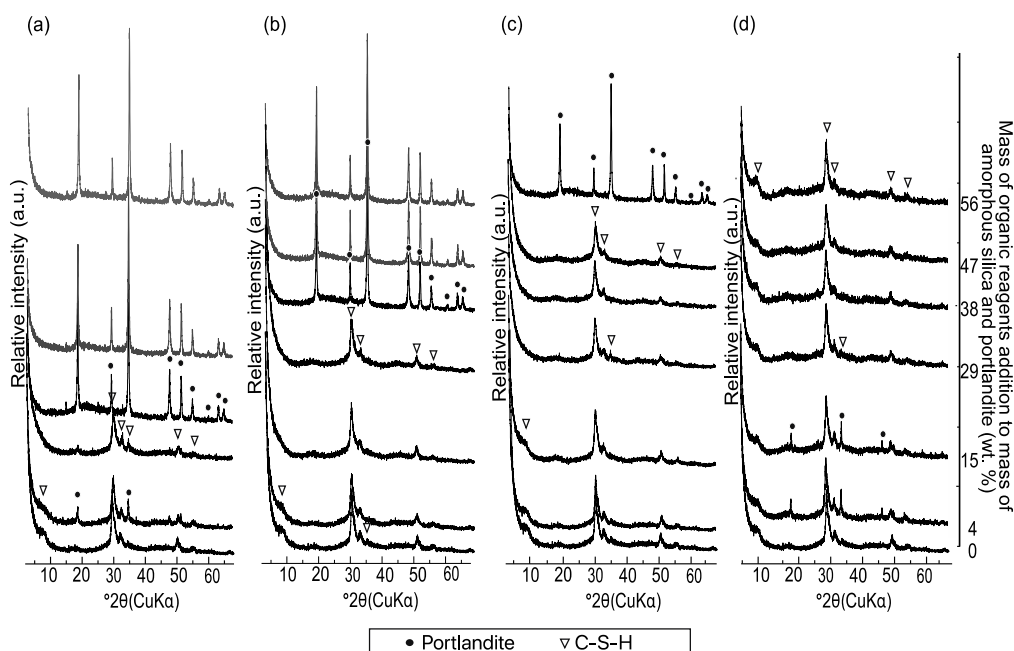
Fig. 5-1 XRD profiles of synthesized products, with (a) Aldrich HA, (b) lignosulfonate, (c) lignin, and (d) Wako HA with increment in the dosage of the reagents. Vertical axis shows the weight percentage of organic reagents against the sum of amorphous silica and portlandite added in the systems.

In addition, as discussed in Chapter 4, the maxima of XRD diffraction corresponding to basal spacing of C-S-H, which appears at 11.2-13.5Å (6.5-7.9°2θ(CuKa)), decreases and disappears as the Aldrich HA, lignosulfonate, and lignin dosage increased. Wako HA did not show the decrease or disappearance of the peak.

5.3.2. *Solution chemistry after C-S-H synthesis*

Calcium, silica and DOC concentrations and pH of solutions after synthesis are shown in **Fig. 5-2**. pH of the solutions in all organic reagent series were around 12.5 regardless to the dosage of organic reagents.

DOC in the solutions increased as organic reagents dosage increased. Gradient of DOC concentration as a function of organic reagent dosage was steeper in the lignin series than

lignosulfonate and Aldrich HA series. Wako HA only slightly increased in DOC concentration. The concentration of DOC at 56 wt.% dosage was 0.17, 0.50, 0.18, and 0.02 mol/L in Aldrich HA, lignosulfonate, lignin, and Wako HA added systems, respectively. Lignosulfonate series increased in DOC concentration drastically after the threshold of C-S-H formation. Whereas, Aldrich HA and lignin did not show the same trend, as the DOC concentration constantly increased. Wako HA did show low increment in DOC concentration, which may result from low solubility of the reagent itself, which was noticed from Wako HA powder remaining undissolved after the synthesis.

Dissolved Ca concentrations were 18.5 mmol/L without organic reagent addition. Dissolved Ca concentration decreased as a function of organic reagent addition in all series, except for the conditions where C-S-H did not form in 38 to 56 wt.% of lignosulfonate addition, and 56 wt.% of lignin addition.

Dissolved Si concentrations were 0.02 mmol/L without organic reagent addition. In all the series, Si concentration was constrained at ca. 0.02 mmol/L while C-S-H was forming. Similarly, Si concentration increased as a function of organic reagent dosage in all series over the threshold of the C-S-H formation. After the C-S-H formation thresholds, Aldrich HA series showed Si concentration between 0.04 to 0.37 mmol/L. Similarly, lignosulfonate series showed Si concentration from 0.20 to 0.70 mmol/L. Lastly, lignin series showed Si concentration of 0.14 mmol/L.
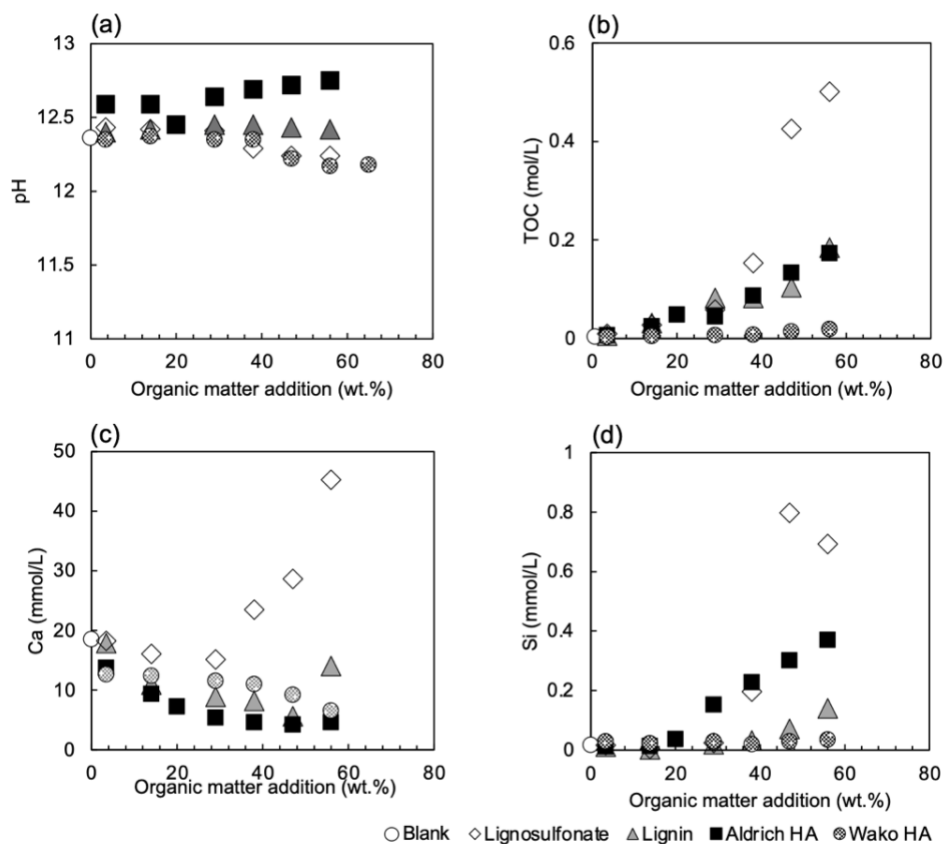
Fig. 5-2 Changes in solution chemistry as a function added weight percentage of organic reagents against amorphous silica and portlandite used in the synthesis (wt.%). Each graph shows (a) pH, (b) Dissolved organic carbon (DOC), (c) calcium concentration and (d) silica concentration of solutions collected after C-S-H synthesis.

5.3.3. Characterization of organic reagents

5.3.3.1. Elemental composition of organic reagents

Elemental analysis data of organic reagents are summarized in **Table 5-1**. C, H, O, and S contents of organic reagents and N content of Aldrich HA and Wako HA was in the range of soil organic matters [9] Nitrogen was under the detection limit for lignosulfonate and lignin, which were not in the range of soil organic matters. No specific elemental

content of organic reagent correlated to their order of the effectiveness to the inhibition of the pozzolanic reaction.

Table 5-1 The elemental compositions of organic reagents.

Samples	Elemental composition (wt.%)					Ash content (wt.%)
	C	H	N	S	O	
Aldrich HA	55.89	4.42	0.86	1.87	37.0	n.d. [1]
Lignosulfonate	47.74	5.21	n.d.[1]	6.78	37.28	3.02
Lignin	56.99	5.04	n.d.[1]	3.04	34.9	n.d. [1]
Wako HA	50.73	3.21	0.98	0.83	27.9	16.4

[1] Not detected. The detection limit of elemental analysis was 0.3 wt.%.

5.3.3.2. Carbon functional groups

The ^{13}C CPMAS NMR spectra of lignosulfonate, lignin, and Wako HA are shown in **Fig. 5-3**. Relative compositions of different carbon functional groups estimated from integration of the spectra and that of Aldrich HA reported on [3] are shown in **Table 5-2**. All organic reagents composed of various carbon functional groups where the abundancy of each groups was different. However, no content of specific carbon functional groups correlated to the trend of the effectiveness of organic reagents to the inhibition of the pozzolanic reaction.
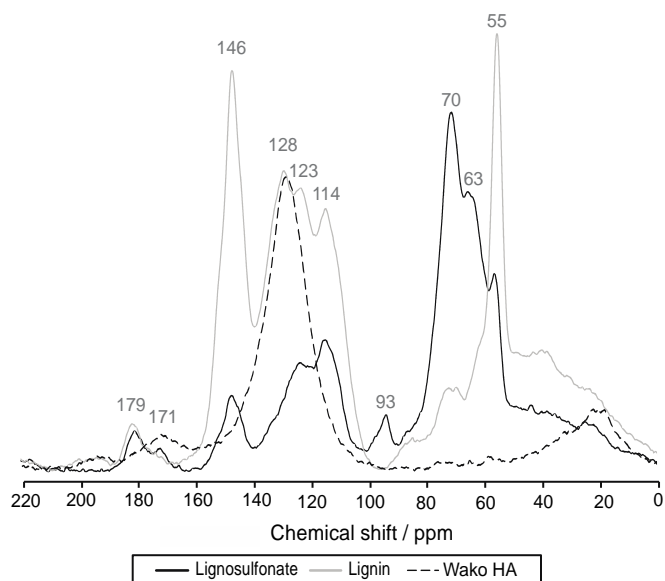
Fig. 5-3 ^{13}C CP MAS NMR spectra of organic reagents. Numbers above the spectra show the chemical shifts of the maxima.

Table 5-2 Relative compositions of different carbon functional groups estimated from solid-state ^{13}C NMR spectra of organic reagents.

Sample	Composition (%)					
	Carbonyl C	Aromatic- or olefin- (C-O)	Aromatic- or olefin- (C-H, C-C)	Polysaccharide	N,O- alkyl- C	Alkyl C
Aldrich HA[1]	12.7	10.8	24.9	8.2	4.5	38.9
Lignosulfonate	3.4	5.1	18.6	46.6	15.8	10.6
Lignin	3.5	18.2	34.8	13.1	17.6	12.9
Wako HA	9.4	9.4	58.8	3.7	1.9	17.0

[1] data from Yabuta et al., (2008)[3].

5.3.3.3. Sulfur redox state

The S XANES spectra of Aldrich HA, lignosulfonate, lignin, and Wako HA are shown in **Fig. 5-4** with square plots. The plots are fitted with standards, which the fit is shown with black bold line. Aldrich HA and Wako HA were relatively richer in reduced form of sulfur in comparison with lignosulfonate and lignin. The result of the quantification of sulfur of reduced (RSSR' and RSH), intermediate (RSOR' and RSO_3^-), and oxidized (SO_4^{2-}) form are shown in **Table 5-3**. Organic reagents mostly composed of reduced or intermediate oxidation states of sulfur, except Wako HA which also composed of significant amount of oxidized sulfur. Content of reduced sulfur was richest in Aldrich HA, followed by Wako HA, lignin, and lignosulfonate. The percent of reduced sulfur of each organic reagent were 51.3, 47.8, 12.2, and 9.0%, respectively. Intermediate oxidation state of sulfur was richest in lignosulfonate, followed by lignin, Aldrich HA, and Wako HA with 91.0, 88.8, 46.7, and 27.3% of the content, respectively. Oxidized form of sulfur was not detected in lignosulfonate and lignin. Wako HA and Aldrich HA contained 24.9 and 2.0% of oxidized sulfur, respectively.
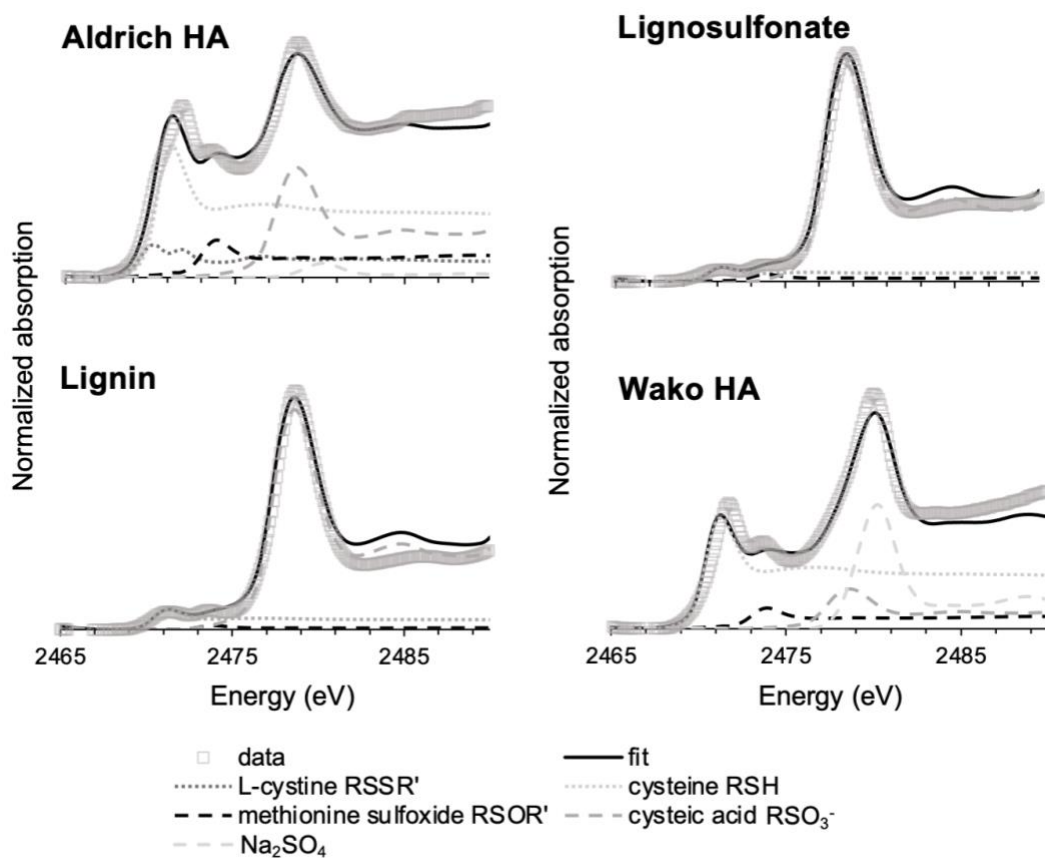
Fig. 5-4 S-K edge XANES spectra of organic reagents. Dashed lines show the reference materials used for linear combination fitting to quantify the redox states of sulfur in organic reagents samples.

Table 5-3 The abundancy of sulfur in oxidized, intermediate, and reduced form calculated from linear combination fitting of S XANES spectra of organic reagents. Oxidized fraction was calculated from peak areas of Na$_2$SO$_4$, intermediate fraction from cysteic acid and methionine sulfoxide and reduced fraction from cysteine and L-cystine.

Redox state	Aldrich HA	Lignosulfonate	Lignin	Wako HA
	Percent of S species (%)			
Oxidized	2.0	n.d.	n.d.	24.9
Intermediate	46.7	91.0	88.8	27.3
Reduced	51.3	9.0	11.2	47.8

5.3.3.4. *Acidic functional groups*

Content of total acidity, carboxylic group, and phenolic group of Aldrich HA, lignosulfonate, and lignin are shown in **Table 5-4**. Total acidity and carboxylic group content of Wako HA were not measured due to their low solubility. Total acidity of Aldrich HA was higher compared to those of lignosulfonate and lignin, both of which were not statistically different. Carboxylic group content was highest in Aldrich HA, followed by lignin and lignosulfonate. Phenolic group content, the difference of total acidity and carboxylic group content, was also not statistically different. The content of carboxylic group, total acidity and phenolic group content did not correlate to the effectiveness of organic reagents to the inhibition of the pozzolanic reaction.

Table 5-4 Total acidity and carboxylic group contents (mequiv/g dry organic reagent) of organic reagents.

Samples	Total acidity	Carboxylic group	Phenolic group
		mequiv/g	
Aldrich HA[1]	7.23±0.75	4.40±0.46	2.86±0.88
Lignosulfonate	1.80±0.53	0.70±0.15	1.11±0.55
Lignin	1.96±0.16	1.50±0.10	0.46±0.19

[1]Calculated from Saito et al., (1980) and Andjelkovic et al., (2006) [7,8].

5.4. Discussion

5.4.1.1. *C-S-H formation thresholds*

The inhibition of the pozzolanic reaction occurred at different thresholds in the dosage of organic reagents, between Aldrich HA, lignosulfonate, lignin, and Wako HA (**Fig.** 5-1). The content of effective organic components to the inhibition of the pozzolanic reaction is suggested to differ between four organic reagents. The effect of organic reagents to the structure of C-S-H is expected to be similar between organic reagents, that interferes with layer stacking of C-S-H, as discussed in Chapter 4.

The causes of the inhibition of the pozzolanic reaction were discussed to originate in the ability of organic matters to (1) buffer the pH to undersaturate against C-S-H; (2) formation of Ca-organic complex to take up Ca and (3) formation of secondary phases that may be impermeable and inhibits the hydration or constrain the solution composition and thermodynamically inhibits the pozzolanic reaction.

Same as the systems investigated in Chapter 2, 3 and 4, organic reagents under the experimental conditions of this study also did not buffer the pH of solutions. The Ca-organic complex formation was insignificant to suppress the Ca supply to the pozzolanic reaction. DOC and Ca concentration was not correlated in Aldrich HA series, in samples over the

threshold of the C-S-H formation. Ca concentrations of the samples over the C-S-H formation thresholds did not show the same trend between organic reagents as a function of the dosage. Lignosulfonate and lignin increased Ca concentration in solution as a function of its dosage over the C-S-H formation threshold though Aldrich HA showed the opposite trend. The interaction of organic reagents and Ca could partition their complex to solid phases, but as discussed in Chapter 4, Ca-organic reagent complex may not be the major cause of the inhibition of the pozzolanic reaction. The existence of portlandite suggested the consumption of Ca to the complex formation was not significant to consume all Ca in starting materials that can inhibit Ca supply to the pozzolanic reaction. The Si concentration of the samples over the C-S-H formation thresholds of all organic reagent series was higher in comparison to samples below the thresholds, unlike Ca concentration in solution. The same tendency of Si concentration that increases over the thresholds between all organic reagent series, infer that the effect of organic reagents to the behavior of silica, maybe triggering the inhibition of the pozzolanic reaction, by forming a secondary phase that influence the concentration of Si in solution. It suggests the formation of secondary phases unlike to C-S-H, which may form an impermeable layer or constrain the solution composition that inhibit the pozzolanic reaction. This discussion also supports the research in Chapter 4, which discussed on how organic matters may inhibit the pozzolanic reaction.

5.4.1.2. *Key component in organic reagents*

Key components in organic reagents that inhibit the pozzolanic reaction were investigated by calculating the amount of specific organic components in the batches at the inhibition of the C-S-H formation. Content of each components in organic reagents at 20, 38, and 56 wt.% addition of Aldrich HA, lignosulfonate, and lignin series, respectively, was calculated. The content of specific organic reagent is hypothesized to be close in values between the batches, which should trigger the inhibition of the pozzolanic reaction.

The comparison of the elemental composition, carbon speciation, and carboxylic group content of organic reagents at the thresholds had different contents of each components (i,e., **Fig. 5-5**, shows the abundancy of milliequivalents of carboxylic group against 1 g of amorphous silica and portlandite used in the synthesis, at the thresholds). The content of phenolic groups may lay in similar value at the thresholds, as the standard errors lay over a range of same content.
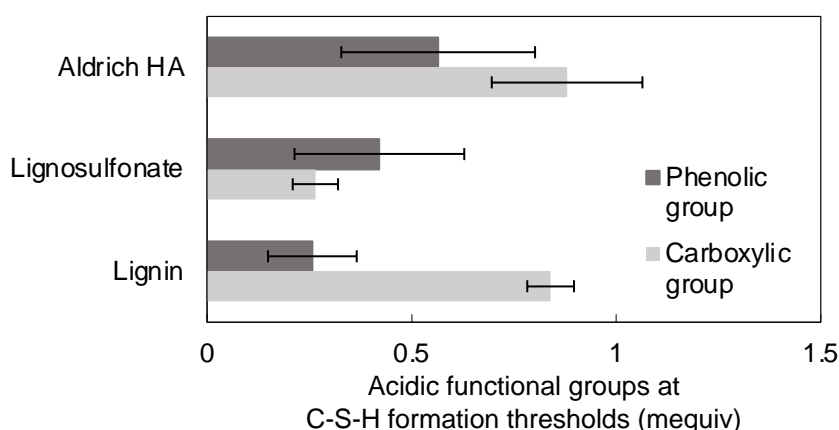
Fig. 5-5 The abundance of acidic functional group at the threshold of C-S-H formation. The content of acidic functional groups was calculated for Aldrich HA, lignosulfonate, and lignin at 20, 38, and 56 wt.% of organic reagent dosages, respectively.

The content of reduced sulfur depicted the thresholds, where the contents showed close values. Reduced sulfur content was 0.19, 0.23, and 0.19 wt.% in Aldrich HA, lignosulfonate, and lignin series, respectively (**Fig. 5-6**). Wako HA, which did not inhibit the formation of C-S-H in the dosage between 0 to 56 wt.%, consisted of 0.12, 0.13, and 0.22 wt.% of oxidized, intermediate, and reduced sulfur, respectively, in the batch of 56 wt.% addition. The amount of reduced sulfur was in the similar value with other organic reagents at the thresholds, though it did not inhibit the pozzolanic reaction. It may result from the insoluble property of Wako HA, that limited the mobility of reduced sulfur. The activity of reduced sulfur was likely retained low compared to other organic reagents that dissolved in the solution. The solubility

of organic matters is determined by the existence of hydrophilic functional groups in the structure.

Overall, the amount of reduced sulfur was suggested as a key component in organic reagents to trigger the inhibition of the pozzolanic reaction. The amount of phenolic group may also be a key component. In addition, the solubility, the abundancy of hydrophilic functional groups in organic reagents, was also suggested important to cause the inhibition of the pozzolanic reaction. The availability of hydrophilic functional groups determines whether soil organic matters can dissolve in solution and affect the pozzolanic reaction. Reduced sulfur is suggested to interact with the pozzolanic reaction, most likely at the surfaces of the solid phases, that forms a secondary phase which may constrain the solution composition or form impermeable layer that inhibit the pozzolanic reaction.
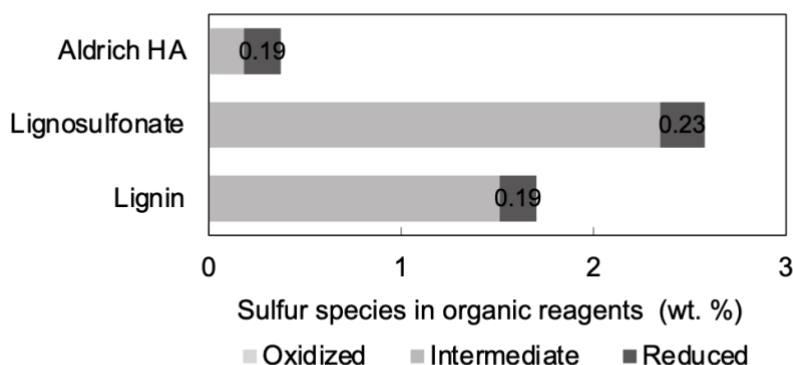
Fig. 5-6 Percent of sulfur oxidation states in organic reagents at the thresholds.

5.5. Conclusions

Four organic reagents caused the inhibition of the pozzolanic reaction at different dosages. Aldrich HA was the most effective organic reagent to the inhibition of the pozzolanic reaction, followed by lignosulfonate, lignin, and Wako HA. The inhibition of the pozzolanic reaction was suggested to result from the formation of secondary phases that forms in coexistence of organic reagents, which either constrain the solution composition or limit the access of water to starting materials that inhibit the hydration.

The components in organic reagents that explained the occurrence of the thresholds was the content of reduced sulfur. Reduced sulfur may play a key role in the inhibition of the pozzolanic reaction. Also, organic reagents with low solubility did not inhibit the pozzolanic reaction, even they contained reduced sulfur. This suggests that the organic reagents must be soluble to water, that enables the key components of organic reagents such as reduced sulfur, to be mobile in the system.

The clarification of the key components in the organic reagents to the inhibition of the pozzolanic reaction is significant in understanding the effective components in soil organic matters that inhibit the pozzolanic reaction. The analysis of the sulfur oxidation states of soil organic matters in waste soils is suggested as a more accurate indicator of the strength development of the mixtures of soils with steel slags. Secondly, this study suggested the possibility to utilize soils that contain organic matters that inhibit the pozzolanic reaction. Existence of the threshold of the dosage in organic matters to inhibit the pozzolanic reaction suggests that addition of other construction materials may enable the utilization of soils. Also, further study to remove or cover the effect of reduced sulfur by additives may enable their utilization.

References

[1]   A. Atkinson, N. Everitt, R. Guppy, Evolution of pH in a radwaste repository: internal reactions between concrete constituents, Harwell, U.K. 20 (1988).

[2]   W. Schoniger, Eine mikroanalytisehe Sehnellbestimmung von Halogen in organischen Substanzen, Microchim. Acta. 43 (1955) 123–129.

[3]   H. Yabuta, M. Fukushima, M. Kawasaki, F. Tanaka, Organic Geochemistry Multiple polar components in poorly-humified humic acids stabilizing free radicals : Carboxyl and nitrogen-containing carbons, Org. Geochem. 39 (2008) 1319–1335. https://doi.org/10.1016/j.orggeochem.2008.05.007.

[4]   H. Knicker, P.G. Hatcher, F.J. González-Vila, Formation of Heteroaromatic Nitrogen after Prolonged Humification of Vascular Plant Remains as Revealed by Nuclear Magnetic Resonance Spectroscopy, J. Environ. Qual. 31 (2002) 444. https://doi.org/10.2134/jeq2002.0444.

[5]   H. Knicker, K.U. Totsche, G. Almendros, F.J. González-Vila, Condensation degree of burnt peat and plant residues and the reliability of solid-state VACP MAS 13C NMR spectra obtained from pyrogenic humic material, Org. Geochem. 36 (2005) 1359–1377. https://doi.org/10.1016/j.orggeochem.2005.06.006.

[6]   M.K. Schnitzer, S.U. Khan, Humic substances in the environment, in: Dekker, New York, 1972: pp. 37–43.

[7]   Y. Saito, S. Hayano, Distribution of Oxygen-Containing Functional Groups and Elements in Humic Acids from Marine Sediments, J. Oceanogr. Soc. Japan. 36 (1980) 59–67.

[8]   T. Andjelkovic, J. Perovic, M. Purenovic, S. Blagojevic, R. Nikolic, D. Andjelkovic, A. Bojic, Spectroscopic and potentiometric studies on derivatized natural humic acid, Anal. Sci. 22 (2006) 1553–1558. https://doi.org/10.2116/analsci.22.1553.

[9]   J.A. Rice, P. MacCarthy, Statistical evaluation of the elemental composition of humic substances, Org. Geochem. 17 (1991) 635–648. https://doi.org/10.1016/0146-6380(91)90006-6.

6. Characterization of humic acids of shallow sea sediments in ports of Japan

Abstract

The utilization of waste soils and industrial byproducts such as dredged soils and steel slags is carried out by mixing the materials together, to apply on construction materials. The mixtures are known to develop strength, though some organic constituents in dredged soils inhibit the strength development of the mixtures, that inhibit the utilization of some dredged soils. The mixtures are known to develop strength by the pozzolanic reaction, that solidifies the mixtures. If the key component in soil organic matters which play a role in the inhibition of the pozzolanic reaction is revealed, the utilization of such soils may become possible. This study focuses on characterizing the soil organic matters in dredged soils in detail, to clarify the specific components that may play a role in the inhibition of the pozzolanic reaction. The content of enriched content of reduced sulfur in soil organic matter fraction was common in dredged soils which formed mixtures without significant strength development. This study also suggested such soils may arise due to the sedimentary conditions which are favorable to conserve polysulfides.

Keywords: Humic acids, marine dredged sediment, cementation

6.1. Introduction

Soil sediments in ports, waterways or dams are dredged frequently to maintain the water depths shallowed by soil particle sedimentation, for safe shipments [1]. Dredged soils are often treated as wastes instead of utilizing as raw materials for construction materials. The

major cause of waste occurrence is the difficultness in improving their physical properties to use them for construction materials. Their physical properties can be improved by addition of alkaline activating materials such as cement, fly-ash, steel slag, CaO and Ca(OH)$_2$ are previously studied [2–7].

Studies on the steel slag and dredged soil mixtures show some dredged soil samples to develop almost no strengths, where other soils do by adding the same steel slags with same mixing ratio and curing duration. Toda et al., 2020 [8] clarified that soil organic matters in dredged soils may inhibit the strength development of the mixtures. Comparison on elemental composition of soil organic matters, humic acids of various dredged soils, stated that higher content of organic sulfur in humic acid fraction can label the dredged soils that exhibit weak or no strength development in comparison with those of dredged soils which develop strengths. Organic sulfur may play a role in inhibiting the strength development of the mixtures or may be positively correlated to the key structure or functional groups which inhibit the strength development of the mixtures. Sulfur in marine sedimentary soils are speciated as sulfide, thiol, sulfonate and sulphate [9,10]. The variation in redox state may infer the reason for organic sulfur enrichment in specific dredged soils and may have different effect to strength development of the mixtures. Soil organic matters has non-stoichiometric structure with various chemical states of carbon composition, from aliphatic to aromatic, with major acidic functional groups of carboxylic and phenolic functional groups which may be correlated to the enrichment of sulfur in humic acids.

The aim of this study is to characterize the humic acids of dredged soils which do and do not develop strengths when mixed with steel slags. Key factors in humic acids which inhibit the strength development of steel slag dredged soil mixtures and factors which may play a role in the occurrence of weak dredged soils is discussed. Characterization of eight humic acids collected in Toda et al., 2018 and 2020 [8,11] are carried out to evaluate sulfur redox state, carbon speciation, and fragment composition.

6.2. Materials

Eight dredged soils used in this study are hereafter named as soil A, B, C, D, E, F, G and H. Strength development variation of steel slag-dredged soil mixtures was compared by forming the mixtures with the same steel slag samples and curing under the same condition. The mixing ratio of steel slag to dredged soils was set to 3:7 in volume, where the water content of dredged soils was normalized as 1.5 times of the respective soil liquid limits with artificial sea water (Aqua Marine for metal corrosion test, Yashima Yakuhin Co., Ltd.). The strength development of the mixtures was measured by uniaxial compressive strength tests. The strength development of dredged soil steel slag mixtures were put into order from strong to weak as follows: Soil A, B, C, E, F and G. Soil A, B, C, D, E and F increased the strengths from during the curing period, but soil F did not increase in its strengths and remained weak [5]. Uniaxial compressive strengths at 28 days of curing were 1070, 810, 660, 480, 250, 30 kPa respective to mixtures made with soil A, B, E, F, C and G (**Table 6-1**). The weakest dredged soils were Soil D and H, which they did not undergo uniaxial compressive strengths tests as demolding the mixture specimen was not successful as the mixtures were not cemented.

Humic acids were extracted from dredged soils A, B, C, D, E, F, G and H. Humic acid samples are hereafter labeled as humic acid (HA) A, B, C, D, E, F, G and H. Humic acids were extracted and purified by dialysis which the method is described on elsewhere [12]. Sulfur content in humic acid fraction was calculated with humic acid quantification and elemental analysis which the data are summarized on **Table 6-1** after Toda et al., 2020. Soil A, B, C, D, E, F, G and H contained 28.3, 54.4, 30.8, 216.9, 18.2, 23.8, 150.7 and 169.0 ppm of sulfur in humic acid fraction, respectively. Humic acid samples were stored in vacuum chamber at least for 24 hours prior to the experiments to eliminate the effect of humidity on their weight measurement.

Table 6-1 Uniaxial compressive strength of steel slag-dredged soil mixtures at 28 days of curing, humic acid content, elemental compositions of humic acids and sulfur content in humic acid fraction of dredged soils (ppm) of soil A, B, C, D, E, F, G and H.

Soils	q_u (kPa)	Humic acid content (wt.%)	Elemental composition of humic acids (%)					Sulfur content (ppm)
			C	H	N	S	O[1]	
Soil A	1070	0.09	45.55	3.61	2.39	3.14	45.31	28.3
Soil B	810	0.20	47.26	4.22	2.73	2.72	43.07	54.4
Soil C	250	0.14	52.03	4.46	2.53	2.20	38.78	30.8
Soil D	n.d.	0.30	41.12	3.57	3.25	7.23	44.83	216.9
Soil E	660	0.16	43.33	3.15	2.13	1.14	50.25	18.2
Soil F	480	0.24	46.17	3.92	2.86	0.99	46.06	23.8
Soil G	30	0.93	51.76	4.12	3.93	1.62	38.57	150.7
Soil H	n.d.	0.24	47.88	4.70	3.92	7.04	36.46	169.0

6.3. Methods

6.3.1. Sulfur K-edge X-ray Adsorption Near Edge Structure (XANES)

XANES experiment was carried out at Beamline BL-11B at the Photon Factory in Tsukuba, Japan. Ni-coated focusing mirror and Si (111) double-crystal monochromator were used to produce a monochromatic X-ray. The reference materials, pyrite, cysteine, L-cystine, methionine sulfoxide, cysteic acid and Na_2SO_4 were measured in total electron yield mode. All reference materials were obtained from FUJIFILM Wako Pure Chemical Corp. (Osaka, Japan), Kanto Chemical Co., Inc. (Tokyo, Japan) or Tokyo Chemical Industries, Co.,Ltd. (Tokyo, Japan). Humic acids A, C, D, E, F and H were measured in fluorescent mode and humic acid B and G in total electron yield mode. Humic acids and reference materials were ground thoroughly and mounted on nickel plate by spreading the sample thinly on carbon tape to set in vacuum chamber (~1×10^{-7} Bar.) at ambient temperature for the measurement.

The data were collected in the energy range of 2460 to 2510 eV, which 2460 to 2465 eV was measured in step width of 0.5 eV, 2465 to 2490 eV with step width of 0.1 eV and 2490 to 2510 eV with step width of 0.5 eV, with duration of each step's data acquisition of 1 second. The S K-edge XANES data analysis was done with program Athena Version 0.9.26. Energy calibration of acquired XANES spectra were done by setting the whiteline maximum of Na2SO4 to 2480.0 eV which then the data were processed for background correction and linear combination fitting to quantify the sulfur oxidation species. All reference materials were set as fitting components on linear combination fitting. The best fit result was picked up for eight humic acid samples.

6.3.2. Solid-state ^{13}C Cross-Polarization/Magic-Angle Spinning Nuclear Magnetic Resonance (CP/MAS NMR)

Solid state ^{13}C CP/MAS NMR spectra were obtained with Bruker DCX-300 spectrometer at a field strength corresponding to 75.5 MHz using a 4-mm CPMAS probe. Samples were packed into 4 mm rotor. The acquisition parameters were as follows: spectral frequency, 99.4 MHz; contact time, 1 ms; pulse delay, 4 s; scan times, 16000; spinning rate, 8 kHz; line-broadening, 50 Hz. Peak assignment and integration of spectra were carried out following chemical shift regions [13–15] as alkyl carbon (alkyl-C):0–45 ppm, alkyl carbon attached to N,O (N,O-alkyl C): 45–60 ppm, alkyl carbon attached to oxygen derived from polysaccharide (polysaccharide-C):60–110 ppm, aromatic and/or olefinic carbon attached to hydrogen or carbon (aromatic-C-H, C-C):110–140 ppm, aromatic and/or olefinic carbon attached to oxygen (aromatic-(C-O):140–160 ppm, and carboxyl and ketones (carbonyl-C): 160–220 ppm. Aliphaticity to aromaticity ratio was also calculated with classification of chemical shift region of 0 to 110 ppm and 110 to 160 ppm, respectively.

6.3.3. Pyrolysis-gas chromatography/mass spectrometry (py-GC/MS)

GC/MS of humic acids were obtained with PY-2020D type Double-Shot Pyrolizer (Frontier Laboratories Ltd.) connected to a Shimadzu GC- 17A/QP5050 type GC/MS system, which pyrolysates were separated with a Quadrex dimethylpolysiloxane (100%) capillary column (0.25 mm x 25 m, 0.25 mm film thickness). A 1.0 ± 0.3 mg of humic acid powder was weighed on a deactivated stainless-steel cup (a 50 ml-volume). A 25 ml aliquot of TMAH in methanol (40 mg/ml) and a 10 ml aliquot of nonadecanoic acid in acetone (0.06 mg/ml) as an internal standard (ISTD) were then added to the cup. Methylation of humic acid by tetramethylammonium hydroxide (TMAH) was employed to reduce the polarity of humic acid components to enable the detection of polar molecules by GC/MS. Solvents were removed under reduced pressure prior to the measurement. After solvent removal, the cup was introduced into the pyrolizer. Helium in 99.995% purity was used as the carrier gas, and the flash pyrolysis of humic acids was carried out at 550 ℃ for 0.4 min. which was then separated in capillary column. The GC oven temperature program was as follows: 50 ℃ for 1.0 min; 50–300 ℃ at a heating rate of 5 ℃/min; 300 ℃ for 5 min. Pyrolysate products detected on GC/MS spectra were assigned by comparison with the library database 107 of National Institute of Standards and Technology (NIST).

6.4. Results and discussion

6.4.1. Reduced sulfur, an indicator of soft mixtures

S K-edge XANES spectra of humic acids are shown on **Fig. 6-1** with the result of linear combination fitting. HA B, C, F and G were fitted with L-cystine, cysteine, cysteic acid and Na_2SO_4. HA A was fitted with pyrite in addition to reference materials used for HA B, C, F and G. HA D, E, and H were fitted with methionine sulfoxide in addition to the reference materials used for HA A.
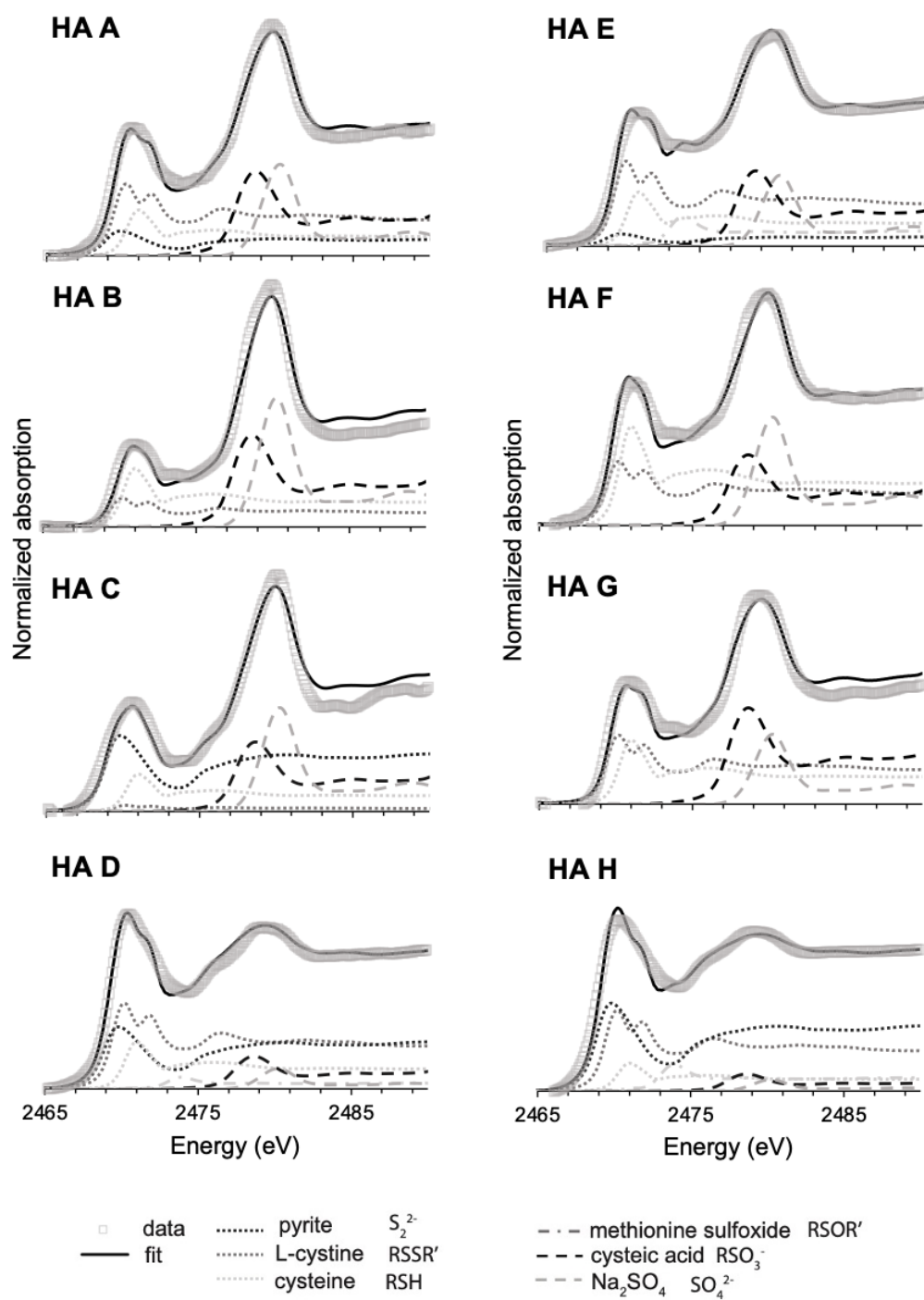
Fig. 6-1 S-K edge XANES spectra of humic acids. Dashed lines show the reference materials used for linear combination fitting to quantify the redox states of sulfur in humic acid samples.

Quantification of sulfur redox state was carried out by classifying reference materials of pyrite, L-cystine and cysteine as reduced sulfur, methionine sulfoxide and cysteic acid as sulfur with intermediate redox state and Na_2SO_4 as oxidized sulfur (**Table 6-2**). All humic acids composed reduced, intermediate, and oxidized sulfur where their proportion varied on the humic acid samples. HA D contained 77.7 % and HA H contained 82.4 % of reduced sulfur, where reduced sulfur fraction of other humic acids varied between 31.7 to 53.8%. Consequently, oxidized sulfur was rather in low concentration in HA D and HA H, which had 3.6 and 2.0 % of $SO4^{2-}$ where that of other humic acids varied between 11.6 to 25.6%. Quantified redox states of sulfur were applied to classify the total sulfur content in humic acids fraction of dredged soils (**Fig. 6-2**). It is clarified that reduced sulfur caused sulfur enrichment in humic acid fraction of dredged soil D and H which contained 169 and 139 ppm, respectively. Dredged soil D and H contained 0.3 and 0.24 wt.% of humic acid in dredged soils, respectively, where other dredged soils except soil F contained 0.24 wt.% or less of humic acids. The sulfur enrichment of sulfur in dredged soil D and H was caused by over 7 wt.% content of sulfur in humic acid composition rather than their humic acid content. Reversely the rich content of sulfur in humic acid fraction of dredged soil F is originating from the 0.94 wt.% content of humic acid. Also, the speciation of sulfur redox state of HA F is rather like that of HA A, B, E, C and F. Hence, high content of sulfur in humic acid fraction in dredged soil F was caused by reduced (66 ppm) and intermediate sulfur (66 ppm), which its enrichment was essentially caused by the content of humic acid itself in dredged soils.

Hence, the existence of reduced (and intermediate) sulfur conservation or addition of humic acids in dredged soil D and H, or the high content of sedimentary humic acids are clarified as the reasons for successful separation of dredged soils which exhibit weak strengths development when mixed with steel slags. The following characterization of humic acids target to extract humic acid components that is enriched in HA D and H.

Table 6-2 The abundancy of sulfur in oxidized, intermediate, and reduced form calculated from linear combination fitting of S XANES spectra of humic acids. Oxidized fraction was calculated from peak areas of Na_2SO_4, intermediate fraction from cysteic acid and methionine sulfoxide and reduced fraction from cysteine, L-cystine and pyrite.

Samples	Oxidized	Intermediate	Reduced
		Percent of S species (%)	
HA A	15.1	32.9	52.0
HA B	25.6	42.6	31.7
HA C	18.0	28.2	53.8
HA D	3.6	18.7	77.7
HA E	11.6	38.2	50.2
HA F	18.8	28.7	52.5
HA G	12.1	44.1	43.8
HA H	2.0	15.6	82.4
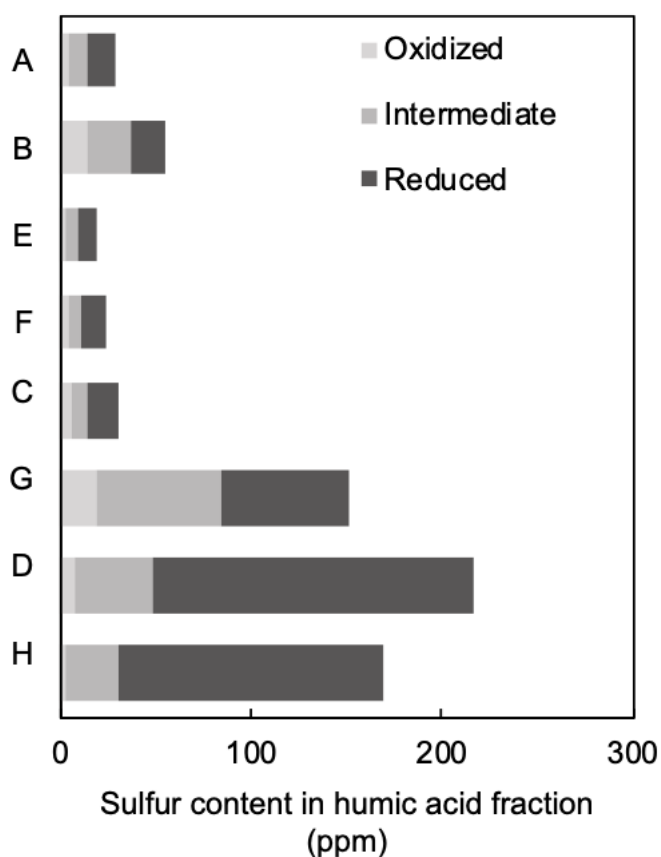
Fig. 6-2 Speciation of sulfur in humic acid fraction of dredged soils. Quantity of classified sulfur redox speciation are plotted on X axis and name of dredged soils are shown on Y axis.

6.4.2. Carbon species of humic acids

To characterize carbon chemical state of humic acids, relative abundance of various carbon species was characterized using solid-state ^{13}C CPMAS NMR. All humic acids consisted of all classification of carbon functional groups (**Fig. 6-3**). Classification of carbon functional groups were divided into carbonyl C (160-220 ppm), aromatic or olefinic C-O (140-160 ppm), aromatic or olefinic C-H and C-C (110-140 ppm), polysaccharide (60-110 ppm), N,O-alkyl C (45-60 ppm) and Alkyl C (0-45 ppm).
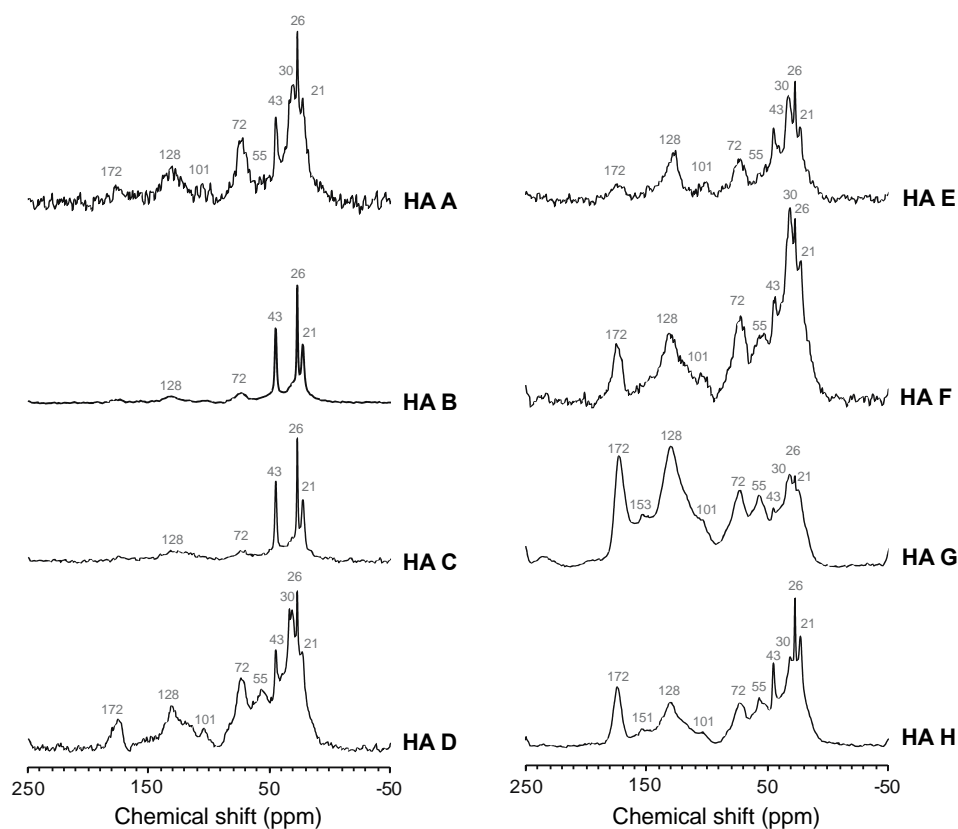
Fig. 6-3 Solid-state 13C CP/MAS NMR spectra of humic acids. The alphabets on the right-hand side of the spectra are the name of humic acid samples. Numbers on the top of spectra indicate the chemical shift of inflection point. The assignment of carbon chemical species are as follows: 21, 26, 30 ,43 ppm: Alkyl-C, 55 ppm: N,O-Alkyl-C,72 ppm: Polysaccharide-C, 101 ppm: Anomeric-C in polysaccharide, 128 ppm: Aromatic-C, 151, 151 ppm: Aromatic- or olefin-(C-O), 172 ppm: Carbonyl-C.

The relative abundance of carbon functional groups was quantified (**Table 6-3**), yet no unique or intensified carbon functional groups were spotted for HA D and H in comparison with other humic acids. Intensity of peak at 128 ppm refers to the degree of humification, which cause the enrichment in aromatic carbon [16], yet the composition of aromatic carbon were not correlated with the enrichment of reduced sulfur in HA D and H. Sugars are known to retard cement hydration [17–19], yet the content of polysaccharides was not enriched in HA D and H. Also, acidic functional groups of organic matters such as carboxylic functional groups are often discussed as the cause of electrostatic interaction between organic polymers with cement hydration reaction [20–22]. However, the composition of carbonyl carbon was not enriched in HA D and H. Due to the limitation of humic acid samples, the titration experiments for acidic functional groups were not carried out. However, as discussed in Chapter 5, the content of phenolic groups may correlate to the strength development degree of the mixtures. Therefore, in further studies, it is recommended to conduct acidic functional groups quantification.

Table 6-3 Relative compositions of carbon functional groups estimated by area integration of solid-state 13C CPMAS NMR spectra of humic acids

Soils	Composition (%)					
	Carbonyl C (160-220 ppm)	Aromatic- or olefin-(C-O) (140-160 ppm)	Aromatic- or olefin-(C-H, C-C) (110-140 ppm)	Polysaccharide (60-110 ppm)	N,O-alkyl-C (45-60 ppm)	Alkyl C (0-45 ppm)
HA A	6.4	3.1	12.8	20.9	6.7	50.1
HA B	5.2	2.6	8.7	13.5	8.6	61.4
HA C	6.3	3.6	14.1	15.3	7.7	53.1
HA D	6.7	3.0	12.9	21.7	12.0	43.7
HA E	5.7	3.9	15.9	19.2	9.2	46.2
HA F	8.2	4.4	15.0	19.2	10.0	43.2
HA G	14.5	9.4	25.0	22.0	8.5	20.5
HA H	11.2	5.3	15.2	16.5	10.6	41.1

6.4.3. Common pyrolysates of humic acids in dredged soils forming soft mixtures

The number of peaks assigned to pyrolysate compounds on the total ion chromatograms were 32, 52, 47, 46, 52, 53, 52, and 51 peaks for HA A, B, C, D, E, F, G, and H, respectively. Pyrolysate compounds that was common in HA D and H are shown in **Table 6-4**. The unique pyrolysates in HA D and H were octadecenoic acid, dimethyl trisulfide and styrene. Unique pyrolysates in HA D, H, and G was phytol and propenioic acid. Dimethyl trisulfide, octadecenoic acid, and propenoic acid suggest the sedimentary environment of soil D and H to be rather reducing which was favorable for sulfur-reducing bacteria to actively metabolize, and to conserve the metabolites within the sediments. Firstly, the formation of polysulfide is attributed to the equilibrium between microbially formed elemental sulfur and sulfides and their abiotic oxidation [23], which such formed polysulfide is suggested possible to consist a structure of humic substances [9]. Secondly, octadecenoic acid is an unsaturated fatty acid[24,25], which may be cis-vaccenic acid, a cellular fatty acid of sulfur-reducing bacteria. Some previous studies discuss the retention time of isomeric fatty acids get fractionated by the position of their unsaturated bonds [26,27], which may distinguish isomers of octadecenoic acids, though the determination of the isomers would need further study. Lastly, propenoic acid is stated as one of metabolites of sulfur reducing bacteria [28].

The existence of styrene and phytol suggest the input of plant-originated organic matters, which was rather well conserved within the sediments. Styrene originates from plants or coal tars, that is a low molecular weight compound that shows solubility in water. Phytol is a plant chlorophyl, which suggests that soils D, H, and G to have input of plant originated organic matters but may also conserve the sedimented organic matters.

Table 6-4 Pyrolysate compounds of HAs. The list contains the compounds commonly detected in HA D and H. Legend ○ show that the fragments was detected in HAs.

Fragment name	Classification	Humic acids							
		A	B	C	D	E	F	G	H
Phosphoric acid, trimethyl ester	P-containing compound	○	○	○	○	○	○	○	○
Hexadecanoic acid (C16), methyl ester	Monocarboxylic acids	○	○	○	○	○	○	○	○
Dimethyl heptene	N-Alkenes	○	○	○	○	○			○
Methanesulfonic acid, methyl ester	S-containing compounds	○		○	○	○		○	○
Dimethyl disulfide	S-containing compounds	○	○	○	○		○		○
3,4-Dimethoxybenzoic acid, methyl ester	Benzoic acid	○		○	○			○	○
Octadecanoic acid (C18), methyl ester	Monocarboxylic acids		○	○	○	○	○	○	○
Methyl Undecene	N-Alkenes		○	○	○	○		○	○
Hentetracontanol	Fatty alcohols		○	○	○				○
Tetradecanoic acid (C14), methyl ester	Monocarboxylic acids		○		○	○		○	○
Tetracosanoic acid (C24), methyl ester	Monocarboxylic acids				○	○	○	○	○
Propenoic acid(C3), methyl dodecyl ester	Monocarboxylic acids				○			○	○
Phytol	Others				○			○	○
Styrene	PAHs*				○				○
Dimethyl trisulfide	S-containing compounds				○				○
Octadecenoic acid (C18), methyl ester	Monocarboxylic acids				○				○

* polycyclic aromatic hydrocarbons

6.5. Conclusion

One of the indicators of the strength development of the mixtures was revealed to attribute to the reduced sulfur content in soil organic matters. However, the bulk analysis of carbon speciation did not indicate intrinsic characteristics of soil organic matters in dredged soils which formed soft mixtures. Through assignment of the pyrolysate compounds on TMAH-py GC/MS, the activity of sulfur reducing bacteria was suggested through the existence of trisulfides, metabolites of sulfur reducing bacteria, and a fatty acid which could be a cellular fatty acid of sulfur reducing bacteria. In addition, the conservation of sedimentary organic matters was suggested in such soils, due to the existence of phytols and styrene,

which are plant chlorophyl and low molecular weight, soluble organic compounds which originate from plants. Overall, this study added an insight to the characteristics of dredged soils which form soft mixtures. The effectiveness of soil organic matters to the pozzolanic reaction may attribute to the input organic matters to sedimentary soils but also how they are conserved and metabolized in the sediment soils.

References

[1]   UNESCO International Sediment Initiative, Sediment issues & sediment management in large river basins interim case study synthesis report, 2011.

[2]   G.-O. Kang, T. Tsuchida, Y.-S. Kim, W.-J. Baek, Influence of humic acid on the strength behavior of cement-treated clay during various curing stages, J. Mater. Civ. Eng. 29 (2017) 1–18. https://doi.org/10.1061/(ASCE)MT.1943-5533.0001919.

[3]   T. Tsuchida, Y.X. Tang, Estimation of compressive strength of cement-treated marine clays with different initial water contents, Soils Found. 55 (2015) 359–374. https://doi.org/10.1016/j.sandf.2015.02.011.

[4]   E. Kiso, M. Tsujii, K. Ito, M. Nakagawa, M. Gomyo, T. Nagatome, Method of dredged soil improvement by mixing with converter steel-making slag, Proc. Civ. Eng. Ocean. 24 (2008) 327–332.

[5]   N.R. Weerakoon, S. Nishimura, H. Sato, K. Toda, T. Sato, Y. Arai, Stiffness and strength mobilisation in steel-slag-mixed dredged clays in early curing, Proc. Inst. Civ. Eng. - Gr. Improv. (2018) 1–17. https://doi.org/10.1680/jgrim.17.00083.

[6]   S. Lirer, B. Liguori, I. Capasso, A. Flora, D. Caputo, Mechanical and chemical properties of composite materials made of dredged sediments in a fly-ash based geopolymer, J. Environ. Manage. 191 (2017) 1–7. https://doi.org/10.1016/j.jenvman.2017.01.001.

[7]   T. Thuy Minh Nguyen, S. Rabbanifar, N.A. Brake, Q. Qian, K. Kibodeaux, H.E. Crochet, S. Oruji, R. Whitt, J. Farrow, B. Belaire, P. Bernazzani, M. Jao, Stabilization of silty clayey dredged material, J. Mater. Civ. Eng. 30 (2018) 1–11. https://doi.org/10.1061/(ASCE)MT.1943-5533.0002391.

[8]   K. Toda, R. Kikuchi, T. Otake, S. Nishimura, Y. Akashi, A. Michihiro, K. Takeshi, T. Sato, Effect of Soil Organic Matters in Dredged Soils to Utilization of their Mixtures Made with a Steel Slag, Materials (Basel). 13 (2020).

[9]   M.A. Vairavamurthy, D. Maletic, S. Wang, B. Manowitz, T. Eglinton, T. Lyons, Characterization of sulfur-containing functional groups in sedimentary humic substances

by X-ray absorption near-edge structure spectroscopy, Energy and Fuels. 11 (1997) 546–553. https://doi.org/10.1021/ef960212a.

[10]   A. Vairavamurthy, W. Zhou, T. Eglinton, B. Manowitz, Sulfonates: A novel class of organic sulfur compounds in marine sediments, Geochim. Cosmochim. Acta. 58 (1994) 4681–4687. https://doi.org/10.1016/0016-7037(94)90200-3.

[11]   K. Toda, H. Sato, N. Weerakoon, T. Otake, S. Nishimura, T. Sato, Key factors affecting strength development of steel slag-dredged soil mixtures, Minerals. 8 (2018). https://doi.org/10.3390/min8050174.

[12]   M. Fukushima, K. Yamamoto, K. Ootsuka, T. Komai, T. Aramaki, S. Ueda, S. Horiya, Effects of the maturity of wood waste compost on the structural features of humic acids, Bioresour. Technol. 100 (2009) 791–797. https://doi.org/10.1016/j.biortech.2008.06.030.

[13]   H. Yabuta, M. Fukushima, M. Kawasaki, F. Tanaka, Organic Geochemistry Multiple polar components in poorly-humified humic acids stabilizing free radicals : Carboxyl and nitrogen-containing carbons, Org. Geochem. 39 (2008) 1319–1335. https://doi.org/10.1016/j.orggeochem.2008.05.007.

[14]   H. Knicker, P.G. Hatcher, F.J. González-Vila, Formation of Heteroaromatic Nitrogen after Prolonged Humification of Vascular Plant Remains as Revealed by Nuclear Magnetic Resonance Spectroscopy, J. Environ. Qual. 31 (2002) 444. https://doi.org/10.2134/jeq2002.0444.

[15]   H. Knicker, K.U. Totsche, G. Almendros, F.J. González-Vila, Condensation degree of burnt peat and plant residues and the reliability of solid-state VACP MAS 13C NMR spectra obtained from pyrogenic humic material, Org. Geochem. 36 (2005) 1359–1377. https://doi.org/10.1016/j.orggeochem.2005.06.006.

[16]   A. Watanabe, H. Takada, Structural stability and natural 13C abundance of humic acids in buried volcanic ash soils, Soil Sci. Plant Nutr. 52 (2006) 145–152. https://doi.org/10.1111/j.1747-0765.2006.00029.x.

[17]   V.S. Ramachandran, M.S. Lowery, Conduction calorimetric investigation of the effect of retarders on the hydration of Portland cement, Thermochim. Acta. 195 (1992) 373–387. https://doi.org/10.1016/0040-6031(92)80081-7.

[18]   M. Bishop, A.R. Barron, Cement hydration inhibition with sucrose, tartaric acid, and lignosulfonate: Analytical and spectroscopic study, Ind. Eng. Chem. Res. 45 (2006) 7042–7049. https://doi.org/10.1021/ie060806t.

[19]   N.L. Thomas, J.D. Birchall, The retarding action of sugars on cement hydration, Cem. Concr. Res. 13 (1983) 830–842.

[20]   H. Matsuyama, J.F. Young, Synthesis of calcium silicate hydrate/polymer complexes: Part I. Anionic and nonionic polymers, J. Mater. Res. 14 (1999) 3379–3388.

[21]   H. Matsuyama, J.F. Young, Synthesis of calcium silicate hydrate/polymer complexes: Part II. Cationic polymers and complex formation with different polymers, J. Mater. Res. 14 (1999) 3389–3396. https://doi.org/10.1557/JMR.1999.0459.

[22]   J. Plank, M. Gretz, Study on the interaction between anionic and cationic latex particles and Portland cement, Colloids Surfaces A Physicochem. Eng. Asp. 330 (2008) 227–233. https://doi.org/10.1016/j.colsurfa.2008.08.005.

[23]   A.J. Findlay, Microbial impact on polysulfide dynamics in the environment, FEMS Microbiol. Lett. 363 (2016) 1–12. https://doi.org/10.1093/femsle/fnw103.

[24]   A. Ueki, T. Suto, Cellular Fatty Acid Composition of Sulfate-Reducing Bacteria, J. Gen. Appl. Microbiol. 25 (1979) 185–196. https://doi.org/10.2323/jgam.25.185.

[25]   G.J. Perry, V. JK, Johns RB, Fatty acids of bacterial origin in contempary marine sediments, 43 (1979) 1715–1725.

[26]   J. Ecker, M. Scherer, G. Schmitz, G. Liebisch, A rapid GC-MS method for quantification of positional and geometric isomers of fatty acid methyl esters, J. Chromatogr. B Anal. Technol. Biomed. Life Sci. 897 (2012) 98–104. https://doi.org/10.1016/j.jchromb.2012.04.015.

[27]   G.W. Francis, Alkylthiolation for the determination of double-bond position in unsaturated fatty acid esters, Chem. Phys. Lipids. 29 (1981) 369–374. https://doi.org/10.1016/0009-3084(81)90070-0.

[28]   D. Suzuki, A. Ueki, A. Amaishi, K. Ueki, Diversity of substrate utilization and growth characteristics of sulfate-reducing bacteria isolated from estuarine sediment in Japan, J. Gen. Appl. Microbiol. 53 (2007) 119–132. https://doi.org/10.2323/jgam.53.119.

7. Microscopic study on the interaction of soil organic matters with the pozzolanic reaction

Abstract

The utilization of waste soils and industrial byproducts such as dredged soils and steel slags are carried out by forming construction materials by mixing them together, as the mixtures develop strength. However, soil organic matters in dredged soils are known to inhibit the cementation reaction of the mixtures, the pozzolanic reaction. It is known that the inhibition of the pozzolanic reaction may occur due to the excess of reduced sulfur and/or phenolic functional groups in the soil organic matter fraction in the dredged soils, though how such organic constituents inhibits the pozzolanic reaction is still unknown. Through STXM study on the samples of the mixtures which did and did not show significant strength development, and the samples of the synthetic products of the pozzolanic reaction with and without excess of organic reagent dosage which did not and did inhibit the pozzolanic reaction, indicated the possibility of aromatic carbon to play a role in the inhibition of the pozzolanic reaction. Because aromatic carbon itself unlikely inhibits the pozzolanic reaction, functionalized aromatic carbon, or organic compounds of, for example, aromatic carbon and reduced sulfur, was suggested to trigger the inhibition of the pozzolanic reaction.

Keywords: Humic acids, marine dredged sediment, pozzolanic reaction, calcium silicate hydrate, STXM

7.1. Introduction

Dredged soils that contain higher reduced sulfur and presumably phenolic groups in soil organic matter fraction was suggested to inhibit the pozzolanic reaction (chapter 5,6). The possibility on how soil organic matters inhibit the pozzolanic reaction have been discussed in chapter 4 and 5. Although the cause of the pozzolanic reaction by soil organic matters were not conclusive, it was clarified that not the pH buffering capacity nor the ability to form calcium complexation of soil organic matters, cause the inhibition. The remaining possibilities were the formation of an impermeable layer around the starting materials that inhibits water to access the materials, which could inhibit the pozzolanic reaction. Alternatively, formation of secondary phases that can form at high dosage of specific soil organic matters, was suggested to constrain the solution composition may inhibit the iterative reaction of the pozzolanic reaction, by keeping portlandite saturated. Therefore, the analysis on the solid-state samples collected in previous chapters, such as the steel slag-dredged soil mixtures and the synthesis products of the pozzolanic reactions, may indicate the cause of the pozzolanic reaction by soil organic matters.

This study focuses on clarifying the interaction of soil organic matters with the pozzolanic reaction in solid phases. The distribution of soil organic matters when the pozzolanic reaction is inhibited was discussed, majorly with the results of elemental mapping and carbon speciation mapping of the synthesis products of the pozzolanic reaction and the powder samples of the steel slag-dredged soil mixtures, under macroscopic scales. The results of the samples which the pozzolanic reaction was and was not inhibited is compared.

7.2. Materials and methods

7.2.1. Materials

7.2.1.1. Synthetic products of the pozzolanic reaction

The products of the C-S-H synthesis experiments via the pozzolanic reaction, carried out in chapter 4, was employed for further microscopic study on the distribution of organic

carbon species. The powders collected from the pozzolanic reaction products synthesized with initial Ca/Si ratio of 1.6 was used for the analysis. The C-S-H particulates synthesized with 15 and 29 wt.% of lignosulfonate, and the pozzolanic reaction products with 56 wt.% of lignosulfonate which the pozzolanic reaction was inhibited, were selected for the comparison. The samples without pretreatment such as pulverization were employed for the analysis under scanning electron microscopy (SEM) and scanning transmission X-ray microscopy (STXM). Powders were placed on the grid for transmission electron microscopy (TEM) made of copper with amorphous carbon support film, Cu400 (JEOL, Japan), for the STXM analysis. The samples were pulverized for the analysis of X-ray adsorption near edge structure (XANES) analysis.

7.2.1.2. *Steel slag-dredged soil mixtures*

The steel slag-dredged soil mixtures, made with soil E and soil H with a steel slag, at 3 days of curing were employed in this study. The characterization of the mixtures is described in chapter 3. The mixture made with soil E and a steel slag is a representative of the mixtures which does develop strength with minor effect or soil organic matters, and mixture made with soil H is a representative of the mixtures which does not develop significant strength with the effect of soil organic matters that inhibits the strength development. The freeze dried mixtures were crushed thoroughly to obtain samples below 25 μ m in diameter. For the STXM analysis, powders were spread by locating the TEM grid in powders which excess of powders were eliminated by tapping the TEM grid while holding it with a tweezer, to eliminate the usage of solutes of organic matters but also the portlandite.

7.2.2. **Methods**

7.2.2.1. *Scanning Electron Microscopy (SEM)*

Synthesized powders via the pozzolanic reaction with addition of lignosulfonate were observed by SEM (Shimadzu, JSM-IT200) to understand the elemental distribution in the

samples with and without C-S-H formation. Synthesized powders were spread on carbon tape which was carbon coated for the observation. Ca, Si and S mapping of the pozzolanic reaction products with and without the C-S-H formation inhibition was carried out.

7.2.2.2. *X-ray Adsorption Near Edge Structure (XANES)*

XANES analysis at C-K edge was carried out for lignosulfonate, humic acids of dredged soil samples, and humic acid standards, Inogashira humic acid (HA) and Dando HA, provided from Japan Humic Substance Society (JHSS). The XANES analysis was carried out at BL-19B in Photon Factory. Monk-Gillieson mounting monochromator with a varied-line-spacing plane grating was used as X-ray monochromator [1]. The XANES spectra were obtained with the total electron yield (TEY). The grinded samples were mounted on copper plate embedded in In metal, which was set in a chamber purged with He gas for the measurement.

7.2.2.3. *Scanning Transmission X-ray Microscopy (STXM)*

STXM analysis was carried out on the pozzolanic reaction products and the mixture samples. Prior to the STXM analysis, SEM analysis on the powder samples on the TEM grid was conducted to determine the grains for the STXM observations. SEM analysis was conducted with minimal exposure to electron beam to avoid the sample damage and carbon contamination. Sample observation was carried out with acceleration voltage of 8 kV at 60 cps.

Submicron distribution images of carbon and calcium speciation of the powder samples of the pozzolanic reaction products, and carbon speciation of the mixtures were obtained in transmission mode by using a compact STXM at BL-19A in Photon Factory [2]. Mapping of transmitted X-ray from pre-edge to post-edge of carbon K-edge and calcium L-edge was obtained using the image stacking method. The TEM grids were loaded on the sample holders and placed in a chamber purged with 0.1 atm He. The sample was scanned by X-

ray beam focused by a Fresnel zone plate with beam diameter minimum of 30 nm. XANES spectra at each edge were obtained using the aXis2000 software.

7.3. Results

7.3.1. SEM

The elemental mapping of the pozzolanic reaction products is shown in **Fig. 7-1**. The distribution of Si, Ca, and S of the C-S-H formed in coexistence of lignosulfonate, with addition of 29 wt.% of lignosulfonate, showed even distribution of the elements (**Fig. 7-1**a). On contrary, the distribution of Ca and Si of the samples which the C-S-H formation was inhibited due to the addition of 56 wt.% of lignosulfonate, showed heterogeneity in the distribution (**Fig. 7-1**b). The distribution of S, probably attributed to the distribution of lignosulfonate, was observed to overlap with the distribution of Si.
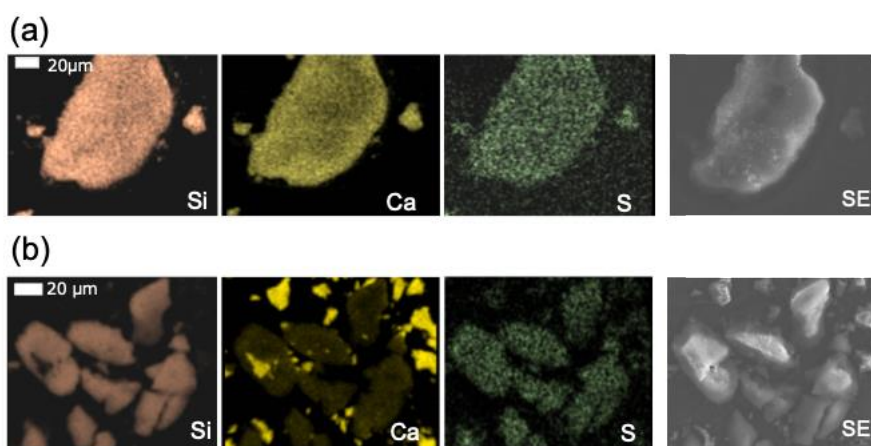
Fig. 7-1 The distribution of Si, Ca, and S elements and SE image of the synthesis products of the pozzolanic reaction of (a) the calcium silicate hydrate (C-S-H) formed with addition of lignosulfonate, and (b) the pozzolanic reaction products which the C-S-H formation was inhibited by lignosulfonate.

7.3.2. STXM

7.3.2.1. The pozzolanic reaction products

STXM images of the products of the pozzolanic reaction at Ca-L edge and C-K edge are shown in **Fig. 7-2** and **Fig. 7-3**, respectively. A particulate with relatively rich content of Si was selected for the observation for the sample of synthesized by the pozzolanic reaction with 56 wt.% of lignosulfonate addition, regarding to the SEM investigation which suggested the selective existence of lignosulfonate with Si rich grains. For particulates of samples with C-S-H formation with addition of lignosulfonate at 29 wt.% of dosage, the synthesized particulates were homogenous, so a particulate with a common composition was selected for the observation. The RGB color-deconvoluted image of the particulate of the pozzolanic reaction products with 56 wt.% of lignosulfonate addition is shown in **Fig. 7-2**(a), and that of C-S-H formed in coexistence of 29 wt.% of lignosulfonate is shown on **Fig. 7-2**(b). Red mapping shows the distribution of portlandite-like state of calcium, and green mapping shows the C-S-H-like state of calcium with irregular symmetry of coordination [3,4]. **Fig. 7-2**(c) shows the regional XANES spectra of extracted regions, corresponding to circled areas on **Fig. 7-2**(a,b).
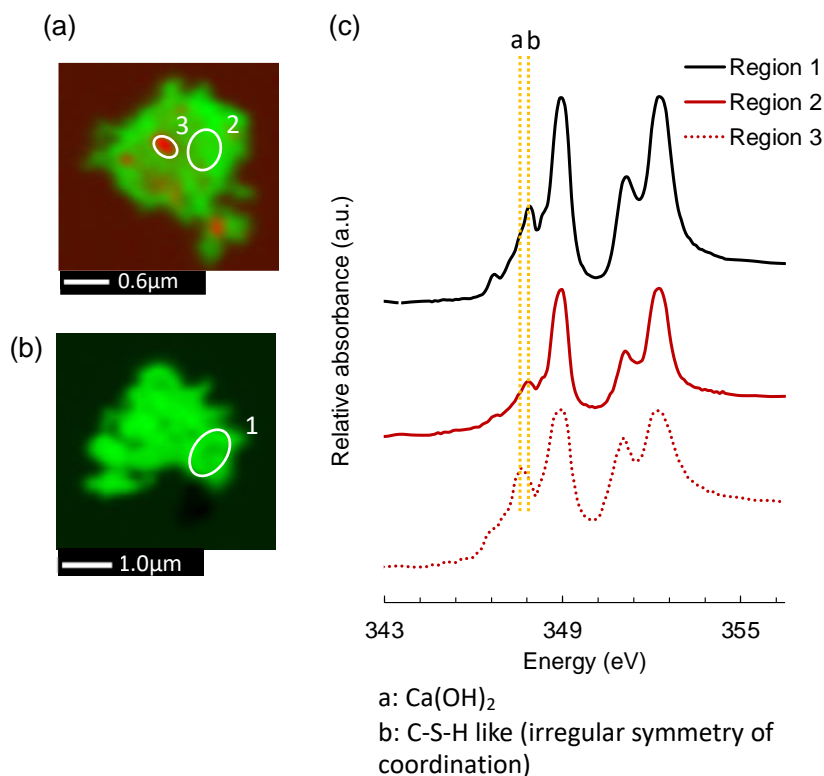
Fig. 7-2 (a) Scanning transmission X-ray microscopy (STXM) image of Ca L-edge of a particulate of the reaction products of the pozzolanic reaction with 56 wt.% dosage of lignosulfonate (b) and of C-S-H formed with addition of 29 wt.% of lignosulfonate. Images in color shows the composition map of Ca with the X-ray adsorption near edge structure (XANES) spectra of extracted regions. Figure (c) shows the XANES spectra at the Ca-L edge extracted from different areas, where the number shown on the figure (a) and (b) corresponds to the area of the extraction.

In contrary to the heterogenous distribution of calcium speciation in the particulate of the samples which the C-S-H formation was inhibited, the STXM image of C-K edge shows homogenous carbon chemical states on the same particulate **Fig. 7-3**(a). The carbon chemical state was homogenous in the particulate which the C-S-H formation was successful **Fig. 7-3**(b). Comparison of the C-K edge XANES spectra extracted from each particulate and the spectra of lignosulfonate reagent show the difference in the peak maxima of aromatic, phenolic, and carboxylic carbon that corresponds to adsorption peaks of 285.1, 286.8, and

288.6 eV, respectively[5]. The carbon species that coexist with solid phases of the pozzolanic reaction products was suggested to be minor in carboxylic groups, that was inferred from lower peak intensity of carboxylic group of region 1, the C-S-H formed sample, and region 2, the sample without C-S-H formation, in comparison with that of lignosulfonate (**Fig. 7-3**(c)). The intensity of aromatic carbon was similar in lignosulfonate and region 2, though lower in region 1, which suggested aromatic carbon as a preferable species to function on the solid phases at the occurrence of the C-S-H formation inhibition. Phenolic carbon had the same tendency with aromatic carbon.

(c) C K-edge NEXAFS of circled regions

(a) Powder of synthesis products with 56 wt.% of lignosulfonate

C distribution

0.6µm

(b) Powder of C-S-H with 29 wt.% of lignosulfonate

C distribution

1.0µm

a: aromatic C=C   c: carboxylic C
b: phenolic C   d: carbonate
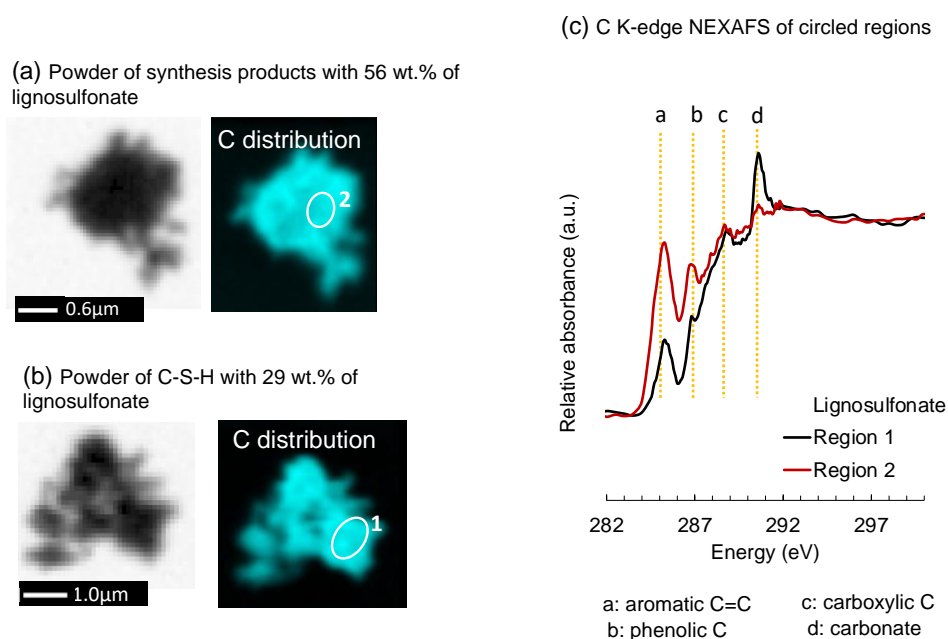
Fig. 7-3 (a) STXM X-ray adsorption image at C L-edge of a particulate of the reaction products of the pozzolanic reaction with 56 wt.% dosage of lignosulfonate (b) and of C-S-H formed with addition of 29 wt.% of lignosulfonate. Images in color shows the composition map of Ca with the XANES spectra of extracted regions. Figure (c) shows the XANES spectra at the C-L edge extracted from different areas, where the number shown on the figure (a) and (b) corresponds to the area of the extraction. XANES spectrum of lignosulfonate is shown together with the regional XANES spectra for the comparison.

Fig. 7-4 shows the XANES spectra of humic acid of dredged soil E, H, and JHSS standards. The humic acids extracted from dredged soils showed similar spectra in comparison with those of JHSS standards, composing of aromatic carbon, carboxylic carbon, and carbonates.

a: aromatic C=C   c: carbonate
b: carboxylic C
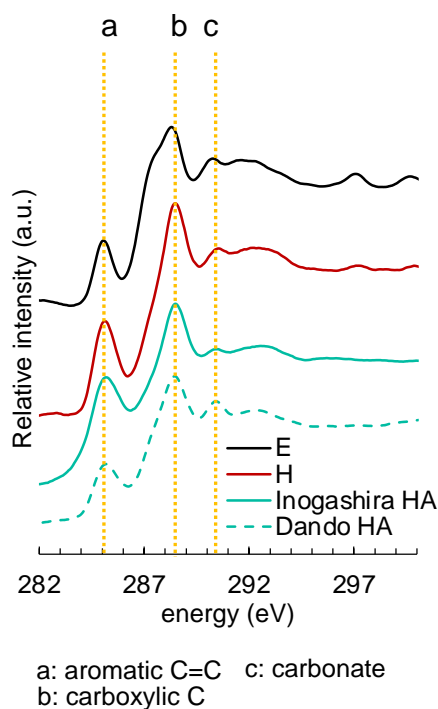
Fig. 7-4 XANES spectra of humic acids extracted from dredged soil E, H, and JHSS standards.

Fig. 7-5(a) shows the particulate of the mixtures made with soil E, and **Fig. 7-5**(b) shows the particulate of the mixtures made with soil H. The former particulate was a common type of particulate in mixture made with soil E, which was composed of Si, Al, C, and O under SEM analysis. Particulates of the latter mixture showed more heterogeneity in the composition of each particulates, hence the particulates which majorly composed of Si, Al, C and O was selected for the analysis. Particle of region 3 was a fragment of diatom frustules, and particle of region 4 maybe volcanic glass from the shape with sharp edges and the elemental composition. **Fig. 7-5**(c) shows the C-K edge XANES spectra of the particulates

of steel slag-dredged soil mixtures. The spectra of region 1 and 2 corresponds to the XANES spectra of the particulate in mixture made with soil E, and region 3, 4, and 5 correspond to that of the particulates in mixture made with soil H. The peak intensity of carboxylic carbon in the region 3, 4, and 5 was comparatively lower from the XANES spectra of humic acid in soil H (**Fig. 7-4**). In contrary, the peak intensity of aromatic carbon was not significantly lowered. The peak intensities of aromatic and carboxylic carbon in region 1 and 2 were like the XANES spectra of humic acid in soil E (**Fig. 7-4**).
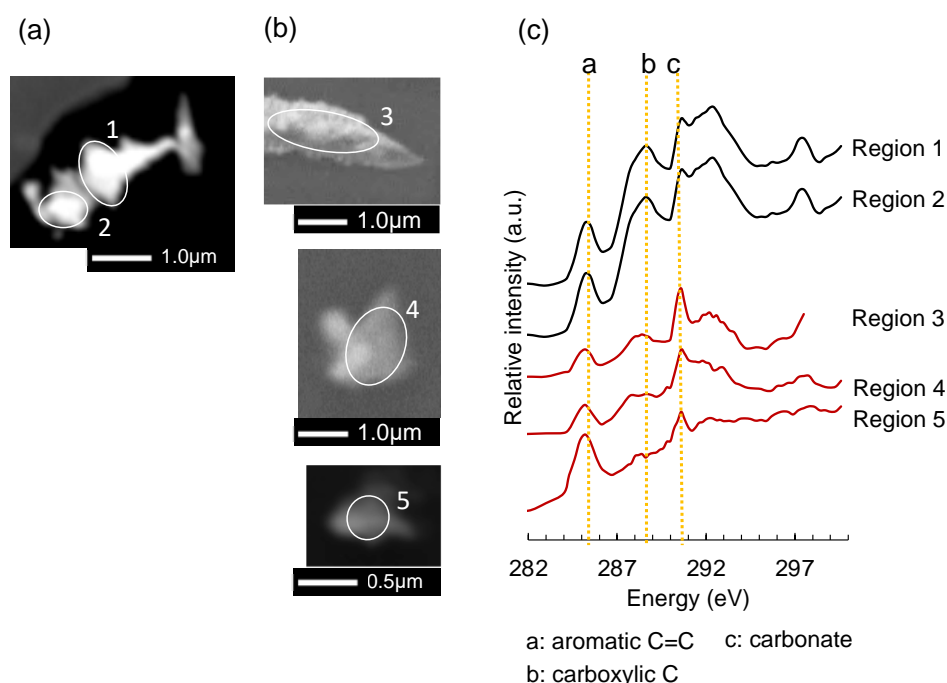
Fig. 7-5 Secondary electron image of (a) particulate of the mixtures made with soil E and (b) mixtures made with soil H. Silica rich particulates were selected for the STXM analysis. The circled regions on figure (a) and (b) are where C K-edge XANES spectra on figure (c) were extracted.

7.4. Discussion

### 7.4.1. Soil organic matters may coexist with Si sources at the inhibition of the pozzolanic reaction

Lignosulfonate selectively coexist with Si rich grains at the inhibition of the pozzolanic reaction (**Fig. 7-1**). Such organic matters, soluble in the pozzolanic reaction, may be attracted to the silica sources. The pozzolanic reaction, interpreted as iterative cycle, initiates at the dissolution of portlandite, which allows amorphous silica to dissolve. The rate-limiting step of the pozzolanic reaction was considered as the dissolution rate of amorphous silica, where portlandite and C-S-H dissolution and precipitation can be considered thermodynamically, though dissolution of amorphous silica must be treated kinetically at the simulation of the C-S-H formation in steel slag-dredged soil mixtures (Chapter 2). Hence, without lignosulfonate dosage which inhibits the pozzolanic reaction, C-S-H would immediately form once amorphous silica supplies dissolved silica. Therefore, the accumulation of lignosulfonate with Si rich grains suggests that it may attribute to the dissolution of amorphous silica, which either the surface of amorphous silica at hydration or the secondary precipitates that form close to Si-rich grains to attract the organic matters. It supports the discussion in chapter 4, which suggested the formation of secondary phases that compose of lignosulfonate and silica, as the cause of the inhibition of the pozzolanic reaction. It was discussed to either limit the hydration of starting materials or constrain the solution composition to inhibit the reaction, though this study revealed that lignosulfonate may favorably function to form such impermeable layer surrounding amorphous silica.

7.4.2. Contribution of aromatic carbon to the inhibition of the pozzolanic reaction

Aromatic carbon commonly coexisted with the particulates which the pozzolanic reaction was inhibited (**Fig. 7-3**, **Fig. 7-5**). In chapter 5, reduced sulfur, and phenolic functional groups, illustrated the thresholds of the organic reagent dosage to cause the inhibition of the pozzolanic reaction (**Fig. 7-6**). In addition to such components in soil organic matters,

aromatic carbon may be playing a key role in the inhibition of the pozzolanic reaction, though it may not be the limiting factor for the initiation of the inhibition of the pozzolanic reaction.

Although phenolic carbon was not detectable for humic acids treated in this study, other soils may contain the phenolic carbon in the amount recognizable under X-ray microscopic studies (i,e,, [6]). Also, the XANES spectra of the region in the particulate from the pozzolanic reaction product with dosage of 56 wt.% of lignosulfonate which the C-S-H formation was inhibited, the peak maxima of phenolic carbon were higher in comparison with that of C-S-H formed particulate. Therefore, this study supports the discovery in chapter 5 which suggested the quantity of phenolic functional group to trigger the inhibition of the pozzolanic reaction, and further suggested the contribution of aromatic carbon to the inhibition of the pozzolanic reaction (**Fig. 7-6**).
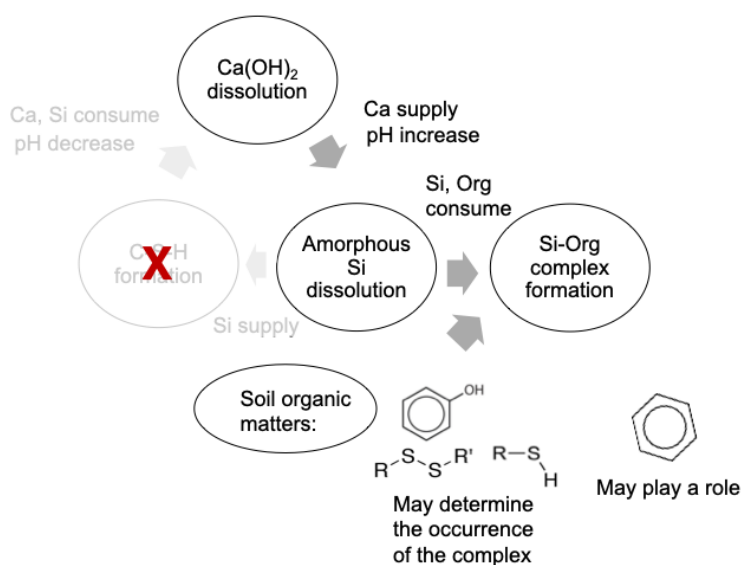
Fig. 7-6 Schematic diagram of the reaction which may occur when soil organic matters inhibit the pozzolanic reaction.

7.4.3.   Interaction of the pozzolanic reaction with the soil organic matters

Reduced sulfur maybe thiols or (poly)sulfides. Sulfides and aromatic carbon are known to interact by the electron lone pairs of sulfides and pi bonds of aromatic carbons, which is known to play a role in forming a macromolecular structure of proteins [7–9] (**Fig. 7-7**). Such macromolecular structure may form the impermeable layer that inhibits the hydration f primary phases in the pozzolanic reaction. Alternatively, the attraction of the electron lone pair to the pi bond cause the pi electron cloud to have slightly negative charge on a side of the aromatic rings, that may be electrostatically attracted to the positively charged surfaces. Such surfaces may be of amorphous silica, where silanol groups are cation exchanged with calcium, that is also known to occur in C-S-H [10].

cation

$R-S-R'$ ◯ electron cloud
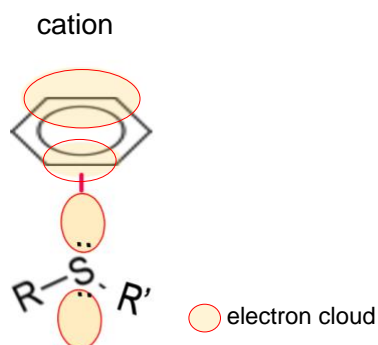
Fig. 7-7 Schematic diagram of lone pair- pi interaction between sulfide and aromatic carbon.

Alternatively, thiols functionalized to aromatic carbon, thiophenols may inhibit the pozzolanic reaction. Thiols are proton donating functional groups that can possess a negative charge after deprotonation, which maybe attracted towards the positively charged surfaces. Thiols are known to have a wide variety of pKa attributed to the carbon structure which thiols are functionalized with [11]. The pKa of thiophenols was modelled to possess pKa in the range of 5.1 to 10.8, hence majority of thiophenols would be deprotonated at a pH of 12.5.

Although the concrete combination of constituents of soil organic matters that inhibits the pozzolanic reaction was not conclusive, this study suggested the possibility of the

contribution of aromatic carbon to the inhibition, and the requirement to consider interactions between organic constituents to interpret the interaction of soil organic matters with the pozzolanic reaction.

7.5. Conclusions

Aromatic carbon was suggested to play a role in the inhibition of the pozzolanic reaction through STXM study of the particulates of steel slag-dredged soil mixtures and the synthetic pozzolanic reaction products. In addition, soil organic matters were suggested to favorably coexist with Si rich grains, that maybe attributed to the location of the secondary phases formation, which is likely to occur close to Si rich grains as dissolution of silicates would be the rate-limiting step of the pozzolanic reaction.

Although the process of aromatic carbon and reduced sulfur, or phenolic functional groups to inhibit of the pozzolanic reaction was not conclusive, this study provides insights into the possibility of the interaction between organic compounds to inhibit the pozzolanic reaction.

References

[1]   K. Amemiya, T. Ohta, Design of a variable-included-angle Monk-Gillieson monochromator with varied-line-spacing gratings, J. Synchrotron Radiat. 11 (2004) 171–176. https://doi.org/10.1107/S0909049503023598.

[2]   Y. Takeichi, N. Inami, H. Suga, C. Miyamoto, T. Ueno, K. Mase, Y. Takahashi, K. Ono, Design and performance of a compact scanning transmission X-ray microscope at the Photon Factory, Rev. Sci. Instrum. 87 (2016). https://doi.org/10.1063/1.4940409.

[3]   G. Geng, R. Taylor, S. Bae, D. Hernández-Cruz, D.A. Kilcoyne, A.H. Emwas, P.J.M. Monteiro, Atomic and nano-scale characterization of a 50-year-old hydrated C3S paste, Cem. Concr. Res. 77 (2015) 36–46. https://doi.org/10.1016/j.cemconres.2015.06.010.

[4]   J. Li, G. Geng, R. Myers, Y.S. Yu, D. Shapiro, C. Carraro, R. Maboudian, P.J.M. Monteiro, The chemistry and structure of calcium (alumino) silicate hydrate: A study by XANES, ptychographic imaging, and wide- and small-angle scattering, Cem. Concr. Res. 115 (2019) 367–378. https://doi.org/10.1016/j.cemconres.2018.09.008.

[5]   C. Le Guillou, S. Bernard, F. De La Pena, Y. Le Brech, XANES-Based Quantification of Carbon Functional Group Concentrations, Anal. Chem. 90 (2018) 8379–8386. https://doi.org/10.1021/acs.analchem.8b00689.

[6]   Y. Takahashi, Q. Fan, H. Suga, K. Tanaka, A. Sakaguchi, Y. Takeichi, K. Ono, K. Mase, K. Kato, V. V. Kanivets, Comparison of Solid-Water Partitions of Radiocesium in River Waters in Fukushima and Chernobyl Areas, Sci. Rep. 7 (2017) 1–11. https://doi.org/10.1038/s41598-017-12391-7.

[7]   A.L. Ringer, A. Senenko, C.D. Sherrill, Models of S/π interactions in protein structures: Comparison of the H 2 S-benzene complex with PDB data , Protein Sci. 16 (2007) 2216–2223. https://doi.org/10.1110/ps.073002307.

[8]   S.K. Singh, A. Das, The n → π∗ interaction: A rapidly emerging non-covalent interaction, Phys. Chem. Chem. Phys. 17 (2015) 9596–9612. https://doi.org/10.1039/c4cp05536e.

[9]   A. Das, S.R. Choudhury, C. Estarellas, B. Dey, A. Frontera, J. Hemming, M. Helliwell, P. Gamez, S. Mukhopadhyay, Supramolecular assemblies involving anion-π and lone pair-π interactions: Experimental observation and theoretical analysis, CrystEngComm. 13 (2011) 4519–4527. https://doi.org/10.1039/c0ce00593b.

[10]   H. Viallis-Terrisse, A. Nonat, J.C. Petit, Zeta-potential study of calcium silicate hydrates interacting with alkaline cations, J. Colloid Interface Sci. 244 (2001) 58–65. https://doi.org/10.1006/jcis.2001.7897.

[11]   Y. Zheng, W. Zheng, D. Zhu, H. Chang, Theoretical modeling of pKa's of thiol compounds in aqueous solution, New J. Chem. 43 (2019) 5239–5254. https://doi.org/10.1039/c8nj06259e.

8. General conclusion

Industrial byproducts and waste soils are environmentally low-impact resources for the construction industry. Construction materials made with such resources are particularly attractive for regional use close to the material sources, because of the feasibility in the transport and application associated with cost savings. Dredged soils excavated sediments of water ways, and steel slags, byproducts of iron making processes, have potential to form civil engineering constructions close to seashores, as their mixtures develop strength. The utilization of such mixtures is still limited due to their unpredictable variation of strength development when different dredged soils or steel slags are applied. Chapter 1 reviewed the literature on the general management of dredged soils and steel slags and current knowledge of technologies on their validation as construction materials, as well as the pozzolanic reaction, chemical reaction that develops strength of the mixtures, to identify the factors affecting the reaction. However, no previous studies have comprehensively investigated the key factors which affects the pozzolanic reaction. This study elucidates the key factors that affects the pozzolanic reaction in steel slag-dredged soil mixtures for the first time by identifying the contributions of both inorganic and organic components in steel slags and dredged soils to the strength development of the mixtures.

8.1. Contribution of inorganic phases

Chapter 2 focused on identifying the factors among inorganic components in dredged soils and steel slags affecting the strength development of the mixtures. Amorphous silica in dredged soils and portlandite in steel slags were identified as the key factors as major Si and Ca sources for the pozzolanic reaction, respectively. The pozzolanic reaction was interpreted as an iterative reaction that continues until the depletion of portlandite or amorphous silica. Hence, the content of both amorphous silica and portlandite in starting materials would be critical in forming a mixture with desired strength development.

Some mixtures, made with dredged soils with enough amorphous silica and steel slag with enough portlandite to develop strength, formed soft mixtures. Therefore, the quantification of inorganic phases was determined as one of the key factors to determine the strength development of the mixtures, that suggested the other key factors that affect the strength development in the mixtures to exist in dredged soils.

8.2. Contribution of organic phases

Chapter 3 focused on identifying the effect of organic components in dredged soils to the strength development of the mixtures. In soft mixtures that contained enough amorphous silica, characteristics of dredged soils such as high sulfur content in soil organic matters fraction was a common characteristic, that suggested the strength development inhibition by soil organic matters.

Chapter 4, 5 and 6 focused on identifying the contribution of soil organic matters to the pozzolanic reaction. Chapter 4 clarified through the synthesis of the secondary phases majorly in charge of the strength development of the mixture, calcium silicate hydrate (C-S-H), via the pozzolanic reaction. It was experimentally proven that the inhibition of the pozzolanic reaction by soil organic matters to occur, with a threshold in the dosage of the organic matter.

Chapter 5 investigated the effectiveness of various organic reagents with similar structural composition to soil organic matters. It was tested with the synthesis of C-S-H via the pozzolanic reaction in coexistence of each organic reagents, which suggested the contribution of phenolic functional groups and reduced sulfur to play a role to the inhibition of the pozzolanic reaction within the macromolecular structure of soil organic matters that compose of numerous carbon species and functional groups.

Chapter 6 focused on the characterization of soil organic matters to prove that such discoveries in chapter 4 and 5 are applicable to the inhibition of the pozzolanic reaction in real steel slag-dredged soil mixtures. Reduced sulfur was the sulfur species, that shaped the

sulfur content in soil organic matters to function as an indicator of soft mixtures. The discovery of reduced sulfur, being the indicator of the inhibition of the pozzolanic reaction in C-S-H synthesis experiment and in real steel slag-dredged soil mixtures, suggested that the inhibition of the pozzolanic reaction was similarly occurring by soil organic matters, in the steel slag-dredged soil mixtures.

In addition to chapter 4, 5 and 6 which focused on identifying the key organic components that trigger the inhibition of the pozzolanic reaction, chapter 7 focused on identifying other organic constituents which may play a role yet does not define the thresholds in their dosage to trigger the reaction that inhibits the pozzolanic reaction. The macroscopic study of the particulates of the mixtures and the synthetic products of the pozzolanic reaction revealed that not only the phenolic groups and reduced sulfur, but aromatic carbon was suggested to play a role in the inhibition of the pozzolanic reaction.

8.3. Research significance

The utilization of dredged soils and steel slags would be enhanced, through the discovery of the indicators of the strength development that would facilitate the evaluation processes of their application to construction materials. Also, the discovery of the key components in soil organic matters that inhibit the pozzolanic reaction and insights into the process of its interaction to trigger the inhibition, is presented as a significant starting point to overcome the issues in the validation of waste soils which were impossible to utilize as construction materials. Overall, outstanding insights are derived from half-splitting analysis of key components in raw materials that promote and inhibit geochemical reactions in control of strength development of such construction materials. These findings in this study are unambiguously useful to enhance utilization of industrial byproducts and waste soils in the construction industry.